

**SOCIAL DIMENSIONS OF URBAN HEAT ISLAND MITIGATION USING  
COMMUNITY GARDENS**

by

William Goldman

A thesis submitted to the Faculty of the University of Delaware in partial fulfillment of the requirements for the degree of Master of Science in Geography

Summer 2017

© 2017 William Goldman  
All Rights Reserved

**SOCIAL DIMENSIONS OF URBAN HEAT ISLAND MITIGATION USING  
COMMUNITY GARDENS**

by

William Goldman

Approved: \_\_\_\_\_  
Dr. Dana Veron, Ph.D.  
Co-Professor in charge of thesis on behalf of the Advisory Committee

Approved: \_\_\_\_\_  
Paul Jackson, Ph.D.  
Co-Professor in charge of thesis on behalf of the Advisory Committee

Approved: \_\_\_\_\_  
Delphis Levia, Ph.D.  
Chair of the Department of Geography

Approved: \_\_\_\_\_  
Mohsen Badiey, Ph.D.  
Acting Dean of the College of Earth, Ocean, and Environment

Approved: \_\_\_\_\_  
Ann L. Ardis, Ph.D.  
Senior Vice Provost for Graduate and Professional Education

## **ACKNOWLEDGMENTS**

I would like to thank the following individuals and groups for their support of my research:

My co-advisor, Dr. Dana Veron, who has supported me in my research endeavors since I was an undergraduate student.

My co-advisor, Dr. Paul Jackson, who first taught me how to frame my work with a critical human geography perspective.

My third committee member, Rodrigo Vargas, for providing me with valuable insights and questions as I conducted my research.

The Neighborhood Gardens Trust, the gardeners of the 2124 Fitzwater Garden, and the residents of Fitzwater Street, who aided in my research by letting me place my sensors on their properties.

The Department of Geography, which has helped me grow as a researcher and a scholar during my time there.

The Mather Graduate Fellows Fund, which provided me the funding for my HOBO sensors, and enabled me to conduct my research.

My friends Nathan Thayer, Casey Smith, and Adrienne Shumlich, who assisted me during my various trips to Philadelphia.

And, last but not least, my parents, for their support over the years, and especially during my time as a graduate student at the University of Delaware.

## TABLE OF CONTENTS

LIST OF TABLES .....	viii
LIST OF FIGURES .....	ix
ABSTRACT .....	xiv

### Chapter

1	BACKGROUND .....	1
1.1	Urban Heat Islands and Park Cool Islands .....	1
1.2	Urban Gardens .....	2
1.3	Thermal Comfort .....	4
1.4	Modelling “Difference” .....	7
2	METHODS .....	9
2.1	Observations .....	9
2.1.1	In situ HOBO sensor data .....	9
2.1.2	Mesowest .....	11
2.2	Observational Data Analysis .....	13
2.2.1	Calculating Urban Heat Island Intensity .....	13
2.2.2	Paired T-test .....	15
2.2.3	Microclimatic Model Forcings .....	16
2.3	Modelling .....	17
2.3.1	Envi-met .....	17
2.3.2	RayMan .....	20
2.3.2.1	Physiological Equivalent Temperature .....	21
2.3.2.2	Predicted Mean Vote .....	22
2.3.3	Analysis of RayMan Results .....	23
2.3.3.1	Hierarchical Cluster Analysis .....	24

3	RESULTS.....	36
3.1	Observational Data Results .....	36
3.1.1	Paired t-test with E4674 .....	36
3.1.1.1	Temperature Differences .....	36
3.1.1.2	Relative Humidity Differences.....	38
3.1.2	Paired t-test with the Garden Sensor .....	40
3.1.2.1	Temperature Differences .....	40
3.1.2.2	Relative Humidity Differences.....	41
3.2	Thermal Comfort Index Results .....	42
3.2.1	Paired t-tests .....	42
3.2.1.1	Street Receptors' PET vs. the Garden Receptor's PET .....	43
3.2.1.2	Hypothetical Model Receptors' PET vs. ActualGarden Model Receptors' PET .....	45
3.2.1.3	Hypothetical Model Receptors' PET vs. 3xGarden Model Receptors' PET .....	46
3.2.1.4	Female PMV vs. Male PMV .....	48
3.2.2	Hierarchical Cluster Analysis.....	49
3.2.2.1	Hierarchical Cluster of the Physiological Equivalent Temperature (PET).....	49
3.2.2.2	Hierarchical Cluster of the Predicted Mean Vote (PMV).....	51
3.2.2.2.1	Male PMV .....	51
3.2.2.2.2	Female PMV .....	52
3.2.3	Diurnal Cycle Graphs .....	52
3.2.3.1	Warming and Cooling Patterns .....	53
3.2.3.2	Diurnal Cycle of the Physiological Equivalent Temperature (PET).....	56
3.2.3.2.1	The Garden Receptor.....	56
3.2.3.2.2	Receptor 1.....	57
3.2.3.2.3	Receptor 2.....	59

3.2.3.2.4	Receptor 3.....	60
3.2.3.3	Comparison of Male and Female Predicted Mean Vote (PMV) Results .....	61
3.2.3.3.1	Male and Female PMV Differences at the Garden Receptor.....	61
3.2.3.3.2	Male and Female PMV Differences at Receptor 1.....	62
3.2.3.3.3	Male and Female PMV Differences at Receptor 2.....	63
3.2.3.3.4	Male and Female PMV Differences at Receptor 3.....	63
4	DISCUSSION.....	116
4.1	Urban Heat Island and Mitigation in Philadelphia .....	116
4.1.1	Philadelphia Urban Heat Island.....	116
4.1.2	Urban Garden Heat Mitigation.....	117
4.2	Thermal Comfort in Urban Community Gardens .....	119
4.2.1	Effects of the Composition of Urban Gardens on Thermal Comfort.....	119
4.2.1.1	The Effect of Tree-Cover and Ground Cover on Thermal Comfort.....	120
4.2.1.2	Male and Female Differences in Thermal Comfort ...	123
4.2.2	Urban Heat Island Mitigation Strategies for Philadelphia .....	126
4.2.2.1	Possibilities.....	126
4.2.2.2	Problems.....	127
4.2.3	Limitations and Future Research.....	129
5	CONCLUSION .....	132
	REFERENCES.....	134

## LIST OF TABLES

Table 3.1: [Urban (LCZ <sub>2</sub> or LCZ <sub>5</sub> ) Sensor Temperature Variable Mean] - [Rural (LCZ <sub>9</sub> ) Sensor E4674 Temperature Variable Mean] .....	38
Table 3.2: [Urban (LCZ <sub>2</sub> or LCZ <sub>5</sub> ) Sensor Relative Humidity Variable Mean] - [Rural (LCZ <sub>9</sub> ) Sensor E4674 Relative Humidity Variable Mean] .....	39
Table 3.3: [Garden Sensor Temperature Variable Mean] - [Other Urban (LCZ <sub>2</sub> ) Sensor Temperature Variable Mean] .....	41
Table 3.4 [Garden Sensor Relative Humidity Variable Mean] - [Other Urban (LCZ <sub>2</sub> ) Sensor Relative Humidity Variable Mean].....	42
Table 3.5: [Garden Receptor Mean PET (°C)] - [Street Receptor Mean PET (°C)] for All Envi-met Models. ( .....	44
Table 3.6: [Theoretical Model Mean PET (°C)] - [ActualGarden Model Mean PET (°C)] for All Receptors. ....	46
Table 3.7: [Theoretical Model Mean PET (°C)] - [3xGarden Model Mean PET (°C)] for All Receptors.....	47
Table 3.8: [Mean Female PMV] - [Mean Male PMV] at Each Receptor for All Models.....	48
Table 3.9: Ranges of PET and PMV values for different levels of thermal comfort and physiological stress (according to Wang et al. 2017).....	53

## LIST OF FIGURES

Figure 2.1: Sensor Locations on Fitzwater St. Philadelphia .....	26
Figure 2.2: ActualGarden Vegetation Model .....	27
Figure 2.2: ActualGarden Soil/Surface Model.....	28
Figure 2.4 3xGarden Vegetation Model.....	29
Figure 2.5 Enlarged Garden Soil/Surface Model (used for 3xGarden, 3xSoyGarden, 3xLoam, and 3xTreeCoveredLoam models).....	30
Figure 2.6 3xSoyGarden Vegetation Model.....	31
Figure 2.7 No-Vegetation Garden Vegetation Model (used in 3xLoam, 3xAsphalt, and 3xConcrete models).....	32
Figure 2.8 Asphalt-Covered Garden Soil (used in 3xAsphalt and 3xTreeCoveredAsphalt models).....	33
Figure 2.9 Tree-Covered Garden Vegetation Model (Used in 3xTreeCoveredLoam and 3xTreeCoveredAsphalt models).....	34
Figure 2.10 Concrete-Covered Soil/Surface Model .....	35
Figure 3.1: Receptor Locations. Receptors are represented as purple cells with abbreviated name (i.e. Garden Sensor = “GS”, Receptor 1 = “R1”, Receptor 2 = “R2” and Receptor 3 = “R3”). The ActualGarden model is shown, but the receptor location is unchanged in each model. ....	64
Figure 3.2: Hierarchical Cluster Analysis Dendrogram of the Physiological Equivalent Temperature (PET) For Each Model and Receptor. The four colors correspond to the four clusters of the dendrogram (which are composed of the same receptor for all eight models). Green represents the Garden Receptor, red represents Receptor 1, blue represents Receptor 2, and brown represents Receptor 3.....	65

Figure 3.3: Hierarchical Cluster Analysis Dendrogram of the Male Predicted Mean Vote (PET) For Each Model and Receptor. The four colors correspond to the four clusters of the dendrogram (which are composed of the same receptor for all eight models). Green represents the Garden Receptor, red represents Receptor 1, blue represents Receptor 2, and brown represents Receptor 3. ....	66
Figure 3.4: Hierarchical Cluster Analysis Dendrogram of the Female Predicted Mean Vote (PET) For Each Model and Receptor. The four colors correspond to the four clusters of the dendrogram (which are composed of the same receptor for all eight models). Green represents the Garden Receptor, red represents Receptor 1, blue represents Receptor 2, and brown represents Receptor 3. ....	67
Figure 3.5: The Diurnal Cycle of the Physiological Equivalent Temperature (PET) of the Garden Receptor for Week 1.....	68
Figure 3.6: The Diurnal Cycle of the Physiological Equivalent Temperature (PET) of the Garden Receptor for Week 2.....	69
Figure 3.7: The Diurnal Cycle of the Physiological Equivalent Temperature (PET) of the Garden Receptor for Week 3.....	70
Figure 3.8: The Diurnal Cycle of the Physiological Equivalent Temperature (PET) of the Garden Receptor for Week 4.....	71
Figure 3.9: The Diurnal Cycle of the Physiological Equivalent Temperature (PET) of Receptor 1 for Week 1. ....	72
Figure 3.10: The Diurnal Cycle of the Physiological Equivalent Temperature (PET) of Receptor 1 for Week 2. ....	73
Figure 3.11: The Diurnal Cycle of the Physiological Equivalent Temperature (PET) of Receptor 1 for Week 3. ....	74
Figure 3.12: The Diurnal Cycle of the Physiological Equivalent Temperature (PET) of Receptor 1 for Week 4. ....	75
Figure 3.13: The Diurnal Cycle of the Physiological Equivalent Temperature (PET) of Receptor 2 for Week 1. ....	76
Figure 3.14: The Diurnal Cycle of the Physiological Equivalent Temperature (PET) of Receptor 2 for Week 2. ....	77

Figure 3.15: The Diurnal Cycle of the Physiological Equivalent Temperature (PET) of Receptor 2 for Week 3. ....	78
Figure 3.16: The Diurnal Cycle of the Physiological Equivalent Temperature (PET) of Receptor 2 for Week 4. ....	79
Figure 3.17: The Diurnal Cycle of the Physiological Equivalent Temperature (PET) of Receptor 3 for Week 1. ....	80
Figure 3.18: The Diurnal Cycle of the Physiological Equivalent Temperature (PET) of Receptor 3 for Week 2. ....	81
Figure 3.19: The Diurnal Cycle of the Physiological Equivalent Temperature (PET) of Receptor 3 for Week 3. ....	82
Figure 3.20: The Diurnal Cycle of the Physiological Equivalent Temperature (PET) of Receptor 3 for Week 4. ....	83
Figure 3.21: The Diurnal Cycle of the Female Predicted Mean Vote (PMV) of the Garden Receptor for Week 1. ....	84
Figure 3.22: The Diurnal Cycle of the Male Predicted Mean Vote (PMV) of the Garden Receptor for Week 1. ....	85
Figure 3.23: The Diurnal Cycle of the Female Predicted Mean Vote (PMV) of the Garden Receptor for Week 2. ....	86
Figure 3.24: The Diurnal Cycle of the Male Predicted Mean Vote (PMV) of the Garden Receptor for Week 2. ....	87
Figure 3.25: The Diurnal Cycle of the Female Predicted Mean Vote (PMV) of the Garden Receptor for Week 3. ....	88
Figure 3.26: The Diurnal Cycle of the Male Predicted Mean Vote (PMV) of the Garden Receptor for Week 3. ....	89
Figure 3.27: The Diurnal Cycle of the Female Predicted Mean Vote (PMV) of the Garden Receptor for Week 4. ....	90
Figure 3.28: The Diurnal Cycle of the Male Predicted Mean Vote (PMV) of the Garden Receptor for Week 4. ....	91
Figure 3.29: The Diurnal Cycle of the Female Predicted Mean Vote (PMV) of Receptor 1 for Week 1. ....	92

Figure 3.30: The Diurnal Cycle of the Male Predicted Mean Vote (PMV) of Receptor 1 for Week 1.....	93
Figure 3.31: The Diurnal Cycle of the Female Predicted Mean Vote (PMV) of Receptor 1 for Week 2.....	94
Figure 3.32: The Diurnal Cycle of the Male Predicted Mean Vote (PMV) of Receptor 1 for Week 2.....	95
Figure 3.33: The Diurnal Cycle of the Female Predicted Mean Vote (PMV) of Receptor 1 for Week 3.....	96
Figure 3.34: The Diurnal Cycle of the Male Predicted Mean Vote (PMV) of Receptor 1 for Week 3.....	97
Figure 3.35: The Diurnal Cycle of the Female Predicted Mean Vote (PMV) of Receptor 1 for Week 3.....	98
Figure 3.36: The Diurnal Cycle of the Male Predicted Mean Vote (PMV) of Receptor 1 for Week 4.....	99
Figure 3.37: The Diurnal Cycle of the Female Predicted Mean Vote (PMV) of Receptor 2 for Week 1.....	100
Figure 3.38: The Diurnal Cycle of the Male Predicted Mean Vote (PMV) of Receptor 2 for Week 2.....	101
Figure 3.39: The Diurnal Cycle of the Male Predicted Mean Vote (PMV) of Receptor 2 for Week 2.....	102
Figure 3.40: The Diurnal Cycle of the Male Predicted Mean Vote (PMV) of Receptor 2 for Week 2.....	103
Figure 3.41: The Diurnal Cycle of the Female Predicted Mean Vote (PMV) of Receptor 2 for Week 3.....	104
Figure 3.42: The Diurnal Cycle of the Male Predicted Mean Vote (PMV) of Receptor 2 for Week 3.....	105
Figure 3.43: The Diurnal Cycle of the Female Predicted Mean Vote (PMV) of Receptor 2 for Week 4.....	106
Figure 3.44: The Diurnal Cycle of the Male Predicted Mean Vote (PMV) of Receptor 2 for Week 4.....	107

Figure 3.45: The Diurnal Cycle of the Female Predicted Mean Vote (PMV) of Receptor 3 for Week 1.....	108
Figure 3.46: The Diurnal Cycle of the Male Predicted Mean Vote (PMV) of Receptor 3 for Week 1.....	109
Figure 3.47: The Diurnal Cycle of the Female Predicted Mean Vote (PMV) of Receptor 3 for Week 2.....	110
Figure 3.48: The Diurnal Cycle of the Male Predicted Mean Vote (PMV) of Receptor 3 for Week 2.....	111
Figure 3.49: The Diurnal Cycle of the Female Predicted Mean Vote (PMV) of Receptor 3 for Week 3.....	112
Figure 3.50: The Diurnal Cycle of the Male Predicted Mean Vote (PMV) of Receptor 3 for Week 3.....	113
Figure 3.51: The Diurnal Cycle of the Female Predicted Mean Vote (PMV) of Receptor 3 for Week 4.....	114
Figure 3.52: The Diurnal Cycle of the Male Predicted Mean Vote (PMV) of Receptor 3 for Week 4.....	115

## **ABSTRACT**

Urban Heat Islands (UHI) occur where urban areas have higher temperatures than their less-developed surroundings, and can be mitigated in part by urban vegetation. In addition, the experience of the UHI varies across populations within a city due to many social and economic factors such as poverty, age, and the residents' biological sex. Urban community gardens have been suggested as a form of urban vegetation which may mitigate local temperature increases associated with the urban heat island in a city as well as providing many other social benefits. However, urban greenspace such as parks vary in cooling capability, and urban gardens are also subject to social forces that influence their composition and may affect their cooling capability. Through an analysis of observed and modelled data from a garden in Philadelphia, the effects of urban garden composition on a neighborhood's thermal comfort was analyzed. It has been demonstrated that urban gardens can reduce temperatures within a city as well as promote thermal comfort, primarily due to the presence of tree cover. The experienced cooling effect of trees varies between the sexes, with females seeing a greater reduction in thermal discomfort than males. However, while urban gardens (and tree cover) may promote thermal comfort, there are many obstacles to cooling the city in this manner. Many of the most popular Philadelphia urban garden crops are non-arboreal. Increasing the cooling impact of an urban garden may require changing garden composition to promote cooling, and trees take years to mature. In addition, residents also face structural inequality and the risk

of gentrification when attempting to maintain urban gardens or increase tree cover in their neighborhoods.

## **Chapter 1**

### **BACKGROUND**

#### **1.1 Urban Heat Islands and Park Cool Islands**

Urbanization leads to increased temperatures in a region when compared to their less-developed surroundings due to changes in land surface properties, a phenomenon known as Urban Heat Islands (UHI; Coseo and Larsen 2014). UHI is caused by the concentration of impervious heat-absorbing materials used in buildings, sidewalks, and streets which absorb more daytime heat (and release it more slowly at night) than natural materials such as soil or vegetation (Harlan et al. 2006). Urban heat islands have been found to reach temperatures that are 6.5 °C warmer in urban areas that replace temperate grasslands and savannas, and 6.5-9 °C warmer when replacing temperate forests (Imhoff et al. 2010). This increased temperature can have multiple effects: increased cooling costs, altered human activity and community interactions, and increased heat stress (Jenerette et al. 2007). In addition, more deaths are attributed to excess heat in cities found within temperate climates when compared to warm climates, due to a lack of acclimatization (Decllet-Barreto et al. 2013). Yet the impact of UHI can be mitigated in part by Park Cool Islands (PCI), which is a pattern of cooler areas created by the presence of vegetation within the Urban Heat Island. Urban vegetation cools its surroundings through a combination of shading and transpirational cooling, and has been found to decrease surface temperatures up to 8.4 °C in Phoenix, AZ (Decllet-Barreto et al. 2013).

However, the Park Cool Island effect is highly variable, due to differences in the extent and composition of urban vegetation. In Florida, forested parks had greater cooling than neighborhoods with extensive vegetation, which in turn had greater cooling than less-vegetated neighborhoods (Jamei et al. 2016). This is consistent with prior research showing that the percentage of impervious surface cover explains approximately 70% of the land surface temperature increase (Imhoff et al. 2010). The size of a park also determines the intensity and extent of its PCI. Cooling is highly localized and decreases away from the park; prior research has shown cooling to extend outside park boundaries by approximately the width of a park and may extend up to 1 to 2 km away in larger parks (Jamei et al. 2016).

The effects of Urban Heat Islands are not evenly distributed among urban populations. Within a city, high mortality is disproportionately impacting marginalized groups, such as the poor, minorities, and the elderly (Harlan et al. 2006). In addition, low-income and minority populations have less access to greenspace and its associated benefits as well (Deplet-Barreto et al. 2013). In fact, Jenerette et al. (2007) found that for every \$10,000 increase in a neighborhood's annual median income, the summer surface temperatures decreased by 0.28 °C. While the Park Cool Island effect has the potential for mitigating Urban Heat Islands, the variability due to both the physical and social influences are important to consider when studying its impact, to understand the experience of heat and how it may differ across an urban population.

## **1.2 Urban Gardens**

One potential method for the mitigation of urban heat islands is through urban gardens, defined as “public spaces managed by member-volunteers who grow food

crops and/or flowers, shrubs, and trees in individual plots and communal growing spaces” (Gregory et al. 2016). Urban gardening has other unique benefits as a type of greenspace. In particular, urban gardens provide healthy and locally produced food to low-income communities (many of which are in “food deserts” with limited access to fresh fruits and vegetables), improve bodily and psychological health, build community resources, and convert vacant land to communal spaces (Poulsen et al. 2014). In addition to these social benefits, there are multiple physical benefits that gardens are purported to have. Many gardeners consider urban gardens as a way to “green up” the city through remediating spaces (Reynolds and Cohen 2014) and there has been recent promotion of urban gardens to mitigate local temperature increases within cities to reduce the effects of energy poverty within cities (Tsilini et al. 2014). In particular, Tsilini et al. (2014) found the addition of an urban garden decreased temperatures during the spring, summer and autumn seasons, and advocated for the use of urban gardens due to their cooling properties and social benefits.

Yet like other forms of greenspace, urban gardens are also subject to social forces that can create disparity. In New York City, Reynolds (2014) found social structures that promote racial and class disparity create differences within the gardens as well, primarily due to the lack of connections to funding and city services among farmers that were non-white or lower income. In general, white gardeners report raising more funding than gardens led by people of color. While one white-led garden was able to raise funds over \$1 million, most non-white gardens were “bare-bones” and struggled to raise money for items such as a \$500 generator. This difference is noticed by both white and non-white gardeners, who both describe the urban gardening as having two distinct, racially-divided parts. These funding differences can

manifest in the size and composition of the gardens; gardeners report that the cost of proper growing media (which includes soil, compost and nutrients) and labor limit the size of their gardens. In particular, a lack of funding makes it difficult to hire labor. Most gardens struggled to pay workers to grow food and relying solely on volunteer labor to manage the gardens was difficult (Cohen and Reynolds 2014).

This disparity between gardens run by white and non-white groups is present in Philadelphia gardens as well. Meenar and Hoover (2012) found that gardeners in Philadelphia reported issues in acquiring and maintaining vacant land, and neighborhoods with less social or political capital have greater difficulty accessing land for gardening. In addition, the gardeners have reported lower-income residents had less time to grow food as well. While Meenar and Hoover's focus precluded discrepancies in funding, the lack of social and political capital that created difficulties in acquiring land likely are also likely to lead existing neighborhood gardens to experience disparity in funding and composition as well. As Reynolds' (2014) reported for New York City, a lack of funding made hiring labor difficult. When Philadelphia residents have little time to grow food due to other jobs, the demand for gardens may be limited.

### **1.3 Thermal Comfort**

While air temperature is an important factor in the thermal sensation of the human body, the heat-balance of the body also relies on other processes affected by the moisture and movement of the air, as well as the radiation balance of the body (Höppe 1999). Therefore, to study the impact of heat on city residents, the use of human-biometeorology can determine the felt impacts of the local climate (Matzarakis

et al. 2007). This can be done through the local observations of both microclimate and human vitals, or through a variety of models. There are several models available.

For this experiment, two commonly-used programs are employed: Envi-met (Envi-met 2016), and RayMan (as described in Matzarakis et al. 2006). Envi-met is a three-dimensional microclimate simulator designed for use in urban and rural environments. Envi-met contains simulation parameters that model plant and surface fluxes, and calculates the thermal comfort index Predicted Mean Vote (PMV) as a result. Due to these capabilities, Envi-met is often used to determine urban biometeorological conditions for varying urban configurations of buildings, street design, vegetation and permeable soils (Salata et al. 2017). Envi-met has been used in research to analyze influences on urban microclimates (Declet-Barreto et al. 2013, Middel et al. 2015, Middel et al. 2015) and to study human thermal comfort in an outdoor urban environment (Salata et al. 2016).

In contrast, RayMan is a radiation model which can be used to calculate the Predicted Mean Vote and Physiological Equivalent Temperature (PET). RayMan uses meteorological variables such as air temperature, humidity, and wind velocity (which may be produced by numerical models such as Envi-met), as well as biological variables such as human body heat production, and heat transfer resistance of clothing in order to calculate the thermal comfort indices (Matzarakis et al. 2006). In addition, RayMan is the most popular method of modelling mean radiant temperature, which is an important variable in the calculation of human thermal comfort (Johansson et al. 2014), and is used to produce the human thermal comfort indices PMV and PET (Matzarakis et al. 2010). While RayMan is only able to model the thermal comfort of a stationary subject (and is thus unable to simulate spatial patterns of comfort), RayMan

is still being used due to its accurate simulation of thermal comfort in urban environments (Matzarakis et al. 2006).

Thermal comfort indices, such as Predicted Mean Vote (PMV) and Physiological Equivalent Temperature (PET), are quantitative ways of determining the felt impact of climate change on humans. The PMV and PET are based on the physiological energy balance of a subject in the experimental study area, but have different forms of determining comfort. Predicted Mean Vote is designed to predict the mean description of an environment by a group of individuals. The PMV scale is based on a seven point Ashrae comfort scale (from -3 for cold to +3 for hot), where the absolute value of the results reflect the predicted thermal stress of the environment (from “no stress” at zero to “”very strong stress” at 3) (Mayer 1993). However, the PMV was designed for indoor conditions and can diverge from an actual survey of thermal comfort in outdoor conditions.

In comparison, the Physiological Equivalent Temperature has been shown to demonstrate better results in outdoor conditions (Rupp et al. 2015). In contrast to the PMV, the PET index calculates the temperature of an indoor environment which would induce the same thermal comfort. Unlike the seven-point PMV scale, the PET scale remains in °C (Mayer 1993), and is based on the Munich energy balance for individuals (MEMI) model (Matzarakis et al. 2006). The MEMI model is heat balance model for the human body, taking into account the metabolic rate, physical heat production, net radiation of the body, convective heat flow, latent heat flow, respiratory heat flow, heat flow due to sweat evaporation, and heat storage (Gosling et al. 2014). PET temperatures around 23 °C are considered neutral (while temperatures at 18 °C and 29 °C would be slightly cool and slightly warm, respectively). The PET

can be adjusted to account for acclimation to warmer temperatures as well, for example, the neutral PET for a warm period is increased to 27 °C (Wang et al. 2017).

In addition to studying the differences in the distribution of potential garden cooling, it is important to examine how human bodies within the neighborhood experience the heat and what disparities may arise. Therefore, in the analysis of the microclimate surrounding and within an urban garden, it is important to study both male and female bodies. Women experience heat differently than men; women are more sensitive to cool temperature, less sensitive to humidity, and more often uncomfortable with an environment than men (Rupp et al. 2015). These differences can lead to disparity in felt impacts of heat in urban population due to the sex of the residents.

#### **1.4 Modelling “Difference”**

With half of the world population currently living in cities (Salata et al. 2016) and expected to increase to 70% of the world population by 2030 (Rupp et al. 2015), it is increasingly important to consider the effect of urban heat island on the population. One proposed method of mitigating the effects of increased urban heat is through the Park Cool Island effect via urban garden vegetation (Tsilini et al. 2014). Initially this idea appears to be a preferable solution to UHI because urban gardens have many additional social benefits compared to other forms of urban vegetation, such as providing fresh food to city residents (Meenar and Hoover 2012, Poulsen et al. 2014) creating community connections, promoting psychological wellbeing, and cleaning up vacant lots (Poulsen et al. 2014). However, many forms of greenspace receive uneven support within a city due to neighborhood characteristics stemming from class and race (Harlan et al. 2006, Jenerette et al. 2007, Declat-Barreto et al. 2013), and urban

gardens suffer from similar disparities as well (Meenar and Hoover 2012, Reynolds 2014, and Reynolds and Cohen 2014). As the Park Cool Island effect is dependent on the size and composition of greenspace (Imhoff et al. 2010, Jamei et al. 2016) and the impact of increased heat is dependent on the residents' bodies (Rupp et al. 2015), while an urban garden's cooling capabilities may be a physical effect but the extent and impact of this cooling may be socially determined. The aim of this project is to examine the physical characteristics of an urban heat island in Philadelphia, PA and its impacts on thermal comfort, with a focus on the social variability and difference in their formation.

## **Chapter 2**

### **METHODS**

#### **2.1 Observations**

Two sets of observations were employed in this study. One set is from a series of *in situ* meteorological sensors installed in and near an urban garden specifically for this study. These sensors were used to determine the air temperature and humidity within and nearby an existing urban garden in the city of Philadelphia. The second set consists of externally-operated sensors that are a part of the Mesowest network. This set of sensors were used to compare the conditions of the earlier set of sensors to urban, peri-urban, and rural areas within and surrounding the city of Philadelphia.

##### **2.1.1 In situ HOBO sensor data**

To determine the cooling capability of an urban garden, temperature and relative humidity data were recorded in situ using Onset HOBO sensors. These HOBO sensors were HOBO U23-001 Pro v2 Temperature/Relative Humidity Data Loggers. These sensors have a temperature range of -40 to 70 °C, an accuracy of  $\pm 0.21$  °C from 0 to 50 °C, and a resolution of 0.02 °C. The relative humidity range of the sensors is 0 to 100%, an accuracy of  $\pm 2.5\%$  from 10%-90% relative humidity (and an accuracy of  $\pm 5\%$  below 10% or above 90% relative humidity), and a resolution of 0.05%. HOBO sensors can store 42,000 measurements and are powered by a

replaceable ½ AA lithium battery. The sensor housing measured 10.2 cm x 3.8 cm (Onset 2016).

Temperature and humidity data were collected at one primary garden site, the 2124 Fitzwater Garden, in the center of Philadelphia, PA. The HOBO sensors recorded temperature and humidity data in five-minute intervals from October 2nd, 2016 to December 4th, 2016. One sensor was situated in the garden, and 4 sensors were located on trees alongside an adjacent street (hereafter referred to as the “Garden Sensor” and Sensors 1 through 4 (based on their proximity to the garden, Figure 2.1). Sensors 1-4 were each attached to the tree on a lower branch (at the most consistent height possible for each tree) and at the midpoint of the branch from base to tip, to provide shielding from direct sunlight through the tree’s canopy. The Garden Sensor was placed in housing that was attached to the trunk of the tree. Sensors 1 through 4 are located sequentially eastward from the garden on Fitzwater Street (the street adjacent to the garden), on the opposite side of the road from the garden. The Garden Sensor was housed in the center of the garden, on the single tree within the boundaries of the garden, at a height of 157 cm from the ground. Sensor 1 was located on a tree diagonally across the street from the garden, at a height of 211 cm. Sensor 2 was down the street from the garden, at a height of 236 cm. Sensor 3 was located further east on the next block, near the corner of Fitzwater Street and S 21st Street, at a height of 203 cm. Lastly, Sensor 4 was placed east of Sensor 3 (but within the same city block) at a height of 201 cm.

The Garden Sensor was placed with the support of the Neighborhood Gardens Trust, which is an organizing body for urban community gardens in Philadelphia (which the 2124 Fitzwater Garden is a part of) as well as the specific gardeners in

charge of the 2124 Fitzwater Garden. Street trees within the city of Philadelphia are the property of the landowners (in this case, the residents of Fitzwater Street), and verbal consent was obtained before placing the Sensors 1-4 on their trees.

### **2.1.2 Mesowest**

In addition, Mesowest data from two sensors located in Philadelphia, and one located on nearby rural land, was used for comparison. Mesowest provides current and archived weather observation-s across the United States, relying upon weather stations managed by a mixture of governmental, educational and private organizations (Mesowest 2017a). Mesowest is an ongoing project between researchers at the University of Utah, the Salt Lake City National Weather Service Office, the NWS Western Region Headquarters, and other agencies, universities and commercial firms. The Mesowest weather-observing networks and database is used by numerous organizations, including by the National Weather Service to monitor weather conditions throughout the country (Mesowest 2017b)

One Mesowest sensor located in Philadelphia and used in this study, E8199, is located in the center of Philadelphia (Latitude: 39.94367, Longitude: -75.15100) at a height of 12 meters (Mesowest 2017c), 2.3 km from the urban garden site. Sensor E8199 records data at 15-minute intervals, and measures temperature, dew point temperature, wet bulb temperature, relative humidity, wind speed, wind gust, wind direction, air pressure, altimeter, solar radiation, precipitation (24 hour), and precipitation since local midnight (Mesowest 2017d). Sensor E8199 is part of the APRSWXNET/Citizen Weather Observer Program. In a manner similar to the 2124 Fitzwater Garden neighborhood, the buildings surrounding the sensor E8199 are typically multi-story buildings that are either attached or in close proximity to each

other. Mesowest shows the land use in the surrounding 1 km<sup>2</sup> of land as the USGS land use classifications “Developed, High Intensity,” and “Developed, Med Intensity” for both the E8199 sensor and the HOBO sensors (Mesowest 2017a). While the E8199 sensor is not in an identical configuration to the garden sensor, the urban environment surrounding both have a similar configuration and density of buildings. Also, as the E8199 sensor is part of the Mesowest network, it is a good, calibrated reference for the HOBO sensors.

Another Mesowest sensor, KPHL, is located at Philadelphia International Airport (Latitude: 39.87327 Longitude: -75.22678) at a height of 2 meters, and is part of the National Weather Service/Federal Aviation Administration (NWS/FAA) network (Mesowest 2017e). The KPHL sensor records data at a five-minute interval, and measures temperature, dew point temperature, wet bulb temperature, relative humidity, wind speed, wind gust, wind direction, pressure, sea level pressure, altimeter, weather conditions, visibility, ceiling, peak wind speed, peak wind direction, and 6-hour high temperature (Mesowest 2017f). The KPHL sensor is located in a noticeably different (peri-urban) environment than sensor E8199; being directly located in USGS land use type “Developed, Open Space” while also located next to “Developed, Med Intensity,” “Cultivated Crops,” “Developed, High Intensity,” “Pasture/Hay,” and “Barren Land” (within the 1 km<sup>2</sup> of land surrounding each site) (Mesowest 2017c). This peri-urban environment is quite different from the interior urban environment shared by E8199 and the garden sensor.

The rural station, E4674, is located outside of the city of Philadelphia at a height of 23 meters above sea level, and is part of the APRSWXNET/Citizen Weather Observer Program (Mesowest 2017g). The E4674 sensor records at 10-minute-long

intervals, and measures temperature, dew point temperature, wet bulb temperature, relative humidity, wind speed, wind gust, wind direction, air pressure, altimeter, solar radiation, precipitation (24 hour), and precipitation since local midnight (Mesowest 2017h). In the 1 km<sup>2</sup> surrounding E4674, the USGS land use is primarily of the types “Deciduous Forest,” “Developed, Low Intensity,” and “Developed, Open Space,” with some smaller quantities (<5% coverage) of “Developed, Med Intensity,” “Woody Wetlands,” “Pasture/Hay,” “Evergreen Forest,” “Cultivated Crops,” and “Developed, High Intensity” (Mesowest 2017h) Therefore, E4674 is used as a rural reference for the UHI impact, while KPHL and E8199 are used to determine the extent and variability of the UHI.

## **2.2 Observational Data Analysis**

### **2.2.1 Calculating Urban Heat Island Intensity**

To determine the UHI intensity and the potential mitigation of the garden, paired t-tests of the data were conducted through JMP. JMP is a statistical package from SAS (2017a and 2017b).

To determine the UHI intensity and the potential mitigation of the garden, the temperature and relative humidity of each sensor was compared using the Local Climate Zone (LCZ) classification proposed by Stewart and Oke (2012). The Local Climate Zones are defined as “as regions of uniform surface cover, structure, material, and human activity that span hundreds of meters to several kilometers in horizontal scale” (Stewart and Oke 2012). Using this classification scheme, the differences that are analyzed are not necessarily “urban-centered” but provide a means of analysis across land cover-land use types (Stewart et al. 2014). For the purposes of this

analysis, the HOBO sensors and Mesowest sensor E8199 are classified as “compact mid-rise” LCZ class (LCZ<sub>2</sub>), defined as a “dense mix of midrise buildings (3–9 stories), few or no trees, land cover mostly paved, [and] stone, brick, tile, and concrete construction materials” (Stewart and Oke 2012). The KPHL sensor is classified as the “open mid-rise” LCZ class (LCZ<sub>5</sub>), defined as an “open arrangement of midrise buildings (3–9 stories), abundance of pervious land cover (low plants, scattered trees), [and] concrete, steel, stone, and glass construction materials” (Stewart and Oke 2012). Lastly, the Mesowest sensor used as a rural proxy, E4674, is defined as the “sparsely-built” LCZ class (LCZ<sub>9</sub>), defined as a “sparse arrangement of small or medium-sized buildings in a natural setting, [and an] abundance of pervious land cover (low plants, scattered trees)” (Stewart and Oke 2012).

The potential UHI was found by analyzing the temperature and relative humidity differential between the HOBO sensors and Mesowest sensors E8199 and KPHL in reference to sensor E4674 (e.g.  $\Delta T_{LCZ_{E8199-E4674}}$  as the temperature difference between the “dense mid-rise” and “sparsely-built” classes). Due to the difference in the temporal resolution of the collected data from the HOBO and Mesowest sensors, the hourly averages of the temperature and relative humidity data are compared for this analysis. In addition, differences in the diurnal temperature range (defined as the difference between the daily maximum and minimum temperatures) are also being analyzed between LCZ classes. This is being done in a manner similar to Stewart et al. (2012), who used a similar analysis to analyze differences in temperature in Nagano, Japan, Vancouver, Canada, and Uppsala, Sweden.

In addition, the daily maximum temperature, minimum temperature, and relative humidity differentials of the HOBO sensors and Mesowest sensors E8199 and KPHL will also be analyzed in reference to sensor E4674, and paired t-tests will be conducted for all variables (hourly average temperature, hourly average relative humidity, diurnal temperature range, daily maximum temperature, and daily minimum temperature). The analysis of daily climate extremes, and the use of paired t-tests, is similar to prior research by Ellis et al. (2015), in which daily maximum and minimum values of urban temperature and humidity data collected from HOBO sensors was analyzed to determine spatial patterns of variability in the UHI of Knoxville, TN.

In this study, to determine the potential mitigation of the urban heat island by the garden, the temperature from the Garden Sensor was compared to temperatures recorded nearby from Sensors 1-4 as well as the temperatures of the independent LCZ<sub>2</sub> sensor E8199. The data from Sensors 1-4 were also compared to the E8199 sensor to determine the extent of any potential cooling outside of the garden boundaries as well as the presence of any other internal temperature variation within the city. Differences in temperature, relative humidity, diurnal temperature range, daily maximum temperature, and daily minimum temperature, as well as paired t-tests for these variables, were conducted on the Garden Sensor data in reference to each LCZ<sub>2</sub> sensor.

### **2.2.2 Paired T-test**

To test for a significant difference in the mean for climatic variables between two sensors, paired t-tests were conducted using the “Matched Pairs” platform in JMP. The Matched Pairs platform compares difference in the values of each row between two columns using a paired t-test. The platform’s results provide the difference

between the means of both tested variables, and uses the paired t-test to determine the p-value of the means' difference (significance:  $p < 0.05$ , SAS 2017a).

To calculate the paired t-test, first the sample mean difference ( $\bar{d}$ ) must be calculated as the mean of the difference for each set of paired values (e.g. the temperature values for the Garden Sensor and Sensor 1 for the first hour) for the study period. The standard error of the mean difference is also calculated as  $SE_{\bar{d}} = s_d / \sqrt{n}$ , where  $SE_{\bar{d}}$  is the standard error of the mean difference,  $s_d$  is the sample standard deviation of the differences, and  $n$  is the sample size. Then the t-statistic is calculated as  $t = \frac{\bar{d} - \mu_{d0}}{SE_{\bar{d}}}$ , where  $\mu_{d0}$  is the mean of the differences ( $d$ ) under the null hypothesis (which equals zero in this case). The t-test has  $n-1$  degrees of freedom (Whitlock and Shluter 2015). Using the t-statistic, JMP finds the probability that the difference of the means equaling zero is not within the 95% confidence limit of the mean difference (SAS 2017a).

### 2.2.3 Microclimatic Model Forcings

The observed HOBO sensor data and the archived Mesowest meteorological data were also used in the creation of parameters for microclimatic simulator Envi-met (2016). In order to model the climate in the garden and surrounding streets, temperature and relative humidity data from Sensor 3 were used for boundary conditions, due to the sensor's location at the edge of the model area. Boundary condition forcings of temperature and relative humidity are determined on an hourly basis in Envi-met (2016), so hourly averages were created for each day of the study period. Then, to reduce the influence of random variation (such as rain or clouds during any particular day) in the study period, weekly averages were created for the hourly temperature and relative humidity data. Envi-met does not simulate rainfall,

and can only produce cloud cover through simplified (i.e. constant) parameters that do not reflect the short-lived nature of cloud cover on the model area's scale, as noted previously by Salata et al. (2016). To reduce –but not necessarily eliminate- the influence of these short-lived fluctuations of temperature and humidity, the average diurnal cycles for each week of the study period were created instead.

In contrast to temperature and relative humidity, wind speed and direction are represented as one value in the configuration of Envi-met (2016). Therefore, average wind speed and direction were determined for each week from the Mesowest sensor E8199's wind speed and direction data. These averages were incorporated in representative parameters for each week of the study period, and each model area configuration was used with these same weekly parameters.

## **2.3 Modelling**

In addition to the comparison of observed data to archived Mesowest meteorological data, the observed data were used to simulate the effects of the garden site and its surroundings on thermal comfort. Two models were employed in this study.

### **2.3.1 Envi-met**

The 2124 Fitzwater garden site was recreated in Envi-met (Envi-met 2016), at a resolution of 2 meters x 2 meters. Envi-met is a three-dimensional microclimate simulator first designed in 1998 to simulate microscale interactions between urban surfaces, vegetation, and the atmosphere (Bruse and Fler 1998). Envi-met is commonly used to determine urban biometeorological conditions. Simulation parameters include complete parameterizations of plant and surface energy and

moisture fluxes, which allows for comparative urban vegetation studies. In addition, Envi-met calculates thermal comfort index Predicted Mean Vote (PMV) as a result (Salata et al. 2016).

A study area map was created using the City of Philadelphia Aerial Photography 2015 dataset (PASDA 2015) to determine building and land cover extents in the garden's surroundings. Building heights were determined using PASDA's Philadelphia Buildings GIS shapefile dataset (PASDA 2016). Receptors were placed in the model area in the locations of the Garden Sensor and Sensors 1-3 (Sensor 4 was located outside of the model area boundaries). Receptors create output files containing the vertical distribution of calculated variables (including, but not limited to, the temperature, relative humidity, wind speed, and mean radiant temperature data used to calculate the thermal comfort indices below) at the receptor location at a higher temporal resolution than the standard output, and provide a temporal focus in contrast to the standard spatial output of Envi-met (2016).

Multiple model areas were constructed, based on variations of garden vegetation and size. ActualGarden was designed to recreate the size and vegetation extent of the existing garden (vegetation model: Figure 2.2, soil/surface model: Figure 2.3). In this instance, the garden is the size of a single building lot, and contains grass and a birch tree (to create ground cover vegetation and a tree with the same relative height to the surrounding buildings). ActualGarden is the only model to contain the standard garden size, as the next models contain garden areas that are the size of three house lots (replacing an adjacent house and its driveway). This increased size was used to exaggerate the effects of different garden compositions and the potential resulting Park Cool Island, which has been previously found to be size-dependent

(Jamei et al. 2016). Because the next seven models represent garden compositions that are not real, they will be referred to as the “hypothetical models,” and due to their increased size, all of the hypothetical models have the prefix “3x.” 3xGarden, in addition to the enlarged garden size, contains grass cover and two birch trees which cover the garden, in order to test the impact of garden size on its mitigation potential (vegetation model: Figure 2.4, soil/surface model: Figure 2.5). 3xSoyGarden contains a garden that is covered entirely with soy (one of the two agricultural plant models in Envi-met (2016)) (vegetation model: Figure 2.6, soil/surface model: Figure 2.5) while 3xLoam replaces the garden with bare loamy soil (vegetation model: Figure 2.7, soil/surface model: Figure 2.5), to determine the influence of plant cover on the garden’s microclimatic impact.

Lastly, the influence of impervious surface cover, albedo and direct sunlight were tested with different combinations of tree and impervious surface coverages in place of the 3xGarden configuration. 3xAsphalt replaces the enlarged garden with asphalt (vegetation model: Figure 2.7, soil/surface model: Figure 2.8), and 3xTreeCoveredAsphalt has asphalt ground cover with additional dense tree cover at a height of 15 m (vegetation model: Figure 2.9, soil/surface model: Figure 2.8). The tree cover allows for comparisons of the impact of shade on human thermal comfort in the modelled conditions. 3xConcrete replaces the asphalt in 3xAsphalt with concrete cover (vegetation model: Figure 2.7, soil/surface model: Figure 2.10). Asphalt and concrete are both treated by Envi-met as impervious surfaces but have different albedo values, and the differences between 3xAsphalt and 3xConcrete will demonstrate any differences arising solely from albedo. Lastly, 3xTreeCoveredLoam replaces the asphalt in 3xTreeCoveredAsphalt with loamy soil (vegetation model: Figure 2.9,

soil/surface model: Figure 2.5). Loam and Asphalt both have lower albedos, but loam is pervious while asphalt is impervious. Through the comparison of 3xTreeCoveredAsphalt and 3xTreeCoveredLoam, the differences between these models will demonstrate the difference in permeable and impermeable surface cover on thermal comfort.

### **2.3.2 RayMan**

In contrast, RayMan is a radiation model that was designed to model the radiation balance of a human body in an urban environment. RayMan can be used to calculate the Predicted Mean Vote, Physiological Equivalent Temperature (PET) and Standard Effective Temperature (SET). RayMan uses variables such as air temperature, vapor pressure, wind velocity, human body heat production, and heat transfer resistance of clothing in order to calculate the thermal comfort indices (Matzarakis et al. 2007).

After the simulations were run for Envi-met, receptor data (for temperature, relative humidity, wind speed, and mean radiant temperature data at locations corresponding to the HOBO sensor locations) were exported for use in RayMan (Matzarakis et al. 2007). Each receptor has a 30-minute output recorded for each variable in the location of the sensor. The meteorological variables of temperature, relative humidity, wind speed, and mean radiant temperature values at a height of 1.4 meters were used for calculating thermal comfort, due to the cell height being the closest height within the model to ISO 7726 standard measuring height of 1.1 m for a standing subject, which is one of the main standards within the field of biometeorology (Johansson et al. 2014). The meteorological variables (and default clothing and activity levels) were used to calculate the Predicted Mean Vote (PMV),

Physiological Equivalent Temperature (PET), and Standard Effective Temperature (SET) in RayMan, in the garden and its surroundings for each model area trial.

### 2.3.2.1 Physiological Equivalent Temperature

RayMan calculates the PET based on the work of Höppe (1999) (Matzarakis 2010). The PET is calculated using the Munich Energy-balance Model for Individuals (MEMI), which is composed of three equations. The first equation, the energy-balance of the human body, is as follows:  $M + W + R + C + E_D + E_{Re} + E_{Sw} + S = 0$ . In the energy balance equation,  $M$  represents the metabolic rate,  $W$  is the physical work output,  $R$  is the net radiation of the body,  $C$  is the convective heat flow,  $E_D$  is the latent heat flow of imperceptible perspiration (water vapor diffusing through the skin),  $E_{Re}$  is the sum of heat flows for heating and humidifying inhaled air,  $E_{Sw}$  is the heat flow due to the evaporation of sweat, and  $S$  is the storage heat flow (for the heating and cooling of the body's mass).

For the energy balance of the human body to be calculated with the above equation, some of the terms are dependent on the conditions of the mean clothing temperature, mean skin temperature, or sweat rate. These conditions are dependent on ambient conditions and the core temperature of the body. In order to calculate the unknown quantities of the variables, two additional equations are used. The second equation describes the heat flow from the body core to the skin surface ( $F_{CS}$ ), which is calculated as  $F_{CS} = v_b * \rho_b * c_b * (T_c - T_{sk})$ . In the second equation,  $v_b$  is the blood flow from the body core to the skin (in  $L/(second * m^2)$ ),  $\rho_b$  is blood density (in  $kg/L$ ),  $c_b$  is for the specific heat (in  $(W * second)/(K * kg)$ ), and  $T_c$  and  $T_{sk}$  are the clothing and skin temperatures (respectively). The third equation describes the heat flow from the skin surface to the clothing layer to the surface of the clothing ( $F_{SC}$ ).

The third equation is  $F_{SC} = (1/I_{cl}) * (T_{sk} - T_{cl})$ , with  $I_{cl}$  representing the heat resistance of the clothing (in  $(K * m^2)/W$ ).

The Physiological Equivalent Temperature is calculated by first calculating the thermal conditions of the body using a given combination of meteorological parameters with the MEMI model (for the purpose of the PET, the metabolism of the body is 80 W (for light activity) and heat resistance of clothing is equivalent to a clothing level of 0.9 clo). Next, the calculated values for the mean skin temperature and core temperature are inserted into the MEMI model for an indoor reference environment in which the mean radiant temperature equals air temperature, air velocity is set at 0.1 m/s, and water vapor pressure is 12 hPA. The resulting air temperature from this calculation is the PET (Höppe 1999).

### 2.3.2.2 Predicted Mean Vote

While Fanger (1972) determined that female bodies have a lower metabolic rate (although it is mitigated by a slightly lower insensible perspiration rate), the PET index uses a standard “body” in its calculation that has a set metabolism (80 W, equivalent to light activity) and clothing parameters (0.9) (Höppe 1999). Therefore, RayMan does not account for differences in the biological sex of the body when calculating PET, but does for PMV. Therefore, the PMV will be used to compare differences in thermal comfort between the biological sexes (and the clothing level will be unchanged).

The PMV was calculated in RayMan based on the work of Fanger (1972), who proposed the PMV index (Matzarakis et al. 2007). The PMV is calculated as follows:

$$PMV = (0.352e^{-0.042(M/A_{Du})} + 0.032) \left[ \frac{M}{A_{Du}}(1 - \eta) - 0.35 \left[ 43 - 0.061 \frac{M}{A_{Du}}(1 - \eta) - p_a \right] - 0.42 \left[ \frac{M}{A_{Du}}(1 - \eta) - 50 \right] - 0.0023 \frac{M}{A_{Du}}(44 - p_a) - 0.0014 \frac{M}{A_{Du}}(34 - \right.$$

$t_a) - (3.4 * 10^{-8})f_{cl}[(t_{cl} + 273)^4 - (t_{mrt} + 273)^4] - f_{cl}h_c(t_{cl} - t_a)]$ , where  $A_{Du}$  represents the surface area of the human body (the “DuBois” area),  $\eta$  represents external mechanical efficiency of the body,  $p_a$  is the partial pressure of water vapor in the ambient air,  $t_a$  is the air temperature,  $f_{cl}$  is the ratio of clothed surface area of the body to unclothed surface area,  $t_{cl}$  is the mean temperature of the outer surface of the clothed area of the human body,  $t_{mrt}$  is the mean radiant temperature, and  $h_c$  is the convective heat transfer coefficient. The temperature of the outer surface of the clothed area of the body,  $t_{cl}$ , is found iteratively, using the equation  $t_{cl} = 35.7 - 0.032 \frac{M}{A_{Du}} (1 - \eta) - 0.18I_{cl}[(3.4 * 10^{-8})f_{cl}[(t_{cl} + 273)^4 - (t_{mrt} + 273)^4] + f_{cl}h_c(t_{cl} - t_a)]$ , where  $I_{cl}$  is the thermal resistance from the skin to the outer surface of the clothed body. The convective heat transfer equation,  $h_c$ , is found with a piecewise equation; where the equations  $20.5(t_{cl} - t_a)^{0.25}$  and  $10.4\sqrt{v}$  (where  $v$  is the relative air velocity) are compared, and the greater resulting value from either of the two equations is used as the convective heat transfer (Fanger 1972).

### 2.3.3 Analysis of RayMan Results

Next, the effects of distance from the garden and garden composition on thermal comfort were determined respectively by comparing the trends and differences between the receptor locations (which correspond to the Garden Sensor and Sensors 1-3), and different model area configurations using the PET and PMV indexes. To test the difference between model configurations, paired t-tests, hierarchical cluster analysis, and diurnal cycle plots of the model runs were used for the PET results. For the comparison of the PMV results in reference to biological sex, paired t-tests and plotting of the model’s diurnal cycle were used as well. Plotting the diurnal cycle is commonly used as a means to demonstrate UHI by showing the

temporal distribution of a variable (such as temperature (Dimoudi et al. 2013, Middel et al. 2014) or temperature differential (Gaffin et al. 2008)) over the course of a day, in order to demonstrate differences between land cover types. For the diurnal cycle, the thresholds for human comfort perceptions (and accompanying biological heat stress) is based on the values provided by Wang et al. (2017), and are overlaid on the diurnal cycle graphs. In addition, hierarchical cluster analysis is used to create dendrogram diagrams, which show model clusters with similar climatological trends. Hierarchical cluster analysis was used by Kim and Baik (2004) and Petralli et al. (2011), who employed the cluster analysis to find climatologically similar stations and cities (respectively) to find trends in urban heat intensity.

### 2.3.3.1 Hierarchical Cluster Analysis

The hierarchical cluster analysis was completed through the use of JMP's "Hierarchical Cluster" platform. The hierarchical clustering method treats each observation as a cluster, then calculates the distances between all pairs of clusters and joins the two closest clusters together. This process repeats until all the points are combined into one cluster. The resulting dendrogram demonstrates the process in which the observations are clustered, and the horizontal distances between each vertical cluster linkage represent the relative distance between observations (SAS 2017b). As with Kim and Baik (2004) and Petralli et al. (2011), Ward's minimum variance method was used to calculate the cluster distances. For this method, the distance between two clusters is the ANOVA sum of squares between two clusters summed over all variables. For clusters  $K$  and  $L$ , the distance is calculated as  $D_{KL} = \|\bar{x}_K - \bar{x}_L\|^2 / (\frac{1}{N_k} + \frac{1}{N_L})$ , where  $\bar{x}_K$  and  $\bar{x}_L$  are the mean of clusters  $K$  and  $L$  respectively,  $\|\bar{x}_K - \bar{x}_L\|$  is the square root of the sum of the squares of the elements of

$\overline{x_K}$  and  $\overline{x_L}$ , also known as Euclidean length, and  $N_k$  and  $N_L$  are the number of observations in clusters K and L respectively (SAS 2017b).

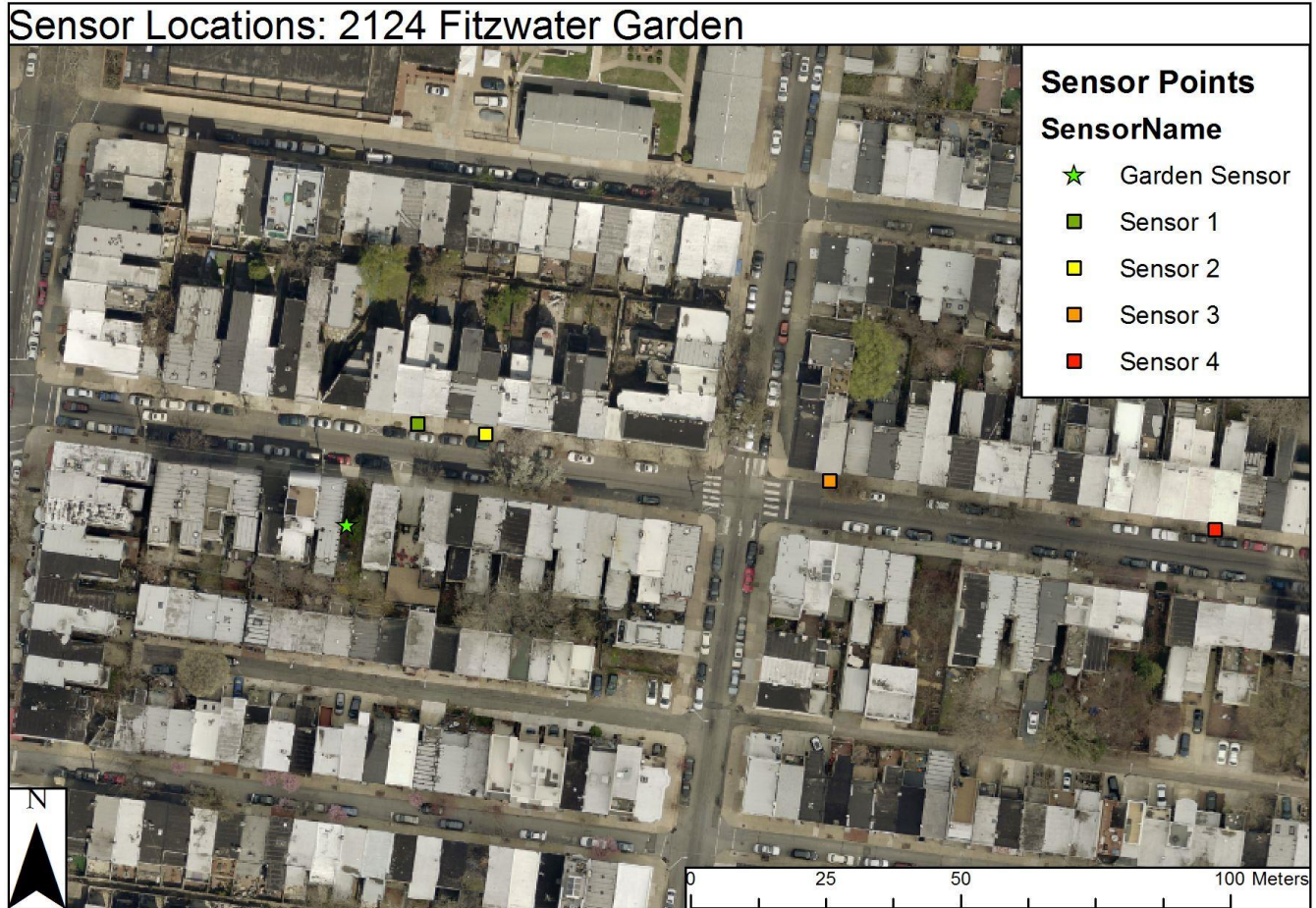


Figure 2.1: Sensor Locations on Fitzwater St. Philadelphia (Background Image, PASDA 2016)

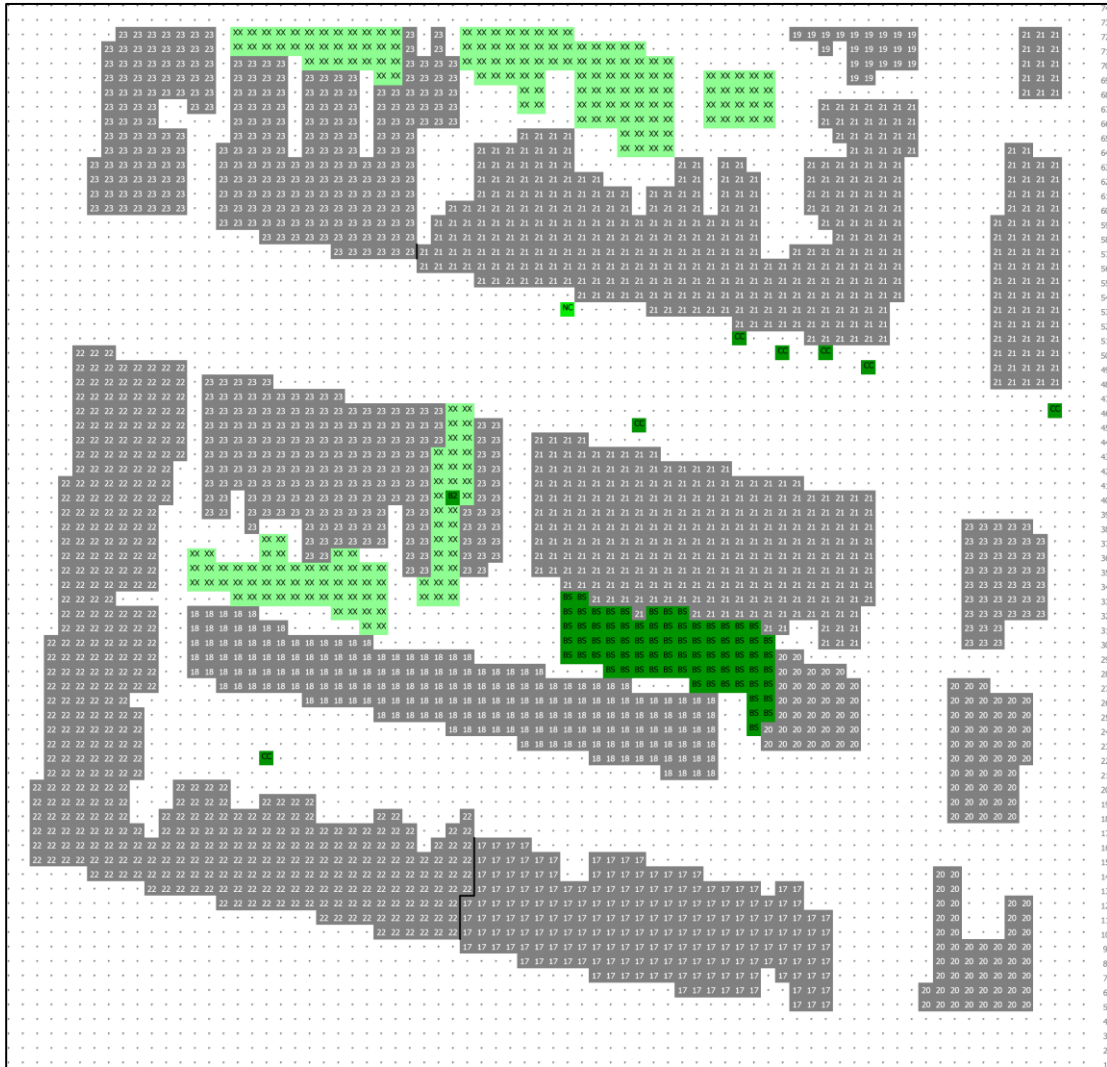


Figure 2.2: ActualGarden Vegetation Model



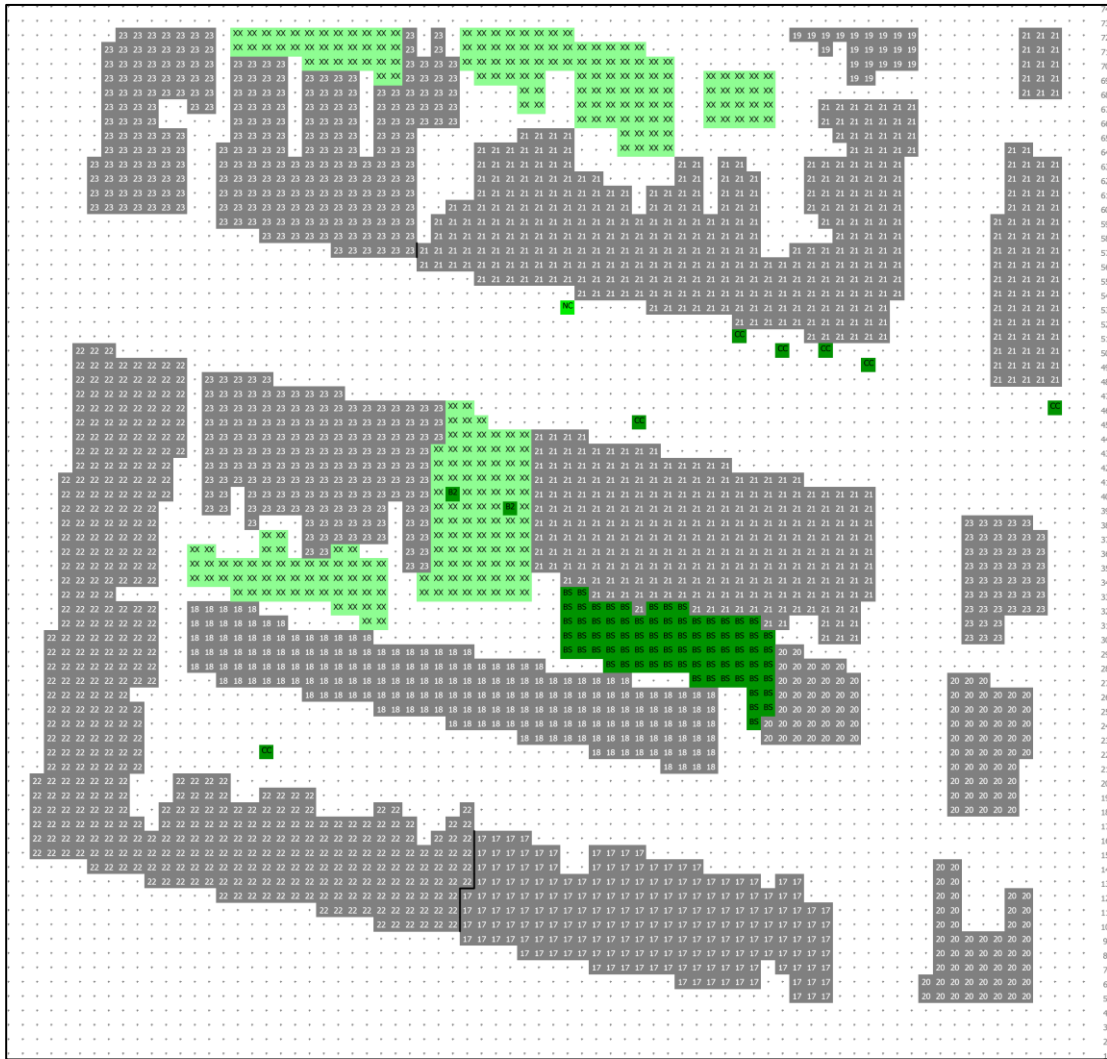


Figure 2.4 3xGarden Vegetation Model

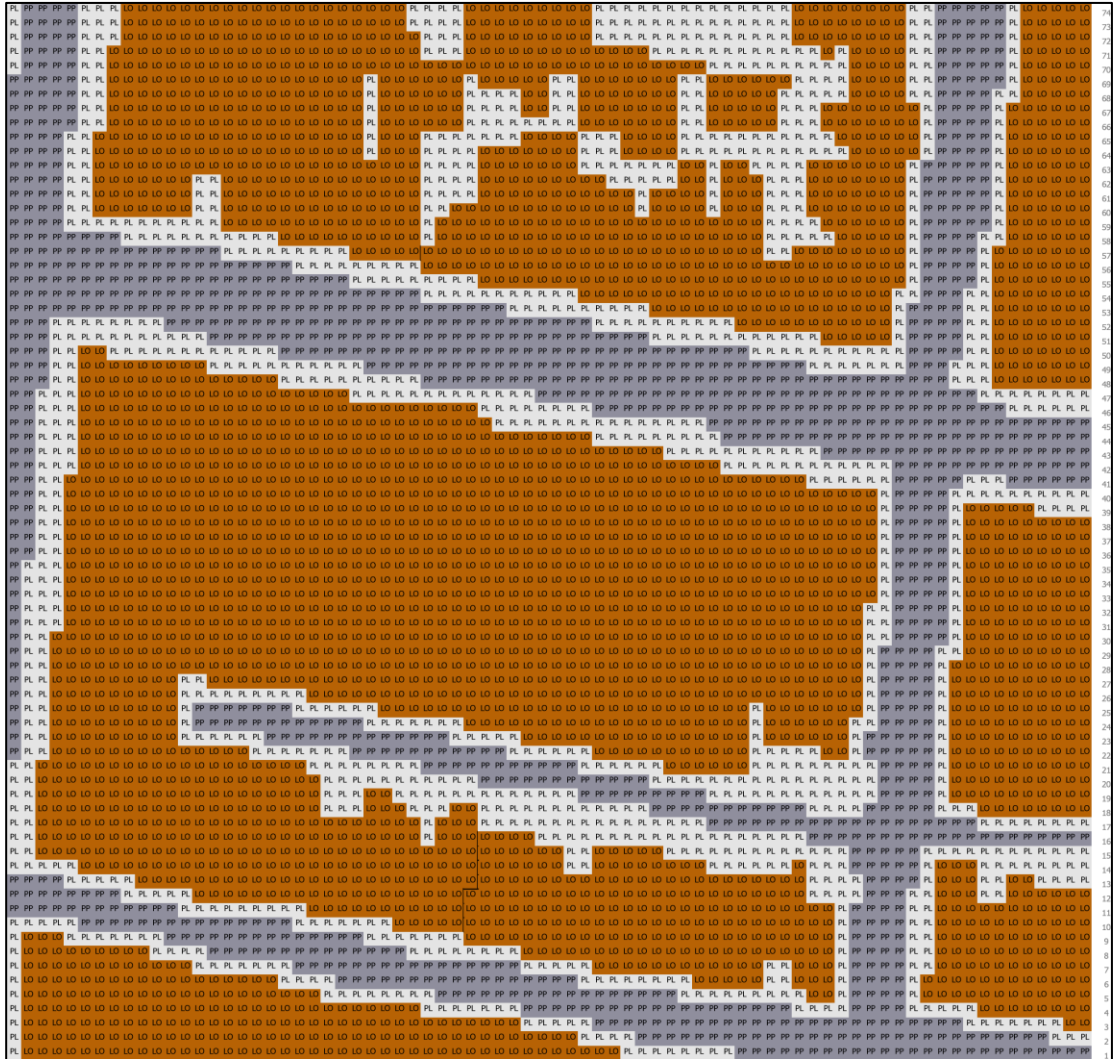


Figure 2.5 Enlarged Garden Soil/Surface Model (used for 3xGarden, 3xSoyGarden, 3xLoam, and 3xTreeCoveredLoam models)



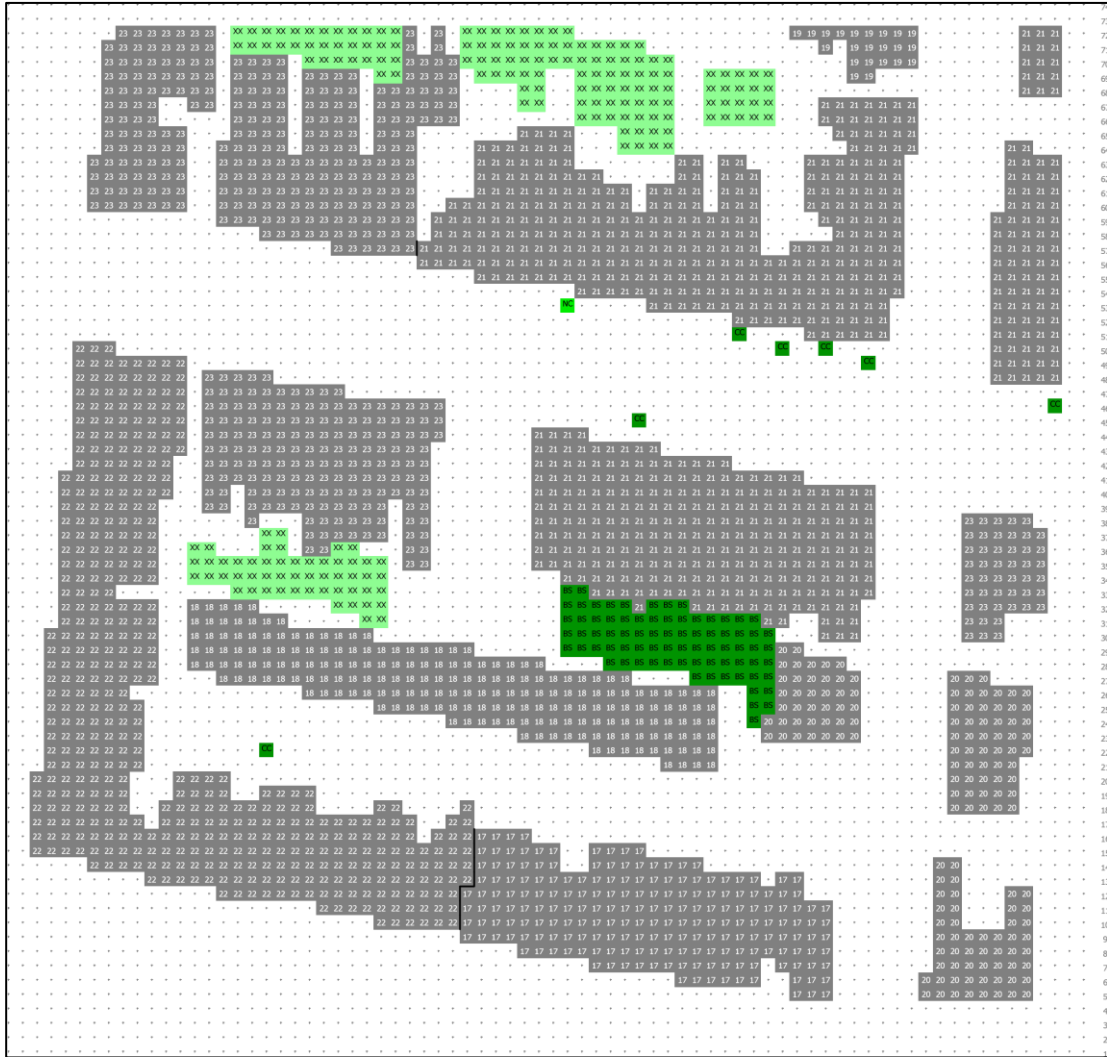


Figure 2.7 No-Vegetation Garden Vegetation Model (used in 3xLoam, 3xAsphalt, and 3xConcrete models)

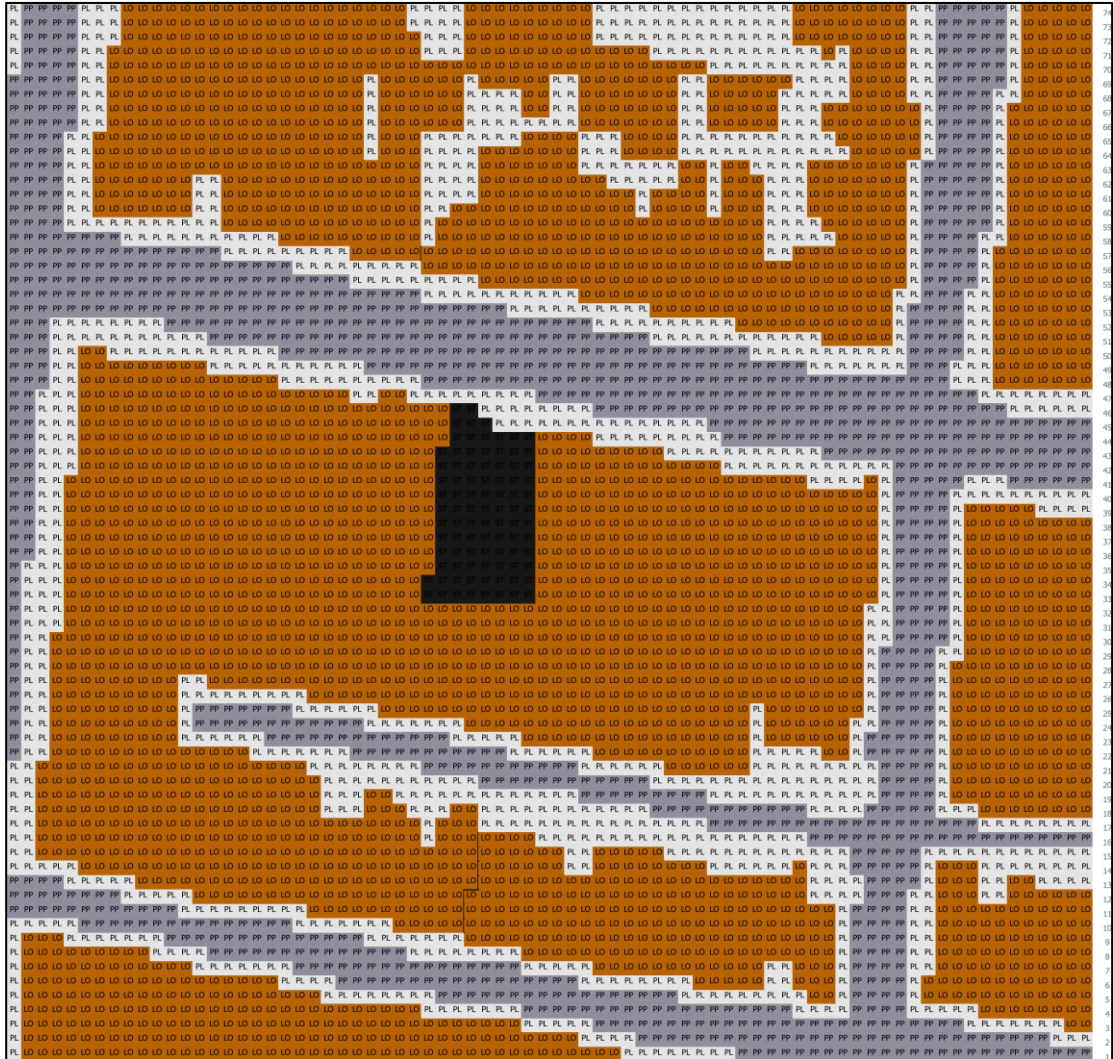


Figure 2.8 Asphalt-Covered Garden Soil (used in 3xAsphalt and 3xTreeCoveredAsphalt models)



Figure 2.9 Tree-Covered Garden Vegetation Model (Used in 3xTreeCoveredLoam and 3xTreeCoveredAsphalt models)

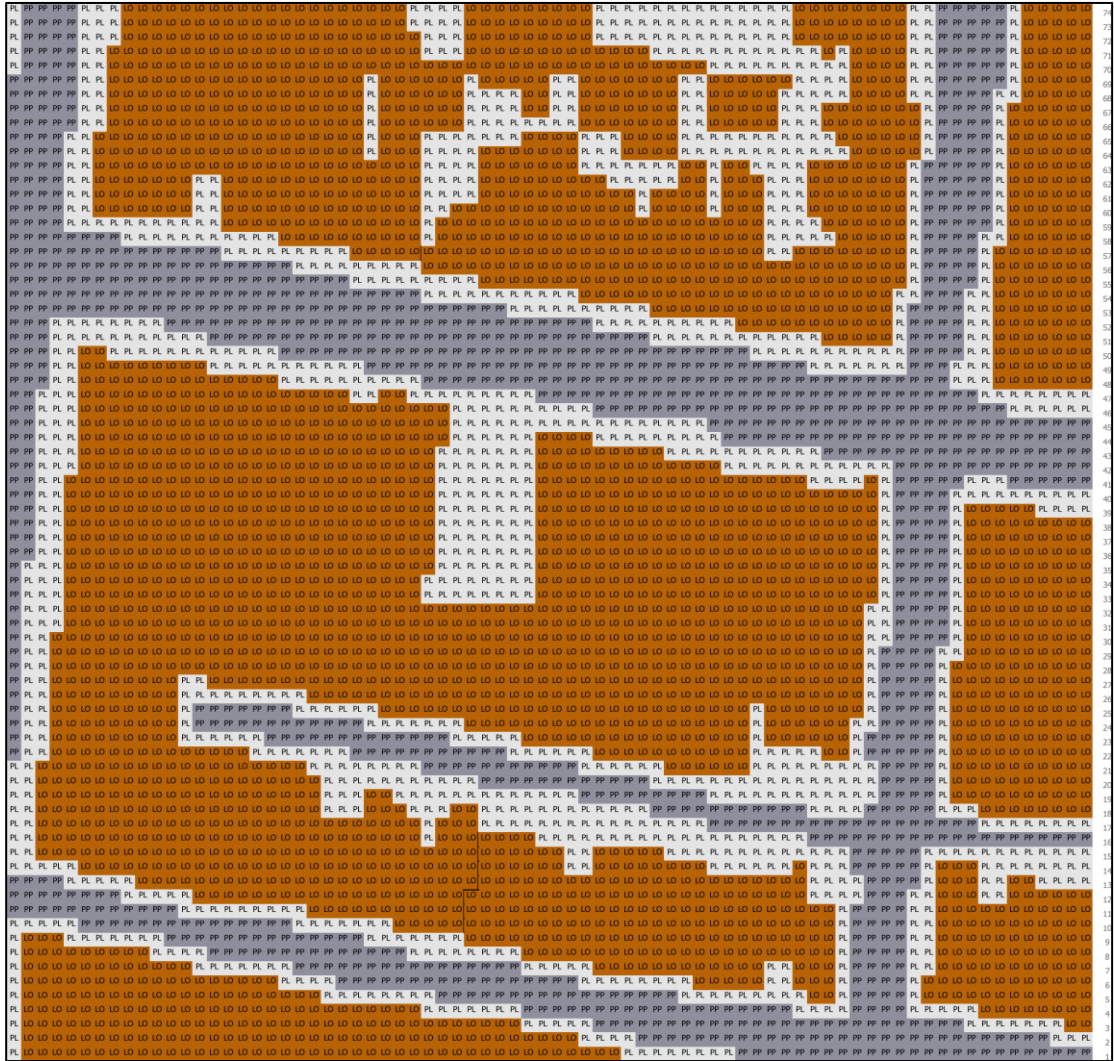


Figure 2.10 Concrete-Covered Soil/Surface Model

## **Chapter 3**

### **RESULTS**

#### **3.1 Observational Data Results**

For the observational data, the variables of daily maximum temperature, daily minimum temperature, daily temperature range, hourly average temperature, daily maximum relative humidity, daily minimum relative humidity, daily relative humidity range, and hourly average relative humidity for the entire study period were analyzed. Each variable was analyzed with paired t-tests, to determine difference in the variables' means from the five HOBO sensors and three Mesowest sensors, with respect to the sensors' LCZs. First, the variables of the Garden Sensor, Sensors 1-4, E81999 (all LCZ<sub>2</sub> sites), and KPHL (an LCZ<sub>5</sub> site) were compared to the sensor E4674 (an LCZ<sub>9</sub> site). For this test, a positive result would indicate a positive bias in the mean for the tested variable at the urban and peri-urban sites in comparison to the rural site E4674. Next, the variables of the Garden Sensor was compared to the other LCZ<sub>2</sub> sites, Sensors 1-4 and E8199. For this test, a positive result would indicate a positive bias at the Garden Sensor compared to the other urban sites.

##### **3.1.1 Paired t-test with E4674**

###### **3.1.1.1 Temperature Differences**

In relation to the “sparsely-built” (Local Climate Zone 9 (LCZ<sub>9</sub>)) rural sensor E4674, temperatures were generally warmer in the “compact mid-rise” (LCZ<sub>2</sub>) urban

sites (Table 3.1). With the exception of the Garden Sensor (which did not yield statistically significant results), maximum temperatures were found to be warmer than E4674, with the difference in the means between the urban sensors and the rural sensor E4674 ranged from 0.62 °C (for E8199) to 3.1 °C (for Sensor 1) warmer than E4674. Minimum temperatures were similarly found to be warmer, with a range in the difference of the means between the urban sites and E4674 being between 0.91 °C (for E8199) to 1.83 °C (for Sensor 3). This positive bias of the urban sites is also reflected in the hourly average temperatures as well, with a difference in the hourly average temperatures ranging from 0.54 °C (for E8199) to 1.25 °C (for Sensor 3). However, the daily temperature range yielded mixed results. The differences of the average daily temperature range for the Garden Sensor was smaller than E4674, Sensors 1, 3, and 4 were larger than E4674, and statistically insignificant for Sensor 2 and E8199.

Between the “open mid-rise” (LCZ<sub>5</sub>) peri-urban sensor KPHL and rural E4674, KPHL was generally warmer as well (though to a lesser degree than the HOBO sensors, Table 3.1). The maximum temperature and hourly average temperatures both had a positive bias in the mean, meaning the peri-urban KPHL sensor was warmer than the rural sensor, with the difference from the mean of E4674 being 0.75 °C and 0.25 °C respectively. The daily temperature range of KPHL also had a positive bias (i.e. larger temperature range) of 0.9 °C compared to E4674. However, the mean difference of the daily minimum temperature with respect to E4674 was not found to be statistically significant.

Table 3.1: [Urban (LCZ<sub>2</sub> or LCZ<sub>5</sub>) Sensor Temperature Variable Mean] - [Rural (LCZ<sub>9</sub>) Sensor E4674 Temperature Variable Mean] (\* represents statistically insignificant results (p>0.05))

	Garden Sensor	Sensor 1	Sensor 2	Sensor 3	Sensor 4	E8199	KPHL
Daily Maximum Temperature (°C)	0.45*	3.19	1.19	2.37	2.71	0.62	0.75
Daily Minimum Temperature (°C)	1.22	1.02	1.18	1.83	1.00	0.91	-0.14*
Daily Temperature Range (°C)	-0.77	2.23	0.03*	0.59	1.76	-0.27*	0.90
Hourly Average Temperature (°C)	0.66	1.06	0.80	1.25	0.93	0.54	0.25

### 3.1.1.2 Relative Humidity Differences

In relation to the rural (LCZ<sub>9</sub>) sensor E4674, daily minimum relative humidity and hourly average relative humidity was found to be lower in the urban (LCZ<sub>2</sub>) sites (Table 3.2). The difference in the means of the daily minimum relative humidity ranged from -1.73% (for the Garden Sensor) to -5.60% (for Sensor 1) when compared to E4674, although the comparison with sensor E8199 was not found to be statistically significant. The differences in the means of hourly average relative humidity had a range of -0.76% (for the Garden Sensor) to -2.70% (for Sensor 3) when compared to E4674. However, the differences of the average daily maximum relative humidity were not consistent, with the Garden Sensor, Sensors 1 and 2, and E8199 results not being significant, and with the Sensors 3 and 4 differences being -2.08% and 1.73% respectively. Despite this, the differences in the average daily relative humidity range was found to be significant for Sensors 1-4, with the differences ranging from 2.85%

(for Sensor 3) to 6.84% (for Sensor 1), meaning that there was greater variation in relative humidity in the city.

Between the “open mid-rise” (LCZ<sub>5</sub>) sensor KPHL and E4674, KPHL had a larger daily relative humidity range (with both statistically significant higher daily maximum relative humidity and lower daily relative humidity) and a lower hourly average relative humidity (equal to -1.86%, Table 3.2). The difference in the average daily minimum relative humidity was found to be 7.56%, with the difference in the average daily maximum relative humidity equaling 2.02%, and the difference in the daily minimum relative humidity equaling -5.54%.

Table 3.2: [Urban (LCZ<sub>2</sub> or LCZ<sub>5</sub>) Sensor Relative Humidity Variable Mean] - [Rural (LCZ<sub>9</sub>) Sensor E4674 Relative Humidity Variable Mean] (\* represents statistically insignificant results (p>0.05))

	Garden Sensor	Sensor 1	Sensor 2	Sensor 3	Sensor 4	E8199	KPHL
Daily Maximum Relative Humidity (%)	0.07*	1.24*	0.39*	-2.08	1.73	-0.5*	2.02
Daily Minimum Relative Humidity (%)	-1.73	-5.60	-3.65	-4.93	-5.58	-0.46*	-5.54
Daily Relative Humidity Range (%)	1.80*	6.84	4.03	2.85	7.31	-0.04*	7.56
Hourly Average Relative Humidity (%)	-0.76	-1.26	-1.45	-2.70	-1.10	-0.52	-1.86

### **3.1.2 Paired t-test with the Garden Sensor**

#### **3.1.2.1 Temperature Differences**

The Garden Sensor was found to have a negative bias in the daily temperature range with respect to the other urban (LCZ<sub>9</sub>) sensors, with the range of differences in the mean of the daily temperature range going from -0.48 °C (when compared to E8199) to -2.94 °C (when compared to Sensor 1, Table 3.3). The daily maximum temperatures had a negative bias for the Garden Sensor in relation to the five other sensors, which had a range of differences in the average daily maximum temperature from -2.74 °C (Sensor 1) to -0.17 °C (E8199). The daily minimum temperatures of the Garden Sensor were warmer than Sensors 1, 4, and E8199 (with mean differences of 0.20°C, 0.22 °C and 0.31 °C respectively), but cooler than Sensor 3 (with a mean difference of -0.60 °C), and with Sensor 2 not having a statistically significant differences in the average daily minimum temperature.

The Garden Sensor also had decreased hourly average temperatures in relation to the other HOBO sensors, with the differences in the mean ranging from -0.11 °C (Sensor 2) to -0.55 °C (Sensor 3). However, the Garden Sensor had warmer hourly average temperatures in relation to E8199, with an average difference of 0.13 °C.

Table 3.3: [Garden Sensor Temperature Variable Mean] - [Other Urban (LCZ<sub>2</sub>) Sensor Temperature Variable Mean] (\* represents statistically insignificant results (p>0.05))

	Sensor 1	Sensor 2	Sensor 3	Sensor 4	E8199
Daily Maximum Temperature (°C)	-2.74	-0.74	-1.92	-2.26	-0.17
Daily Minimum Temperature (°C)	0.20	0.04*	-0.60	0.22	0.31
Daily Temperature Range(°C)	-2.94	-0.79	-1.32	-2.48	-0.48
Hourly Average Temperature (°C)	-0.36	-0.11	-0.55	-0.23	0.13

### 3.1.2.2 Relative Humidity Differences

The Garden Sensor was generally found to have an decreased daily relative humidity range with respect to the other LCZ<sub>9</sub> sensors (except E8199), with the differences in the mean daily relative humidity range having a range of -1.26% (when compared to E8199) to -5.04% (when compared to Sensor 1, Table 3.4). Similarly, the daily minimum relative humidity of the Garden Sensor had a positive bias when compared to other the sensors (except E8199), with a range of -1.26% (when compared to E8199) to 3.87% (when compared to Sensor 1). The differences in the mean daily maximum relative humidity were more variable between sensors, with an increase of 2.15% when the Garden Sensor is compared to Sensor 3, and Sensors 1 and 2 being offset by -1.17% and -1.67% respectively. Comparison with Sensor 2 and E8199 did not yield statistically significant results. Overall, the Garden Sensor had higher hourly average humidity then the other HOBO sensors (with the exception of Sensor 4, which was statistically insignificant) with a range of 0.37% (Sensor 1) to

1.79% (Sensor 3). However, the hourly average relative humidity of the Garden Sensor had a negative bias in relation to E8199, with a mean difference of -0.25%,

Table 3.4 [Garden Sensor Relative Humidity Variable Mean] - [Other Urban (LCZ<sub>2</sub>) Sensor Relative Humidity Variable Mean] (\* represents statistically insignificant results (p>0.05))

	Sensor 1	Sensor 2	Sensor 3	Sensor 4	E8199
Daily Maximum Relative Humidity (%)	-1.17	-0.32*	2.15	-1.66	0.57*
Daily Minimum Relative Humidity (%)	3.87	1.92	3.20	3.85	-1.26
Daily Relative Humidity Range (%)	-5.04	-2.24	-1.05	-5.51	1.83
Hourly Average Relative Humidity (%)	0.37	0.56	1.79	0.20*	-0.25

### 3.2 Thermal Comfort Index Results

To find the impact of the urban garden's form on thermal comfort in the urban environment, the PET and PMV were calculated for each garden type, and compared using paired t-tests, hierarchical cluster analysis, and diurnal graphs.

#### 3.2.1 Paired t-tests

The paired t-tests were conducted in four different manners. First, the PET of three points outside the garden (analogous to Sensors 1-3, and referred to as Receptors 1, 2, and 3) were compared to the PET of the receptor within the garden (at a spot

analogous to the Garden Sensor, referred to as the Garden Receptor, Figure 3.1). For this paired t-test, positive offsets represents an increased mean PET at the street receptor in comparison to the Garden Receptor of the particular model. Second, the PET results of the hypothetical models (i.e. all models prefixed with “3x”) were compared with respect to ActualGarden model’s receptor PET results between analogous receptors (e.g. 3xGarden Garden Receptor PET results vs. ActualGarden Garden Receptor PET results). Lastly, the hypothetical models’ PET results were also compared with respect to the 3xGarden model’s analogous receptor results, to compare vegetation and soil/surface cover differences without differences in garden size. For both paired t-tests, positive results indicate a positive bias in mean PET from the hypothetical model compared to the ActualGarden or 3xGarden model.

Lastly, the Male and Female PMV was compared at each receptor for each model (e.g. ActualGarden Garden Receptor Male PMV results vs. ActualGarden Garden Receptor Female PMV results) to find the difference in the average PMV for male and female bodies. A positive result represents an increased mean PMV for the female body in comparison to the male body.

### **3.2.1.1 Street Receptors’ PET vs. the Garden Receptor’s PET**

The ActualGarden, 3xGarden, 3xTreeCoveredLoam, and 3xTreeCoveredAsphalt models were the only models with statistically significant results for all receptors (Table 3.5). For all four models, the street receptors had a positive bias in the PET than the garden sensor. In addition, the farther a receptor is from the garden, the positive bias of the difference in the mean PET (between the receptor and the Garden Receptor) increased. The smallest increase in the bias as distance increased from the garden was from 0.57 °C to 1.84 °C (a range of 1.26 °C,

for 3xTreeCoveredAsphalt). The largest increase in the biases from the garden was from 0.70 °C to 2.27 °C (a range of 1.56 °C, for ActualGarden). The model with the largest difference in the mean PET between the street receptors and the Garden Receptor was consistently 3xGarden, with a differences in the mean of 0.92 °C, 1.55 °C, and 2.39 °C for Receptors 1, 2, and 3 respectively. The model with the smallest differences in the mean PET of the street receptors relative to the Garden Receptor was consistently 3xTreeCoveredAsphalt, with differences in the mean of 0.57 °C, 1.02 °C, and 1.84 °C for Receptors 1, 2, and 3 respectively.

Table 3.5: [Garden Receptor Mean PET (°C)] - [Street Receptor Mean PET (°C)] for All Envi-met Models. (\* represents statistically insignificant results (p>0.05))

	Receptor 1	Receptor 2	Receptor 3
ActualGarden	0.70	1.41	2.27
3xGarden	0.92	1.55	2.39
3xSoyGarden	-0.77*	-0.21*	0.43*
3xLoam	-0.50*	0.07*	0.71*
3xTreeCoveredLoam	0.68	1.13	1.95
3xTreeCoveredAsphalt	0.57	1.02	1.84
3xAsphalt	-0.85	-0.28*	0.36*
3xConcrete	-0.66*	-0.26*	0.39*

### **3.2.1.2 Hypothetical Model Receptors' PET vs. ActualGarden Model Receptors' PET**

In the models 3xSoyGarden, 3xLoam, 3xAsphalt, and 3xConcrete the PET results at the receptors had positive bias when compared to the PET of the ActualGarden at the same locations (Table 3.6). The differences in the mean PET were consistently largest at the Garden Receptor, and decreased farther away from the garden. 3xAsphalt and 3xConcrete had the largest differences in the Mean PET relative to ActualGarden. The range of the differences of the mean PET for 3xAsphalt was the largest, ranging from 0.08 °C to 1.98 °C (a total range of 1.91 °C).

The models 3xTreeCoveredLoam and 3xTreeCoveredAsphalt both had warmer PET results for the Garden Receptor and Receptor 1, statistically insignificant results for Receptor 2, and cooler PET results for Receptor 3. 3xTreeCoveredAsphalt had slightly warmer mean PET differences (<1 °C) than 3xTreeCoveredLoam for each receptor, and a larger range in the receptors than 3xTreeCoveredLoam (0.43 °C compared to 0.32 °C respectively).

The model 3xGarden had cooler PET results for the Garden Receptor and Receptor 3 (differences in the mean PET of -0.16 °C and -0.03 °C respectively) relative to the ActualGarden model, and statistically insignificant results for Receptors 1 and 2.

Table 3.6: [Theoretical Model Mean PET (°C)] - [ActualGarden Model Mean PET (°C)] for All Receptors. (\* represents statistically insignificant results (p>0.05))

	Garden Receptor	Receptor 1	Receptor 2	Receptor 3
3xGarden	-0.16	0.06*	-0.02*	-0.03
3xSoyGarden	1.88	0.40	0.25	0.04
3xLoam	1.60	0.40	0.26	0.04
3xTreeCoveredLoam	0.28	0.26	-0.001*	-0.04
3xTreeCoveredAsphalt	0.41	0.28	0.01*	-0.02
3xAsphalt	1.98	0.42	0.29	0.08
3xConcrete	1.95	0.59	0.27	0.07

### 3.2.1.3 Hypothetical Model Receptors' PET vs. 3xGarden Model Receptors' PET

The models 3xSoyGarden, 3xLoam, 3xAsphalt, and 3xConcrete all consistently had a positive bias in the PET compared to the 3xGarden PET (Table 3.7). As with respect to the ActualGarden model, the mean differences of the PET were largest at the Garden Receptor, and decreased as distance from the garden increased. In addition, 3xAsphalt and 3xConcrete had the largest differences in the mean PET compared to the 3xGarden model, and the range for the mean differences of 3xAsphalt was the largest with a range from 0.11 °C to 2.14 °C (a total range of 2.02 °C).

The models 3xTreeCoveredLoam and 3xTreeCoveredAsphalt had a greater positive bias in the PET values (compared to the 3xGarden model) closer to the garden site, and statistically insignificant differences further from the garden. For

3xTreeCoveredLoam, the mean PET of the Garden Receptor and Receptor 1 was higher than 3xGarden at the same locations (with differences in the mean of 0.44 °C and 0.20 °C respectively) but differences in the mean of Receptors 2 and 3 were statistically insignificant. The 3xTreeCoveredAsphalt model had differences in the mean of 0.56 °C, 0.22 °C, and 0.04 °C for the Garden Sensor, Receptor 1, and Receptor 2 (respectively) with respect to the 3xGarden model, but the results were statistically insignificant at Receptor 3.

Table 3.7: [Theoretical Model Mean PET (°C)] - [3xGarden Model Mean PET (°C)] for All Receptors. (\* represents statistically insignificant results (p>0.05))

	Garden Receptor	Receptor 1	Receptor 2	Receptor 3
3xSoyGarden	2.03	0.34	0.27	0.08
3xLoam	1.76	0.34	0.28	0.08
3xTreeCoveredLoam	0.44	0.20	0.02*	-0.0048*
3xTreeCoveredAsphalt	0.56	0.22	0.04	0.01*
3xAsphalt	2.14	0.36	0.31	0.10957
3xConcrete	2.10	0.52	0.29	0.10106

### 3.2.1.4 Female PMV vs. Male PMV

For all models, the Female PMV had a lower mean than the Male PMV (i.e. the differences in the mean Female PMV relative to the Male PMV were negative for all models) (Table 3.8). However, two trends were apparent in the differences in the means of the Female and Male PMV. For the models ActualGarden, 3xGarden, 3xTreeCoveredLoam, and 3xTreeCoveredAsphalt, all the models had much lower differences (in the mean Female PMV relative to the Male PMV) compared to the other four models (an average mean difference of -1.77, compared to -1.56). However, every model had similar differences in the mean PMV for the street receptors (Receptors 1, 2, and 3, with an average of -1.66, -1.59, and -1.61 respectively). Among the street receptors, each model had the largest differences in mean Female PMV (compared to the mean Male PMV) with Receptor 1, and the smallest mean difference with Receptor 2.

Table 3.8: [Mean Female PMV] - [Mean Male PMV] at Each Receptor for All Models. (\* represents statistically insignificant results (p>0.05))

	Garden Receptor	Receptor 1	Receptor 2	Receptor 3
ActualGarden	-1.74	-1.68	-1.59	-1.61
3xGarden	-1.80	-1.68	-1.61	-1.62
3xSoyGarden	-1.56	-1.65	-1.58	-1.59
3xLoam	-1.59	-1.65	-1.58	-1.59

Table 3.8 cont.

3xTreeCoveredLoam	-1.76	-1.67	-1.61	-1.63
3xTreeCoveredAsphalt	-1.76	-1.66	-1.61	-1.62
3xAsphalt	-1.56	-1.65	-1.58	-1.59
3xConcrete	-1.56	-1.64	-1.57	-1.59

### 3.2.2 Hierarchical Cluster Analysis

For the hierarchical cluster analysis, dendrograms were created for the PET and PMV results. For the PET results, the dendrogram is grouping the results from each receptor for all eight models. The receptors that are most closely related form the lowest-level clusters on the left (as pairs). Clusters are formed by the vertical linkages, and the horizontal distance between the vertical linkages represent the similarity of the joining clusters. Eventually all of the receptors are linked at the far right of the diagram. For the PMV results, the Male and Female results are provided in two separate dendrograms, to compare the changes in relationships between the biological sexes. The names of the receptors are formatted as “[Model Name] [Receptor Abbreviation],” where the cluster abbreviation is GR for the Garden Receptor and R1, R2, and R3 for Receptors 1, 2 and 3 respectively.

#### 3.2.2.1 Hierarchical Cluster of the Physiological Equivalent Temperature (PET)

The hierarchical cluster of the PET (Figure 3.2) clustered the analogous receptors of each model into their own cluster. In terms of the Receptor clusters, the Receptor 1 and 2 clusters are the most closely related, followed by the Garden Receptor cluster and the Receptor 3 cluster.

Within the clusters for the Garden Receptor, Receptor 2, and Receptor 3, a pattern emerges. For each of the receptors, the ActualGarden and 3xGarden models, the 3xTreeCoveredLoam and 3xTreeCoveredAsphalt models, and 3xAsphalt and 3xConcrete models form the lowest-level clusters on the dendrogram. In addition, the ActualGarden and 3xGarden cluster is most closely related to the 3xTreeCoveredLoam and 3xTreeCoveredAsphalt cluster. Similarly, the 3xAsphalt and 3xConcrete cluster is most closely related to of the 3xSoyGarden and 3xLoam. For Receptor 1 and Receptor 2, the 3xAsphalt and 3xConcrete cluster is paired with a 3xSoyGarden and 3xLoam cluster. For the Garden Receptor, however, 3xSoyGarden and 3xLoam cluster is separated, with the 3xAsphalt and 3xConcrete cluster being more closely related to 3xSoyGarden than 3xLoam.

Despite this, the main division within the three receptor clusters were between the model with trees (ActualGarden, 3xGarden models, 3xTreeCoveredLoam, and 3xTreeCoveredAsphalt) and those without trees (3xSoyGarden, 3xLoam, 3xAsphalt and 3xConcrete). The 3xAsphalt and 3xConcrete cluster was the most closely related model pairs (although the other two tree-less models were similarly close in Receptors 2 and 3), while the ActualGarden and 3xGarden cluster were the least similar of the lowest-level clusters in all the receptor clusters.

For Receptor 1's cluster, the clustering was different than the other receptors. While the ActualGarden and 3xGarden models, the 3xSoyGarden and 3xLoam models, and the 3xTreeCoveredLoam and 3xTreeCoveredAsphalt are still the lowest-level clusters, the pairings within the Receptor 1 cluster changes. 3xAsphalt is extremely similar to the 3xSoyGarden and 3xLoam cluster (i.e. there is very little horizontal distance between their linkages). The three models are most closely related to the

3xTreeCoveredLoam and 3xTreeCoveredAsphalt cluster, which is then related to the 3xConcrete model. These six models then form their own cluster within the Receptor 1 cluster, which is then linked to the remaining two models in the ActualGarden and 3xGarden cluster to complete the Receptor 1 cluster.

### **3.2.2.2 Hierarchical Cluster of the Predicted Mean Vote (PMV)**

While the PMV dendrograms share many similarities with the PET dendrogram. The individual receptors each form the four main clusters, and the lowest-level pairs are similar to the pairs of the PET dendrogram. However, there are also multiple differences between the Male dendrogram, Female dendrogram, and the PET dendrogram, in which the lowest-level pairs are either split or paired with other clusters in a different manner than the other dendrograms.

#### **3.2.2.2.1 Male PMV**

The Male PMV dendrogram (Figure 3.3.) is similar to the PET dendrogram in regards to the corresponding Receptor 3 clusters. However, the other three clusters are structurally different from the corresponding clusters in the PET dendrogram. For the Garden Receptor cluster, the 3xGarden model is most similar to the 3xTreeCoveredSoil and 3xTreeCoveredAsphalt cluster, and then this three-model cluster is linked to the ActualGarden model. For the Receptor 1 cluster, the 3xLoam model and 3xAsphalt model are a lowest-level cluster pair, then the 3xSoyGarden model is the closest related to the pair (that is, the 3xAsphalt and 3xSoyGarden models switch relative positions). For the Receptor 2 cluster, the ActualGarden model was more closely related to the tree-less garden-site models than the other tree-covered garden-site models.

#### **3.2.2.2.2 Female PMV**

Structurally speaking, the Female PMV dendrogram (Figure 3.4) is similar to the Male PMV dendrogram. However, there are two minor differences in the Receptor 1 and 2 clusters. While the Male PMV dendrogram had the 3xLoam and 3xAsphalt models as a lowest-level cluster pair for Receptor 1, the Female PMV Receptor 1 structure is structurally the same as the PET dendrogram (i.e. 3xLoam and 3xSoyGarden are more closely related, then 3xAsphalt is most similar). In the Receptor 2 cluster, the 3xSoyGarden and 3xLoam garden were not paired, but instead 3xLoam was more closely related to the 3xAsphalt and 3xConcrete cluster than 3xSoyGarden.

#### **3.2.3 Diurnal Cycle Graphs**

For both the PET and PMV indices, the weekly average diurnal cycle of the four modelled weeks were plotted for all the models. The models are also graphed against the human comfort (and heat stress) thresholds for the PET and PMV (respectively) as used by Wang et al. (2017) (Table 3.9). The PET, Male PMV, and Female PMV results contained values that exceeded the “warm” value (correlated with moderate heat stress, 35 °C for the PET, and 2.5 for the PMV and reached the “cool” value (correlated with moderate cold stress, 13 °C for the PET and -1.5 for the PMV). However, the warmest weeks for all three indices were Week 1 and Week 3 (with the extreme results indicating a “hot” environment and strong heat stress and the coldest week was Week 4 (with results indicating a generally cold environment).

Table 3.9: Ranges of PET and PMV values for different levels of thermal comfort and physiological stress (according to Wang et al. 2017).

PET (°C)	PMV	Thermal Comfort	Physiological Stress
4	-3.5	Very Cold	Extreme Cold Stress
8	-2.5	Cold	Strong Cold Stress
13	-1.5	Cool	Moderate Cold Stress
18	-0.5	Slightly Cool	Slight Cold Stress
23	0.5	Neutral	No thermal stress
29	1.5	Slightly Warm	Slight Heat Stress
35	2.5	Warm	Moderate Heat Stress
41	3.5	Hot	Strong Heat Stress

### 3.2.3.1 Warming and Cooling Patterns

For all four modelled weeks, there was a consistent pattern in the model’s responses during the diurnal cycle for the Garden Receptor. Starting at 00:30 (the earliest receptor results from Envi-met), the PET and PMV values decrease until the minimum values of the diurnal cycle are reached right before sunrise, at which point the PET and PMV began to rise again. During this early period, the tree-less garden models (3xSoyGarden, 3xLoam, 3xAsphalt, and 3xConcrete) are cooler than the tree-covered garden models (the ActualGarden, 3xGarden, 3xTreeCoveredLoam, and 3xTreeCoveredAsphalt models). Then, during the early morning, the PET and PMV values begin to converge between models before diverging as the tree-less models warm faster at 09:30. During the day, tree-covered garden models demonstrate an increase in PET and PMV values that level out at 13:00 (in the range between the “neutral” and “slightly warm” thermal comfort values) before slowly decreasing for the rest of the cycle. However, the treeless models (the 3xSoyGarden, 3xLoam,

3xAsphalt, and 3xConcrete models) demonstrate a sudden increase in PET and PMV values (between 09:30 and 10:00) in which the values reach or exceed the “warm” threshold values for all four weeks. The thermal comfort indices then increase until 12:00, and by 12:30 the thermal comfort indices return to below the “slightly warm” threshold and follow a similar pattern to the tree-covered models.

However, within the tree-less and tree-covered model groups, some additional trends are apparent. The tree-covered models diverge into two groups over the course of the day. The ActualGarden and 3xGarden models are the coolest models, while the 3xTreeCoveredLoam and 3xTreeCoveredAsphalt models are both much warmer than the first two models (and are similar in warmth to the tree-less models after 12:30). Within the tree-less models, the 3xLoam covered model is cooler during the day (including during the period of elevated warmth in the late morning) than the other tree-less models. The 3xLoam model is also similar to the 3xTreeCoveredLoam and 3xTreeCoveredAsphalt models before 09:30 and after 13:00 during Weeks 2-4, and cooler in the same time period during Week 1.

For Receptor 1, the pattern is similar across all weeks, but Weeks 3 and 4 are structured more similarly than compared to the prior two weeks. For each week (and across all three indices), the minimum values are in the early morning (similar to the Garden Receptor). Then, the indices begin to increase, with a rapid increase from 08:00 to 08:30 and subsequent decrease from 09:00 to 09:30. A similar increase and decrease occurs between 12:30 to 14:30 for the every model but the 3xGarden model and Actual Garden. The 3xGarden model levels off around 13:00 before decreasing in the afternoon and evening. For Weeks 1 and 2, the ActualGarden model diverges from the 3xGarden model, and warms from 12:30 to 13:00 (in a similar intensity to the tree-

less models) and then cools from 13:00 to 13:30. For Weeks 3 and 4, however, the ActualGarden model behaves similarly to the 3xGarden model. In addition, for Week 1, the Concrete model shows strong divergence from the other models during the small daytime peaks.

For Receptor 2, the model follows the same general diurnal cycle pattern of minimum PET and PMV values in the early morning which then increase before levelling off in the early afternoon. However, during the morning, there is a peak in the PET/PMV values for Weeks 1 and 4, and two peaks for Weeks 2 and 3. During Week 1, the thermal comfort indices sharply increase from 07:00 to 09:30, before decreasing from 09:30 to 11:00. For Weeks 2 and 3, there are instead two peaks, with local maxima at 08:00 and 09:30 for both weeks. For Week 4, the PET and PMV values increase sharply from 6:30 to 8:00 before decreasing suddenly from 8:00 to 8:30.

Receptor 3 shows a consistent pattern for each of the modelled weeks. As with the other receptors, the temperature minimum is in the early morning (for Receptor 3, at 06:30 in all cases). Then the temperature begins to increase sharply before levelling off and reaching a local maximum at 11:30, decreasing sharply from 11:30 to 12:00, having a slight increase in PET/PMV from 12:30 to 13:00, and a sharp peak at 14:00 (of a similar intensity to the decrease at 11:30) before gently decreasing for the rest of the diurnal cycle.

### **3.2.3.2 Diurnal Cycle of the Physiological Equivalent Temperature (PET)**

#### **3.2.3.2.1 The Garden Receptor**

During Week 1 at the Garden Receptor (Figure 3.5), the PET ranged from approximately 13 °C to 45 °C (for the tree-less models) and from 14.3 °C to 27.3 °C (for the coolest tree-covered model, 3xGarden model). When the tree-less models diverge from the tree-covered models between 09:30 to 10:00, the tree-less models increase approximately 20 °C in 30 minutes, and go from a PET just below the neutral threshold (23 °C ) to exceeding the “hot” threshold of 41 °C (indicating strong heat stress). The tree-less models maximum PET, 44.5 °C (at 12:00) is the warmest of all four weeks, and 17.9 °C warmer than the warmest tree-covered models (3xTreeCoveredLoam and 3xTreeCoveredAsphalt). After the peak PET at 12:00, the tree-less models cool until they are comparable to the tree-covered models at 12:30 (for example, 27.3 °C for 3xConcrete and 26.8 °C for 3xTreeCoveredAsphalt at 12:30), and are between the “neutral” and “slightly warm” thresholds (at 23 °C and 29 °C respectively).

During the Week 2 (Figure 3.6), the PET values follow a similar pattern, but ranged from “cold” (indicating moderate cold stress, threshold at 8 °C) at night to “warm” (35 °C for the tree-less models in the late morning. For the tree-covered models, the PET never increased above the “neutral” threshold. The highest mid-day maximum PET was 37.7 °C for the tree-less models (except for 3xLoam) at 12:00, and the coolest mid-day maximum PET was 18.7 °C for 3xGarden (from 13:30 to 14:30).

Week 3 (Figure 3.7) had similarly high PET when compared to Week 1. The tree-less models all exceeded the “warm” threshold after diverging from the tree-covered models in the late morning, and reached 41 °C (the “hot” threshold) at 12:00

before cooling to levels similar to the tree-covered models at 12:30. In addition, models were at or above the “neutral” threshold at during the mid-day, although at slightly cooler PET values than Week 1.

During Week 4 (Figure 3.8), the coldest week, primarily had values below the “Slightly Cool” (18 °C) threshold, with the only models that exceeded the threshold being the tree-less models, during the period of extra warmth in the late morning. During the warm period for the tree-less models, the maximum PET barely exceeded the “warm” threshold (reaching 35.5 °C) at 12:30, before dropping below the “slightly cool” threshold at 13:00.

#### **3.2.3.2.2 Receptor 1**

Receptor 1 is located across the street from the garden, at a distance of 30 meters from the garden boundary in the ActualGarden model. For Week 1 (Figure 3.9), the only model to exceed the “slightly warm” was the 3xConcrete model (which had a maximum of 40 °C, just below “hot”), while the other models reached a maximum just below the threshold. Most of the models (except 3xConcrete and 3xGarden) have a range from approximately 13 °C to 28 °C. However, the 3xGarden model diverges from the other models at 12:00 and does not have a small peak in PET between 13:00 to 14:00, so the 3xGarden maximum PET is approximately 25 °C. In contrast, the 3xConcrete model has exaggerated peaks at 8:30 to 9:00 and 13:00 to 14:00 (approximately 10 °C and 12 °C larger than the other models), with a maximum PET of approximately 40 °C. In addition, the 3xConcrete model also has PET values approximately 1 °C less than the other models during the nighttime as well.

For Week 2 (Figure 3.10), the all models have a maximum PET at 12:30, however the 3xTreeCoveredLoam and 3xTreeCoveredAsphalt are about a degree

cooler than the tree-less models. In addition, the ActualGarden model is a degree cooler than the 3xTreeCoveredLoam and 3xTreeCoveredAsphalt, and 3xGarden is approximately 5 °C cooler than the other tree-covered models.

For Receptor 1, the models only exceeded PET values above the “slightly warm” threshold for Week 3 (Figure 3.11). In addition, the PET of Receptor 1 consistently has a range of 1 to 2 °C outside of the mid-day divergence in PET values. From 00:30 to 06:30, the ActualGarden model is slightly warmer than the other models until the minimum PET (which was approximately 15 °C to 16 °C for all models), at which point 3xGarden reaches similar PET values to ActualGarden. The ActualGarden and 3xGarden models then warm at a lesser rate than the other models beginning at 10:00 (at which point the two models become cooler than the other models) and reach a maximum PET of about 26 °C at 13:00. In addition, the 3xTreeCoveredLoam and 3xTreeCoveredAsphalt follow a similar pattern to the tree-less models (including a small peak in PET at 13:00 and 13:30), although the two models are consistently cooler than the tree-less models. The 3xTreeCoveredLoam and 3xTreeCoveredAsphalt models have a maximum PET of approximately 32 °C, and the tree-less models have a maximum PET of approximately 33 °C.

For Week 4 (Figure 3.12), the PET follows a similar pattern as Week 3, but with less variation between models (i.e. the models have similar PET values until the mid-day divergence), and much lower values. The PET never exceeds the “neutral” threshold during Week 4, with a maximum PET of approximately 21 °C. The minimum PET is also the lowest of any Receptor 1 PET values, at approximately 7 °C.

### 3.2.3.2.3 Receptor 2

Receptor 2 is located east of Receptor 1 and to the west to the intersection of a street perpendicular to Fitzwater Street (the street that the 2124 Fitzwater Garden site is located on), at a distance of 41 meters from the garden boundary in the ActualGarden model. For Receptor 2. During Week 1 (Figure 3.13), the thermal comfort indices sharply increase from 07:00 to 09:30 (with an approximately 20 °C increase in PET from the beginning of the peak to its apex), before decreasing from 09:30 to 11:00 (a decrease of approximately 10 °C in PET), forming a local minimum at 11:00 as the PET slightly rises until mid-day. The maximum PET is approximately 33 °C (slightly below the “warm” threshold), at 09:30, with a minimum PET of approximately 12 °C (slightly below the “cool” threshold). The models have a high similarity with each other for Week 1, with the largest variation between models being less than 1 °C.

For Weeks 2 and 3 (Figure 3.14 and Figure 3.15), there are instead two peaks, with local maxima at 08:00 and 09:30 for both weeks. For both weeks, the two peaks have increases of approximately 20 °C (with an approximately 15 °C decrease after the peak). For Week 2, the first peak reaches 31 °C (above the “slightly warm” threshold) and the second peak reaches 37 °C (above the “warm” threshold). The models also see some divergence between the tree-less and tree-covered models from 10:00 to 16:00, with the tree-less models being slightly warmer than the tree-covered models by a 1 °C. For Week 3, the first peak reaches 34 °C (slightly below the “warm” threshold) and the second peak reaches 41 °C (the “hot” threshold). Similarly to Week 2, Week 3 has a PET range during the mid-day with a 1 °C between the warmest models (the tree-less models) and coolest models (ActualGarden and 3xGarden).

For Week 4 (Figure 3.16), the PET has a range of approximately 1 °C to 2 °C between the models throughout the diurnal cycle. The minimum PET is approximately 7 °C (below the “cold” threshold) at 06:30. The PET then increases sharply to the maximum PET of approximately 25 °C (slightly above the “slightly cool” threshold) at 8:30, before decreasing to approximately 11 °C at 8:30. Then all the model PET values increase until approximately 18 °C to 20 °C at 12:30, before decreasing in the afternoon.

#### **3.2.3.2.4 Receptor 3**

Receptor 3 is located at the intersection, across the street that runs perpendicular to Fitzwater Street, at a distance of 80 meters from the edge of the ActualGarden model. For all four weeks, the pattern is consistent between all the models. Week 1 (Figure 3.17) and Week 2 (Figure 3.18) are structurally identical, with Week 2 being slightly colder than Week 1. However, Week 3 (Figure 3.19) and Week 4 (Figure 3.20) have a small range in the PET (a maximum of 1 °C) between the models during the daytime. The extreme PET values also occur at the same time for each week, with the minimum PET at 06:30, and the maximum PET at 14:00 (which is slightly warmer than the PET before the sharp decrease from 12:00 to 13:30). For Week 1, the PET has a range of approximately 11 °C to 36 °C, going from below the “cool” threshold to above the “warm” threshold. For the PET has a range of approximately 7 °C to 35 °C, going from below the “cold” threshold to the “warm” threshold. For Week 3, the warmest week, the range is from approximately 14 °C (slightly above the “cool” threshold) to 45 °C (above the “hot” threshold). Week 4, the coldest week, has a minimum PET of approximately 6 °C (below the “cold”

threshold) and a maximum PET of 33 °C (between the “slightly warm” and “warm” threshold). Week 4 also has the largest range of PET values.

### **3.2.3.3 Comparison of Male and Female Predicted Mean Vote (PMV) Results**

For the PMV results, the PET, Male PMV, and Female PMV diurnal cycles have similar trends. However, while the Female PMV has a lower mean than the Male PMV (see Section 3.2.1.4 above), the Male and Female PMV results also have strong differences in their extreme values. While the Male and Female PMV results both have periods of hot and cold, the Female PMV has exaggerated deviations from neutral PMV values. Female bodies were more likely to feel cold during the course of a diurnal cycle (due to the model being generally cooler during the study period), and when the Male PMV increased, the Female PMV increased more. This phenomenon is apparent in all four receptor locations.

#### **3.2.3.3.1 Male and Female PMV Differences at the Garden Receptor**

The differences between the Male and Female PMV are most clearly demonstrated at the Garden Receptor. For Week 1, the Female PMV (Figure 3.21) of the tree-less models (which experience a period of increased warmth in the late morning) ranges from -3 to 5 (from below the “cold” threshold to far above the “hot” threshold), while the Male PMV (Figure 3.22) had a range of -1 to 4 (from below the “slightly cool” threshold to just above the “hot” threshold). However, the tree-covered models have a Male PMV range of approximately -1 to 1 (“slightly cool” to between “neutral” and “slightly warm”), and a Female PMV of approximately -2 to 0 (“cold” to between “slightly cool” and “neutral”) For the tree-less models Week 2 has an even larger range for the Female PMV (-4.5 to 4) (Figure 3.23), while the Male PMV has a

range of -2 to 3.25 (Figure 3.24). This pattern of difference in extreme PMV for the tree-less models repeats in Week 3, with a Female PMV range of -3 to 5 (Figure 3.25) and Male PMV range of -1 to 4 (Figure 3.26), and Week 4, with a Female PMV range of -5 to 3 (Figure 3.27), and a Male PMV of -2.5 to 2.5 (Figure 3.28). For the tree-covered models, the Female PMV instead reaches a maximum PMV of -1.5, -0.5, and -2 while the maximum Male PMV was 0, 1, and -1 for Weeks 2, 3, and 4, respectively.

#### **3.2.3.3.2 Male and Female PMV Differences at Receptor 1**

The maximum PMV values at Receptor 1 were generally close to the neutral threshold for all models during Weeks 1-3, so there was minor variation during those Weeks. However, the 3xConcrete model had elevated PMV values compared to the other models during Week 1, and this increased PMV is much greater for the Female PMV (Figure 3.29) than the Male PMV (4 and 3, respectively) (Figure 3.30). In addition, the minimum PMV values were much lower for the Female PMV than Male PMV for all three weeks. For the first three weeks, Female and Male PMVs had a respective minimums of -3.5 and -1.4 for Week 1, -3.5 and -1.5 for Week 2 (Figure 3.31 and Figure 3.32), and -2.5 and -1.75 for Week 3 (Figure 3.33 and 3.34). For Week 4, the maximum PMV was colder than normal, so the Female PMV ranged from -5 to -0.5 (Figure 3.35), and the Male PMV ranged from -2.25 to 0.5 (Figure 3.36). In addition, during Week 4, the treeless models were higher than the 3xTreeCoveredLoam and 3xTreeCoveredAsphalt by 1 (for the Female PMV) and 0.5 (for the Male PMV) at the time of maximum PMV.

### **3.2.3.3.3 Male and Female PMV Differences at Receptor 2**

For the Weeks 1 and 2, the differences in Receptor 2 PMV values between the Male and Female behaved similarly as Receptor 1, with greater variation among minimum PMV values than maximum PMV values. For Week 1, the Female PMV ranged from approximately -3.5 to 1.75 (Figure 3.37), and the Male PMV ranged from approximately -1.25 to 2.75 (Figure 3.38). For Week 2, the Female PMV ranged from approximately -4 to 2.75 (Figure 3.39), and the Male PMV ranged from approximately -2 to 2.5 (Figure 3.40). However, for Weeks 3 and 4 the maximum PMVs had greater variation. For Week 3, the Female PMV ranged from approximately -2.5 to 3.75 (Figure 3.41), while the Male PMV ranged from approximately -0.75 to 3 (Figure 3.42). For Week 4, the Female PMV ranged from approximately -5 to 0 (Figure 3.43), while the Male PMV ranged from approximately -2.4 to 1 (Figure 3.44).

### **3.2.3.3.4 Male and Female PMV Differences at Receptor 3**

For Receptor 3, the greatest differences in the Male and Female PMV extremes was the minimum PMV. For Week 1, the Female PMV ranged from approximately -4 to 2.25 (Figure 3.45) while the Male PMV ranged from approximately -1.75 to 2.25 (Figure 3.46). For Week 2, the Female PMV ranged from approximately -5 to 2 (Figure 3.47), while the Male PMV ranged from approximately -2.5 to 2 (Figure 3.48). For Week 3, the Female PMV ranged from approximately -3 to 5 (Figure 3.49), while the Male PMV ranged from 1 to 4 (Figure 3.50). Lastly, for Week 4, the Female PMV had an approximate range of -5.75 to 2.75 (Figure 3.51), and the Male PMV had an approximate range of -2.75 to 2.5 (Figure 3.52).



Figure 3.1: Receptor Locations. Receptors are represented as purple cells with abbreviated name (i.e. Garden Sensor = “GS”, Receptor 1 = “R1”, Receptor 2 = “R2” and Receptor 3 = “R3”). The ActualGarden model is shown, but the receptor location is unchanged in each model.

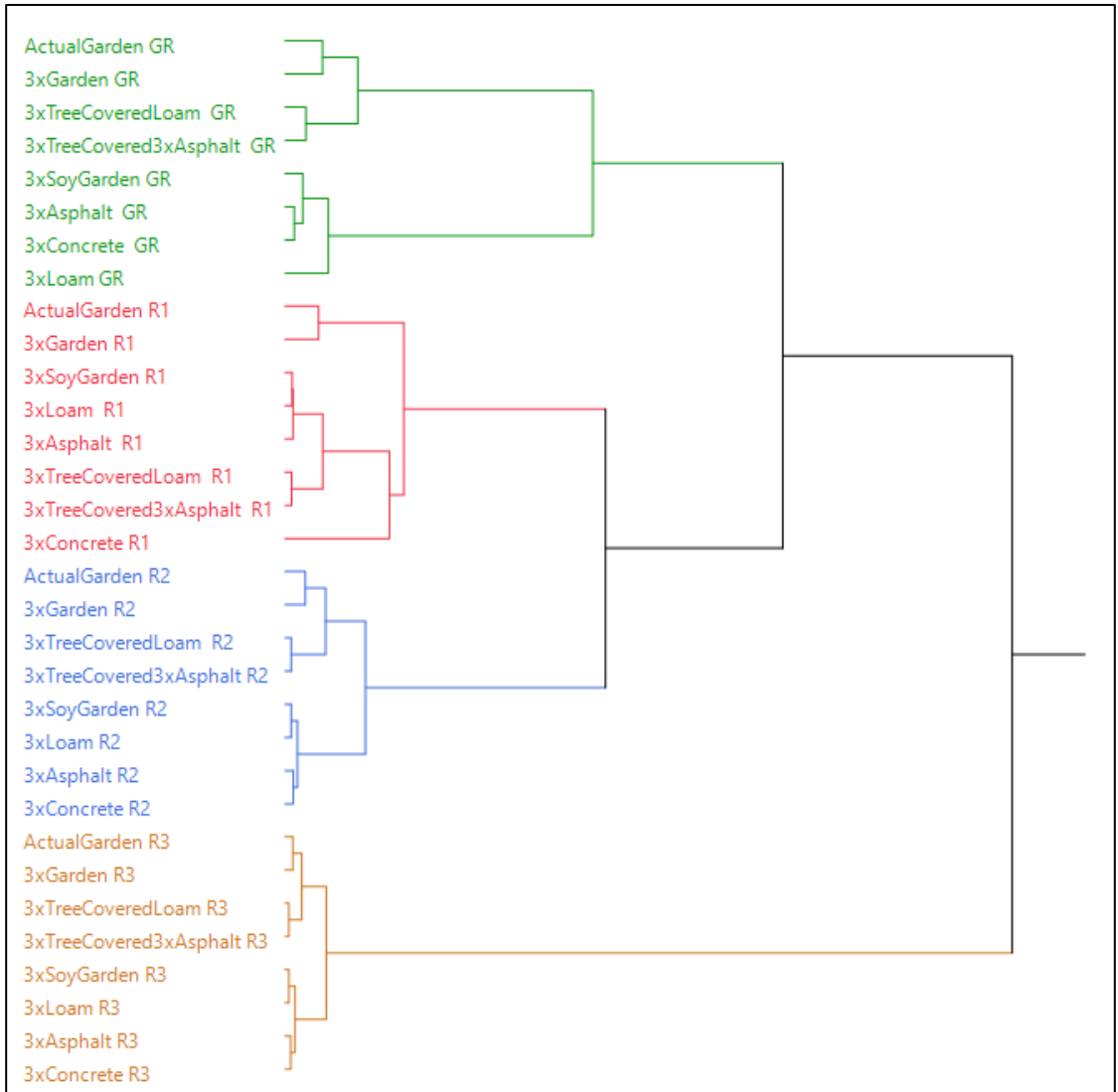


Figure 3.2: Hierarchical Cluster Analysis Dendrogram of the Physiological Equivalent Temperature (PET) For Each Model and Receptor. The four colors correspond to the four clusters of the dendrogram (which are composed of the same receptor for all eight models). Green represents the Garden Receptor, red represents Receptor 1, blue represents Receptor 2, and brown represents Receptor 3.

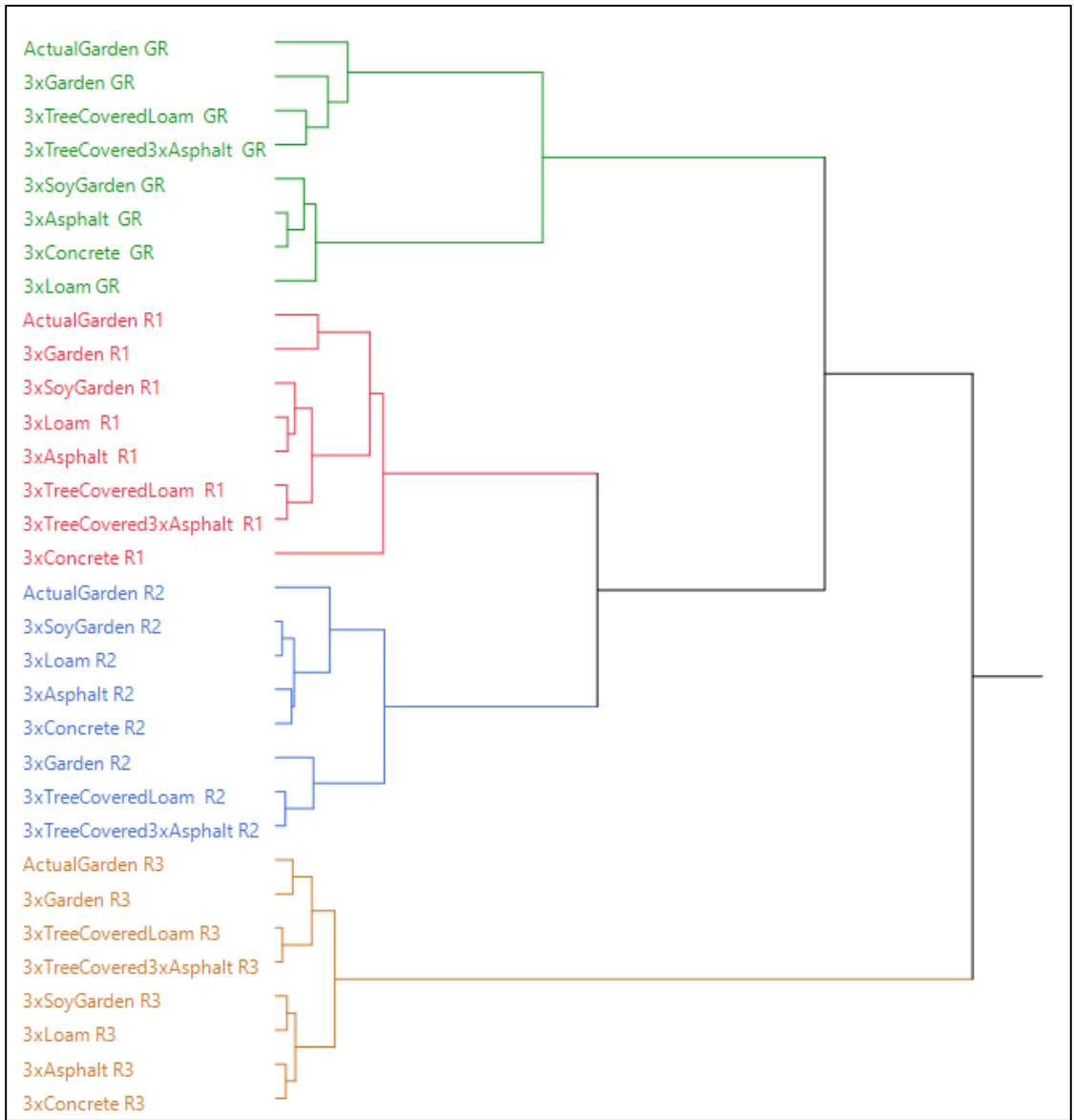


Figure 3.3: Hierarchical Cluster Analysis Dendrogram of the Male Predicted Mean Vote (PET) For Each Model and Receptor. The four colors correspond to the four clusters of the dendrogram (which are composed of the same receptor for all eight models). Green represents the Garden Receptor, red represents Receptor 1, blue represents Receptor 2, and brown represents Receptor 3.

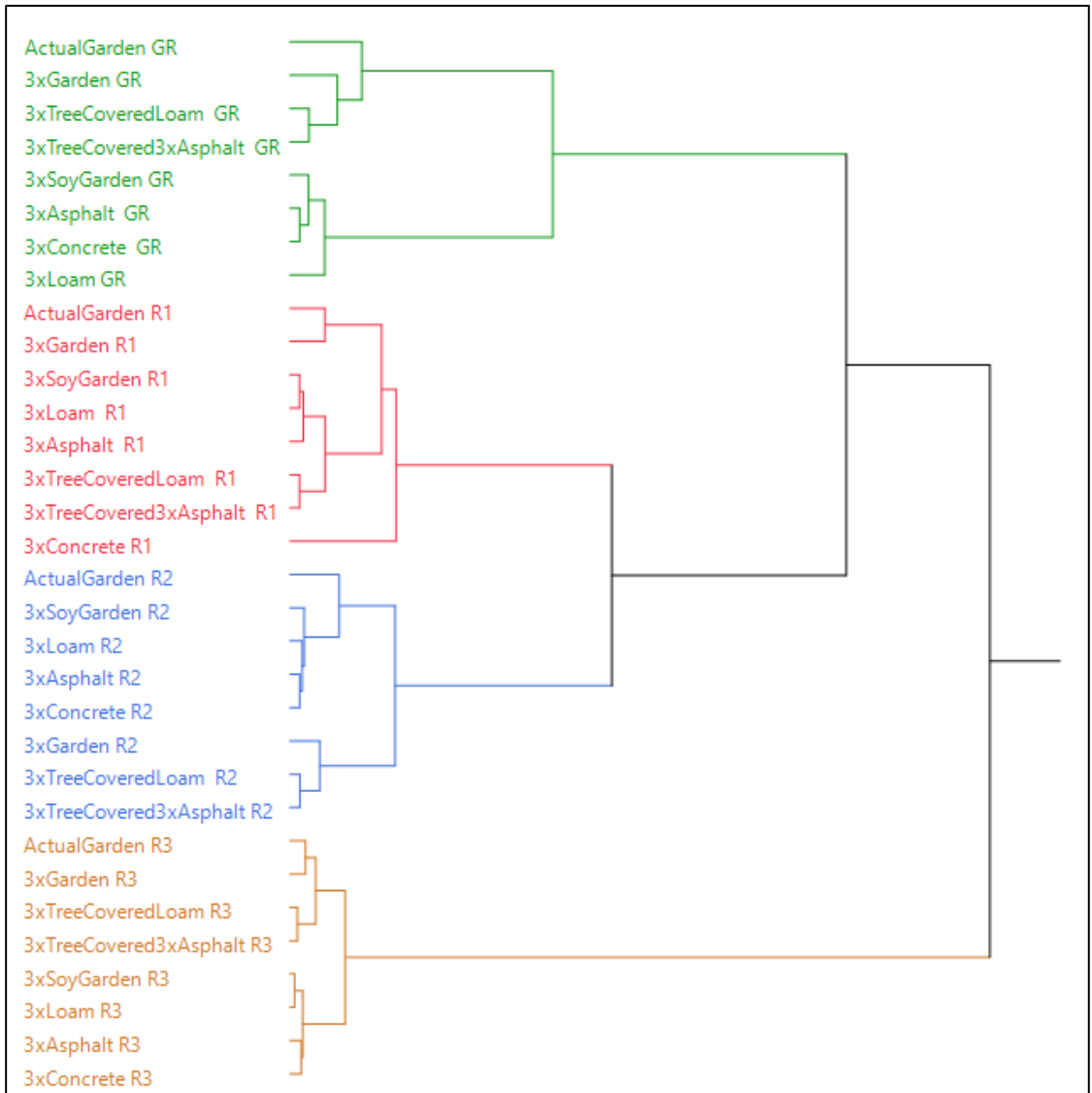


Figure 3.4: Hierarchical Cluster Analysis Dendrogram of the Female Predicted Mean Vote (PET) For Each Model and Receptor. The four colors correspond to the four clusters of the dendrogram (which are composed of the same receptor for all eight models). Green represents the Garden Receptor, red represents Receptor 1, blue represents Receptor 2, and brown represents Receptor 3.

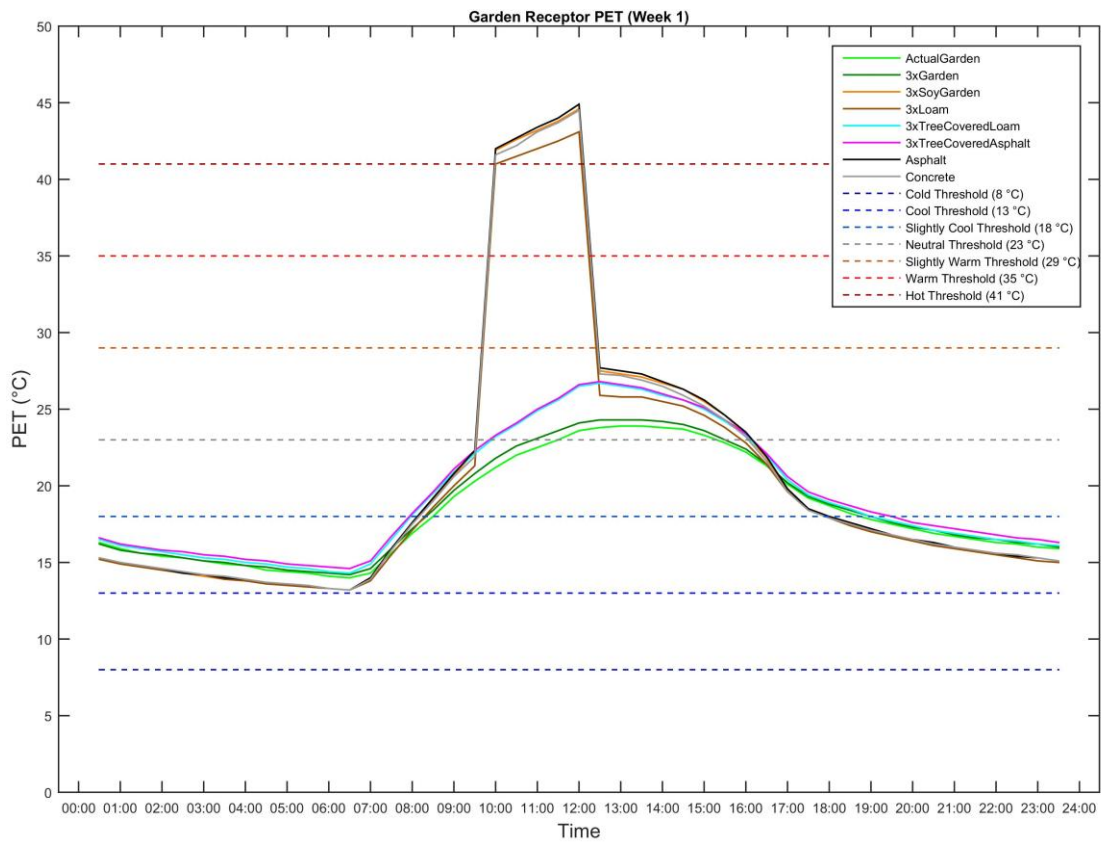


Figure 3.5: The Diurnal Cycle of the Physiological Equivalent Temperature (PET) of the Garden Receptor for Week 1.

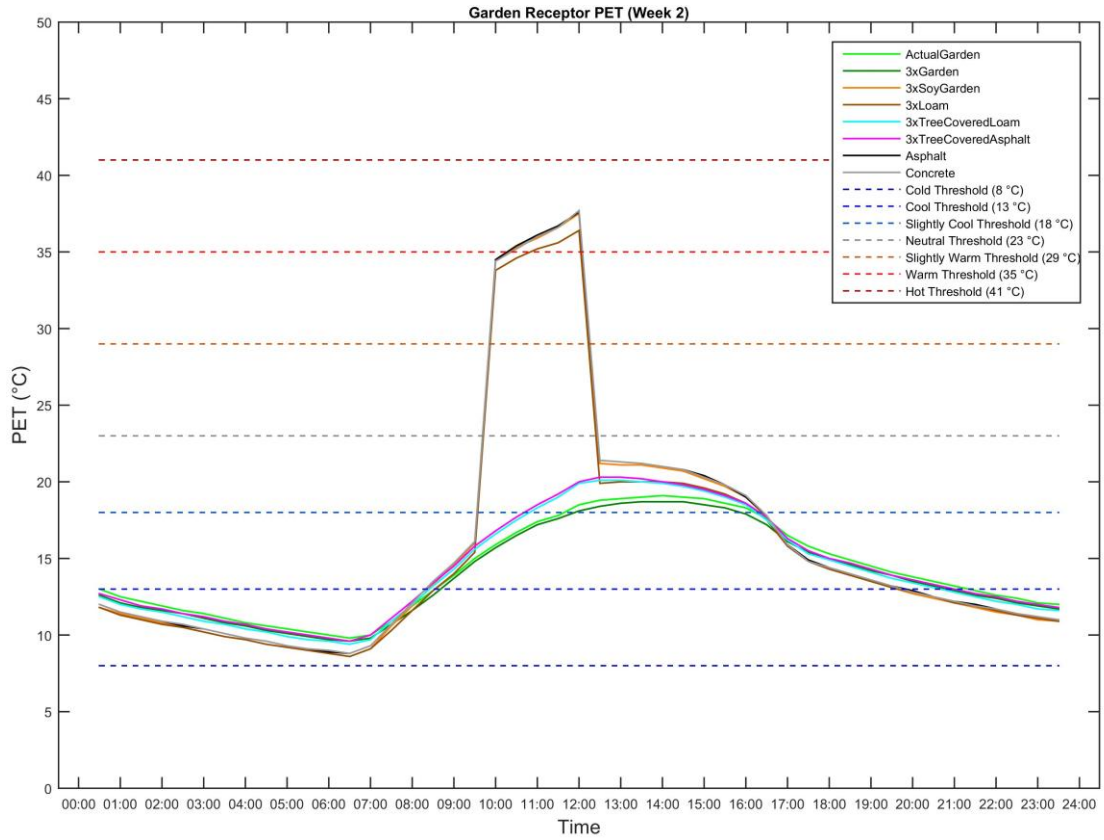


Figure 3.6: The Diurnal Cycle of the Physiological Equivalent Temperature (PET) of the Garden Receptor for Week 2.

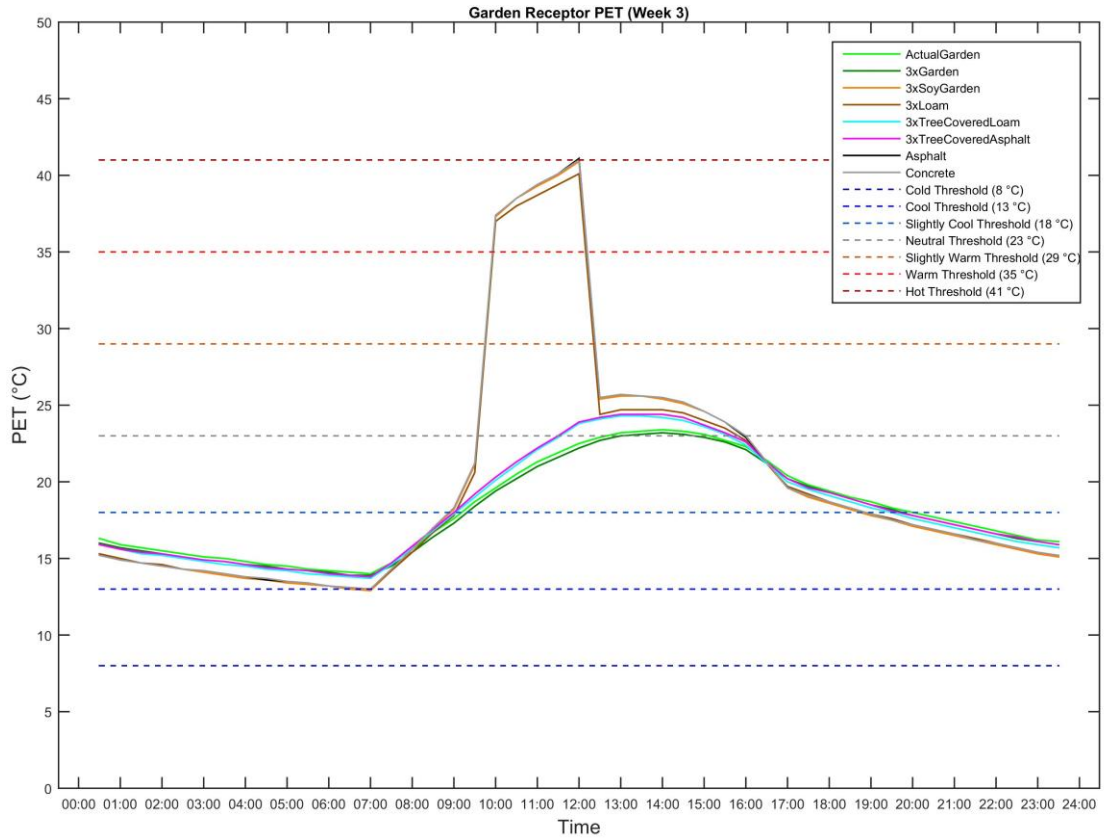


Figure 3.7: The Diurnal Cycle of the Physiological Equivalent Temperature (PET) of the Garden Receptor for Week 3.

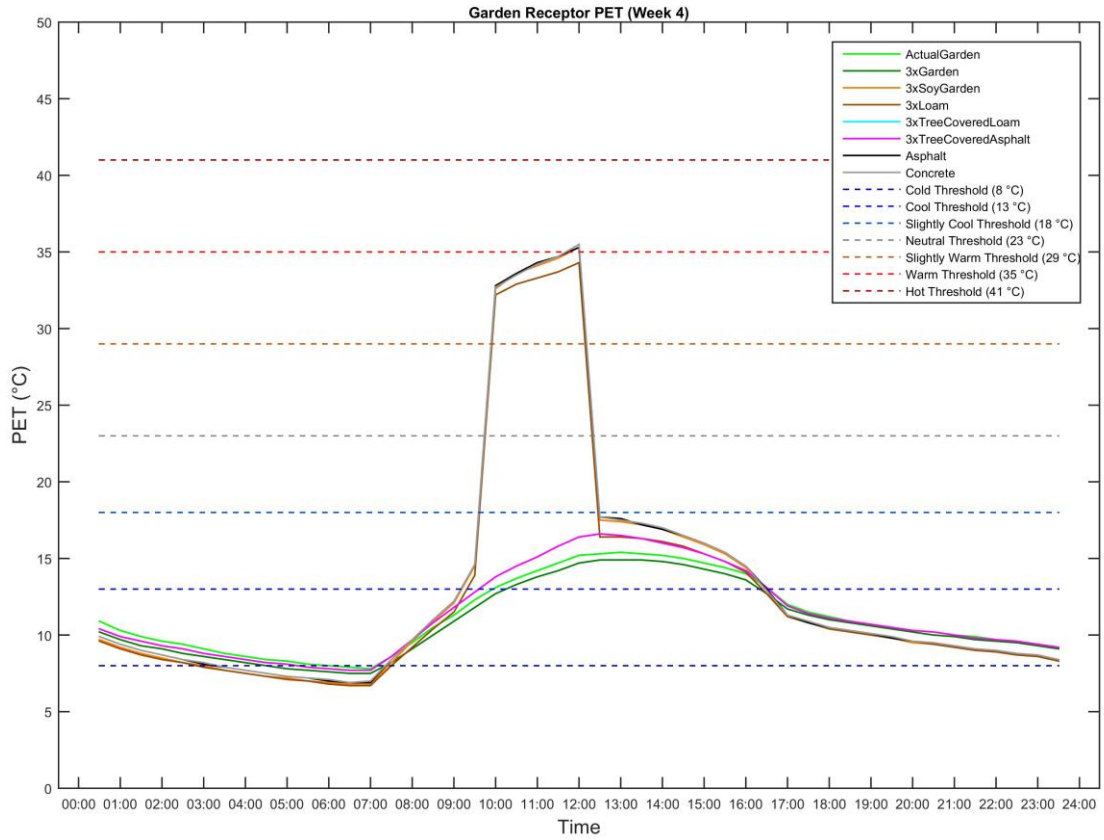


Figure 3.8: The Diurnal Cycle of the Physiological Equivalent Temperature (PET) of the Garden Receptor for Week 4.

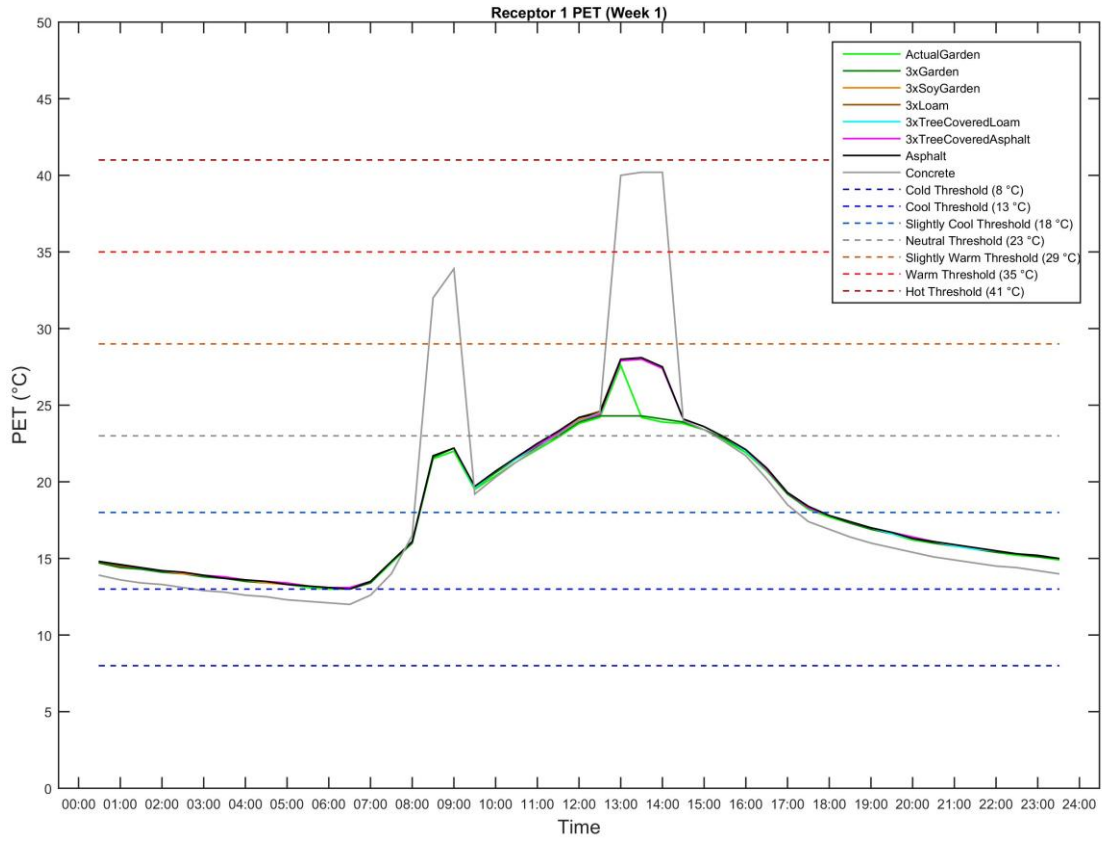


Figure 3.9: The Diurnal Cycle of the Physiological Equivalent Temperature (PET) of Receptor 1 for Week 1.

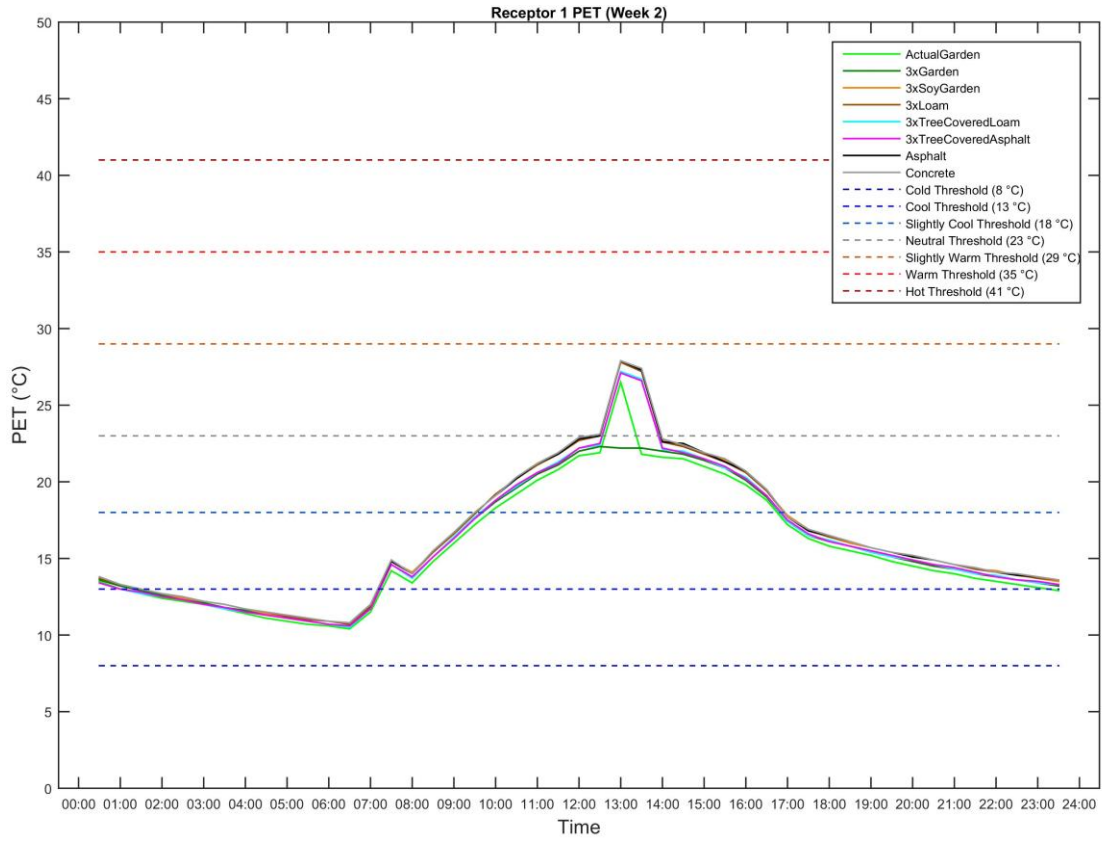


Figure 3.10: The Diurnal Cycle of the Physiological Equivalent Temperature (PET) of Receptor 1 for Week 2.

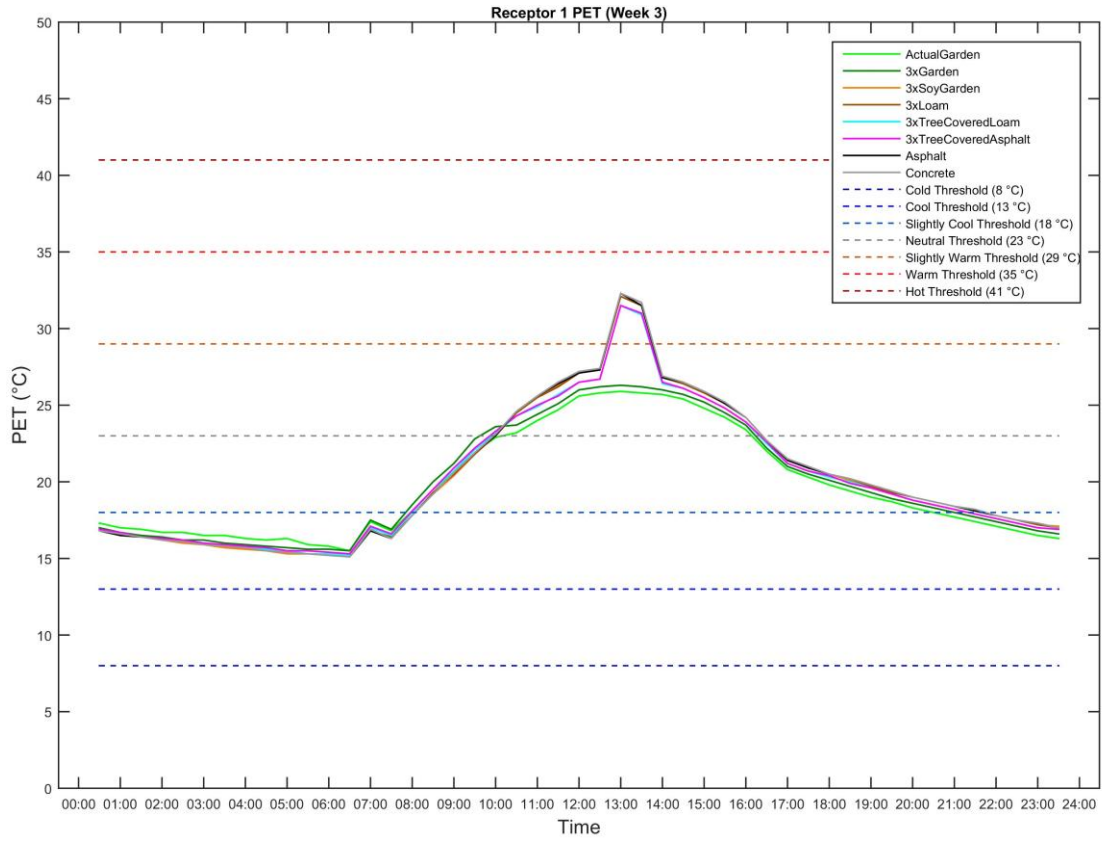


Figure 3.11: The Diurnal Cycle of the Physiological Equivalent Temperature (PET) of Receptor 1 for Week 3.

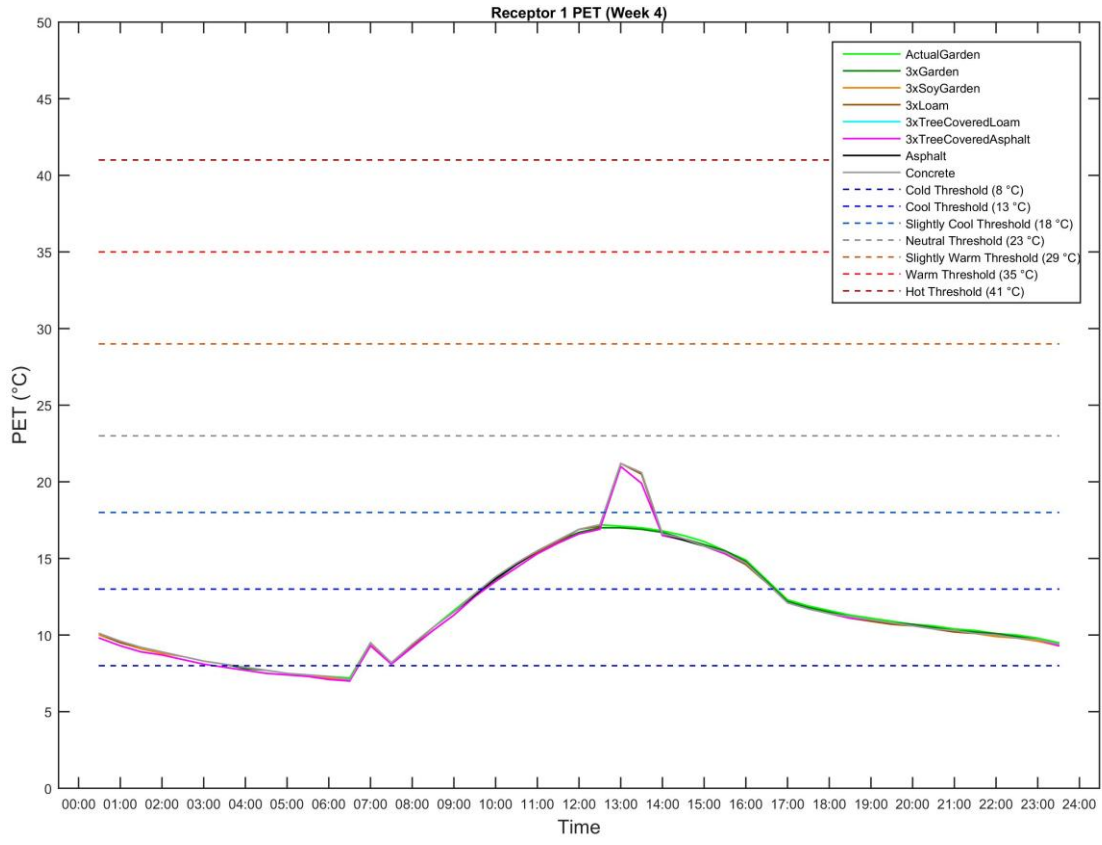


Figure 3.12: The Diurnal Cycle of the Physiological Equivalent Temperature (PET) of Receptor 1 for Week 4.

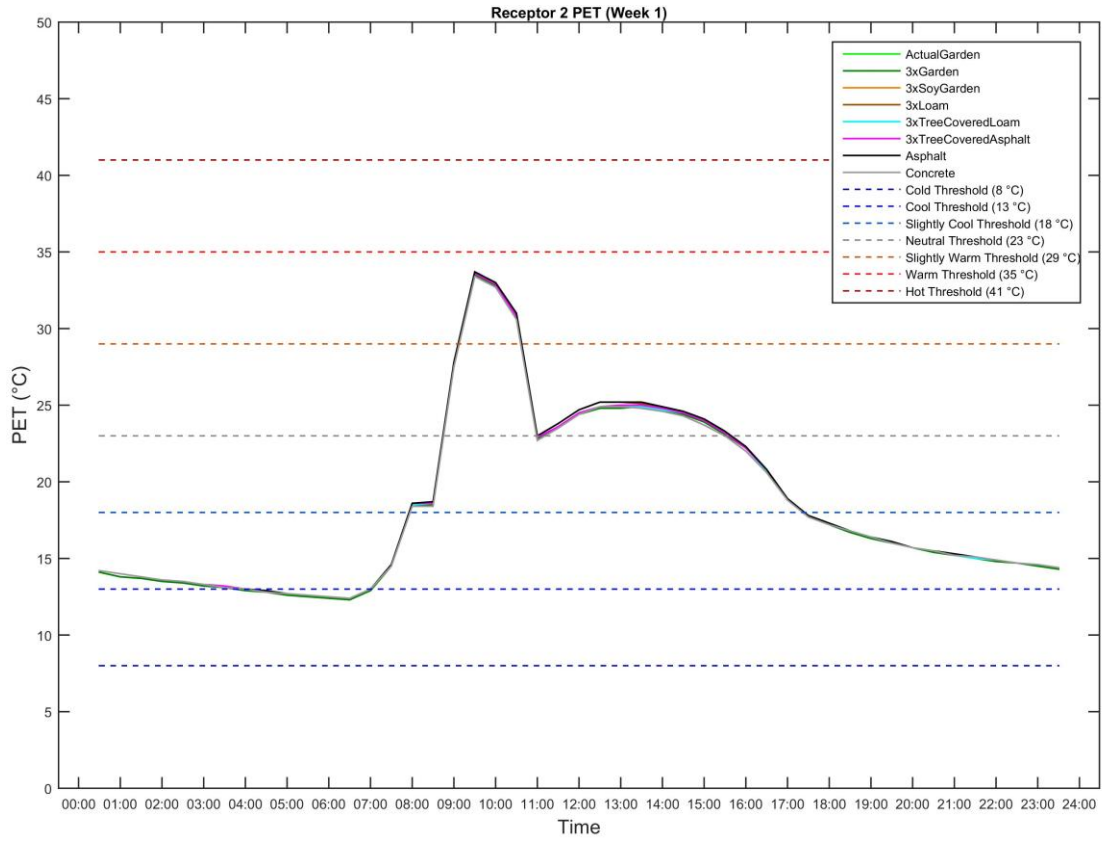


Figure 3.13: The Diurnal Cycle of the Physiological Equivalent Temperature (PET) of Receptor 2 for Week 1.

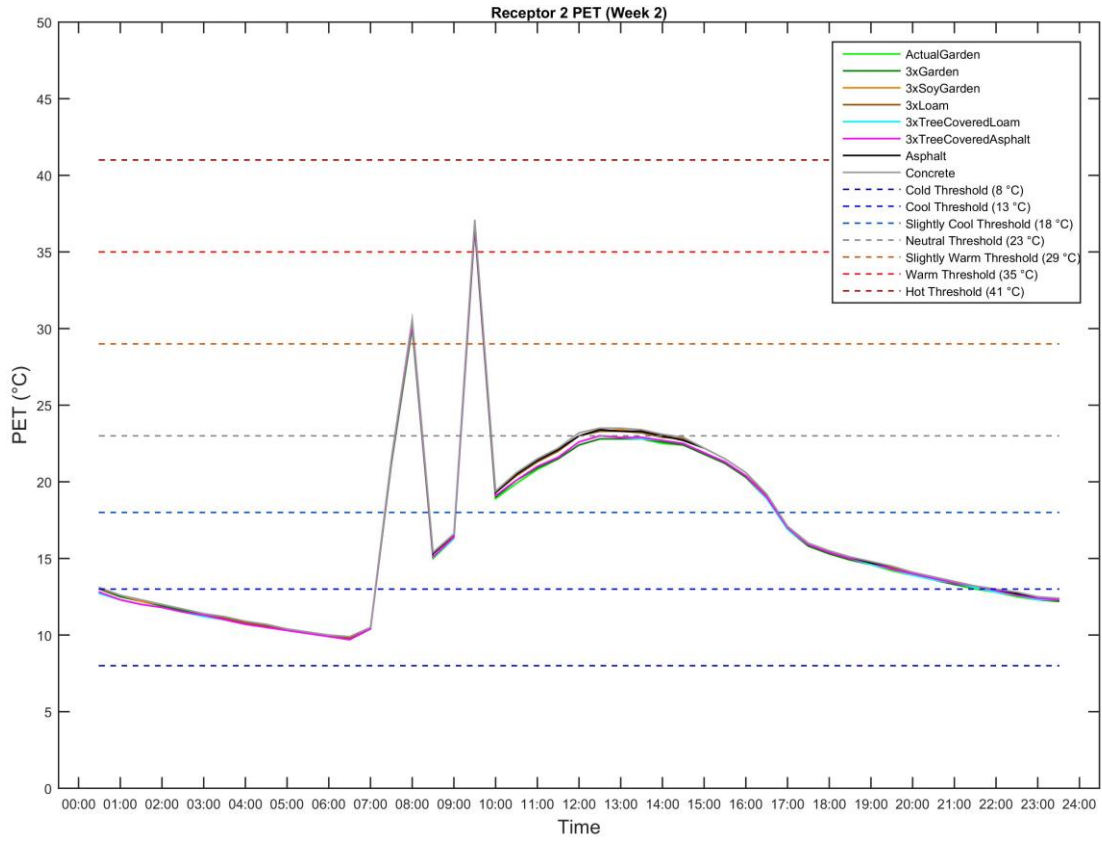


Figure 3.14: The Diurnal Cycle of the Physiological Equivalent Temperature (PET) of Receptor 2 for Week 2.

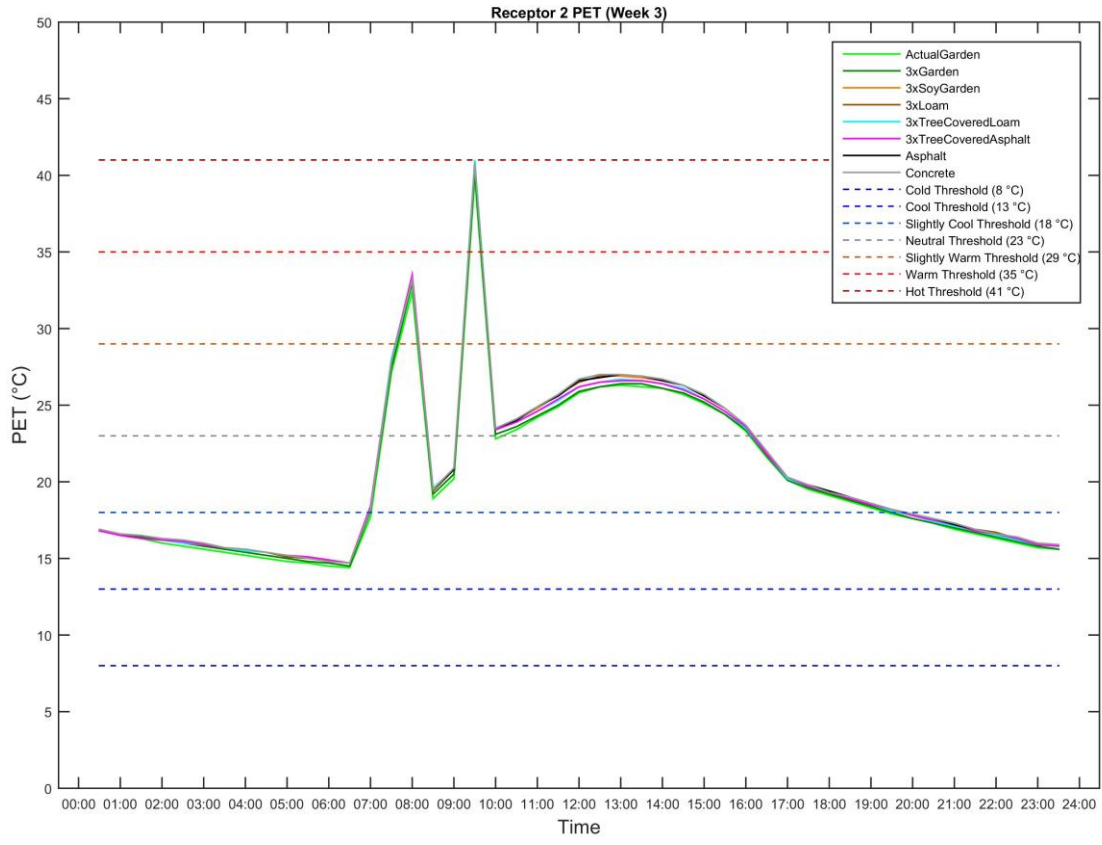


Figure 3.15: The Diurnal Cycle of the Physiological Equivalent Temperature (PET) of Receptor 2 for Week 3.

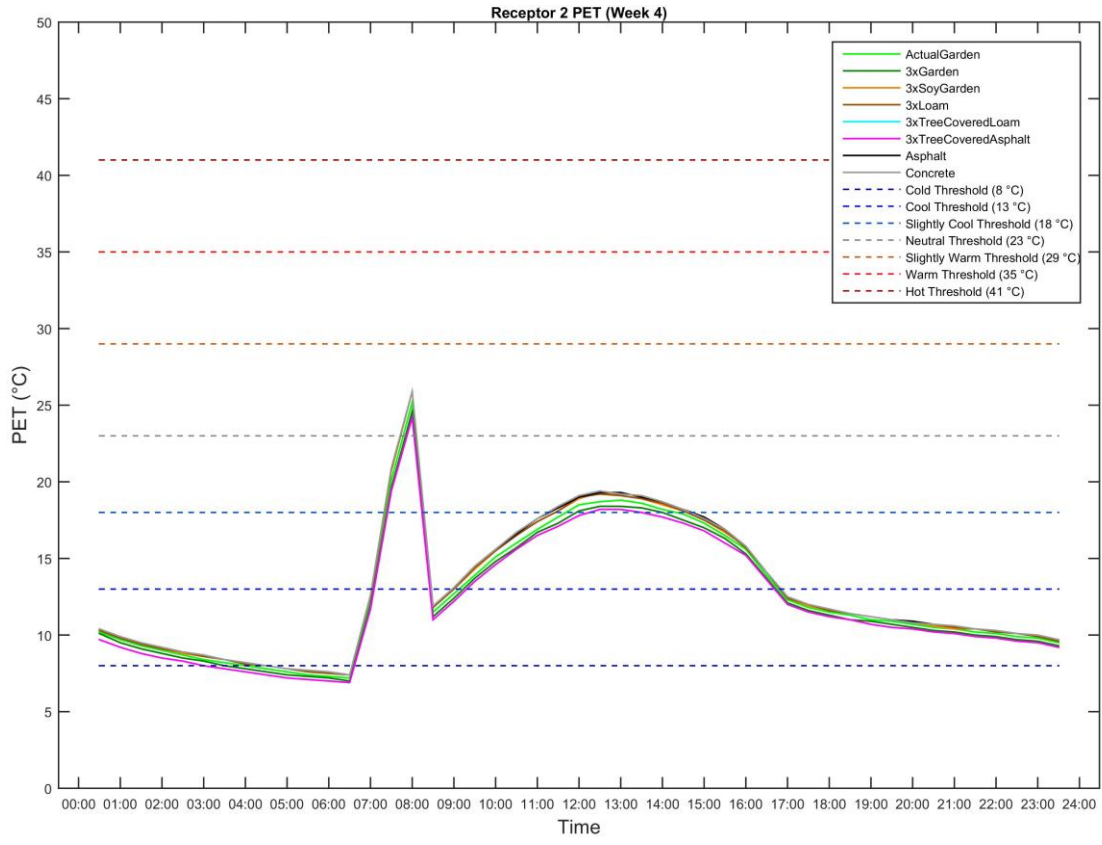


Figure 3.16: The Diurnal Cycle of the Physiological Equivalent Temperature (PET) of Receptor 2 for Week 4.

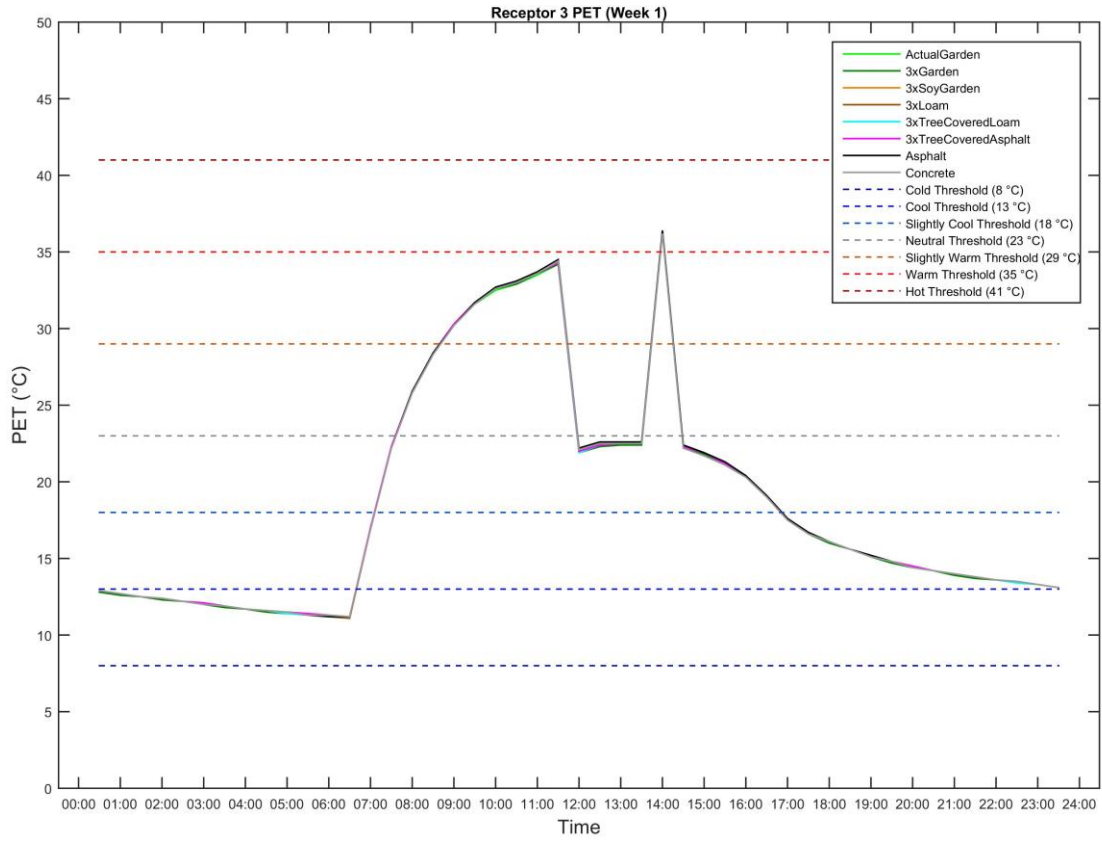


Figure 3.17: The Diurnal Cycle of the Physiological Equivalent Temperature (PET) of Receptor 3 for Week 1.

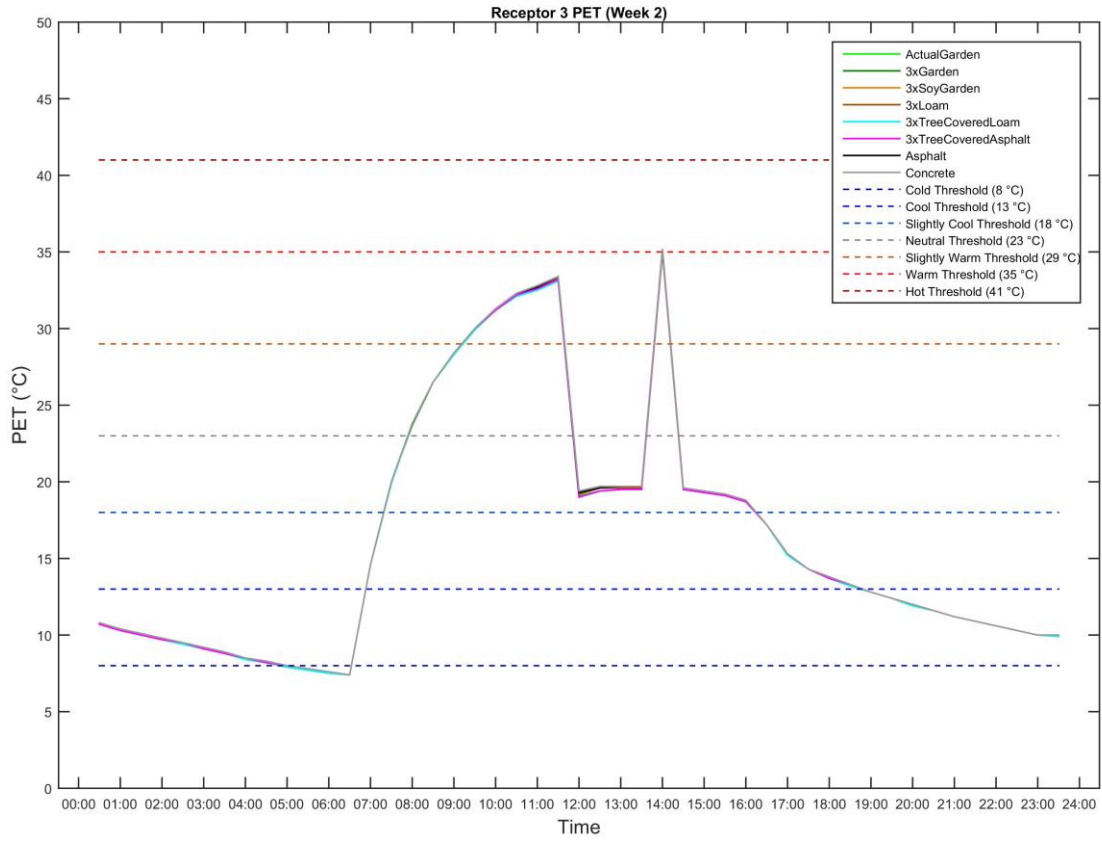


Figure 3.18: The Diurnal Cycle of the Physiological Equivalent Temperature (PET) of Receptor 3 for Week 2.

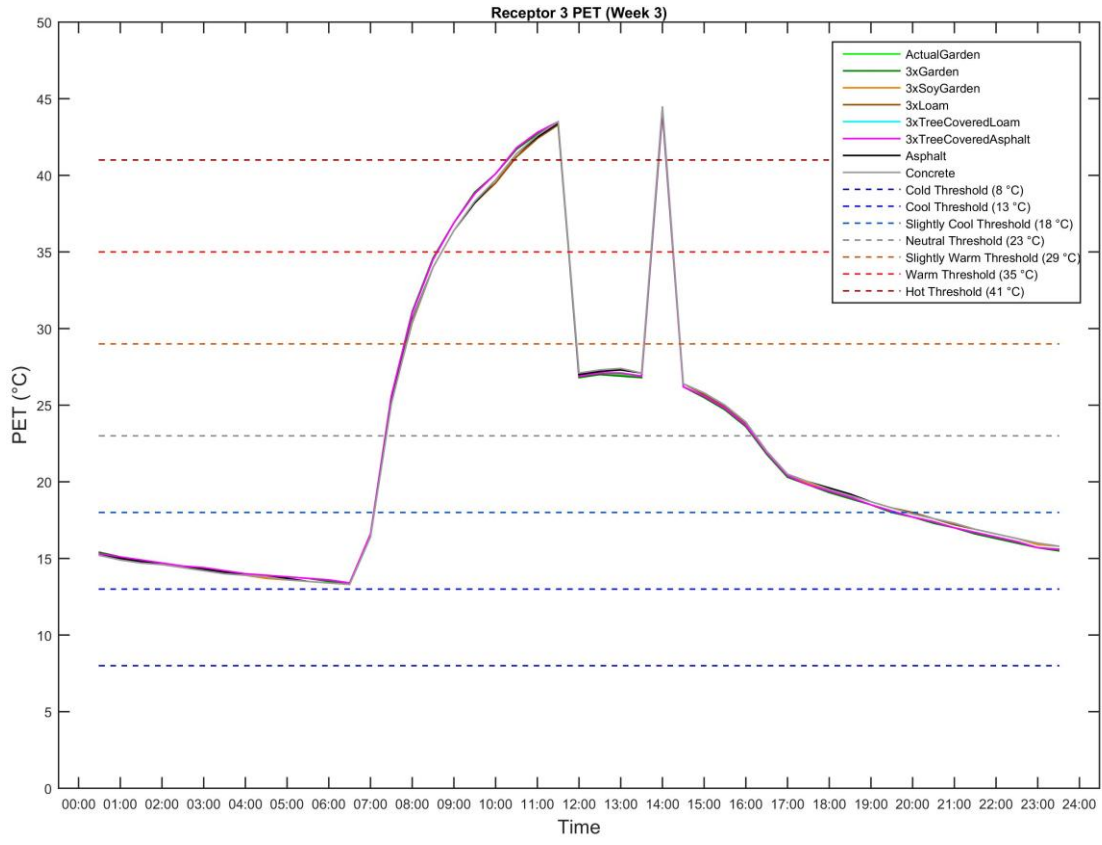


Figure 3.19: The Diurnal Cycle of the Physiological Equivalent Temperature (PET) of Receptor 3 for Week 3.

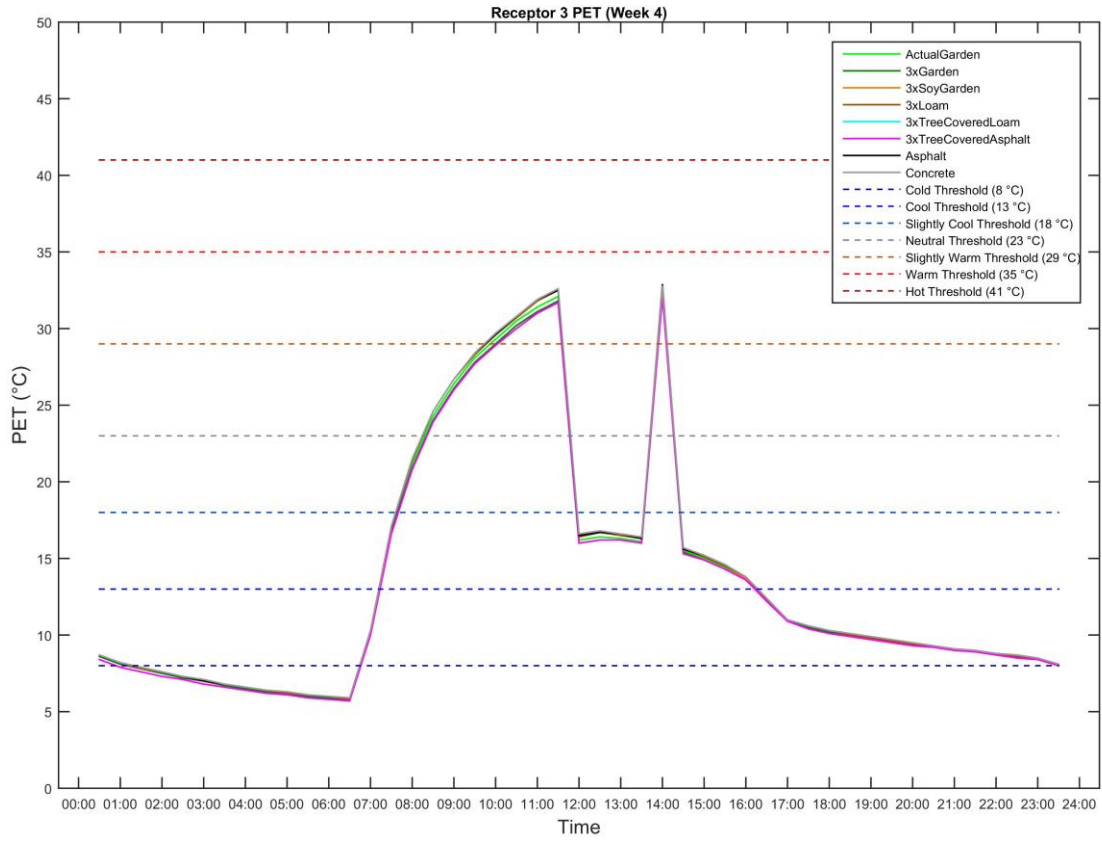


Figure 3.20: The Diurnal Cycle of the Physiological Equivalent Temperature (PET) of Receptor 3 for Week 4.

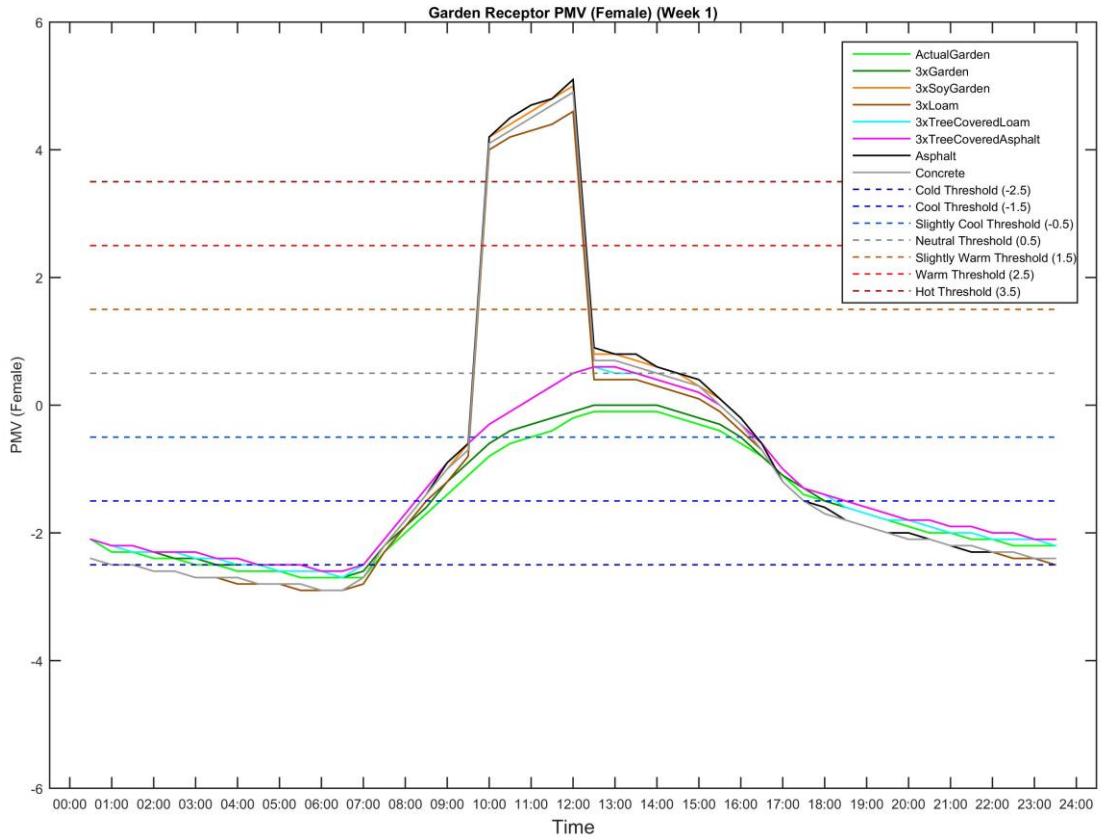


Figure 3.21: The Diurnal Cycle of the Female Predicted Mean Vote (PMV) of the Garden Receptor for Week 1.

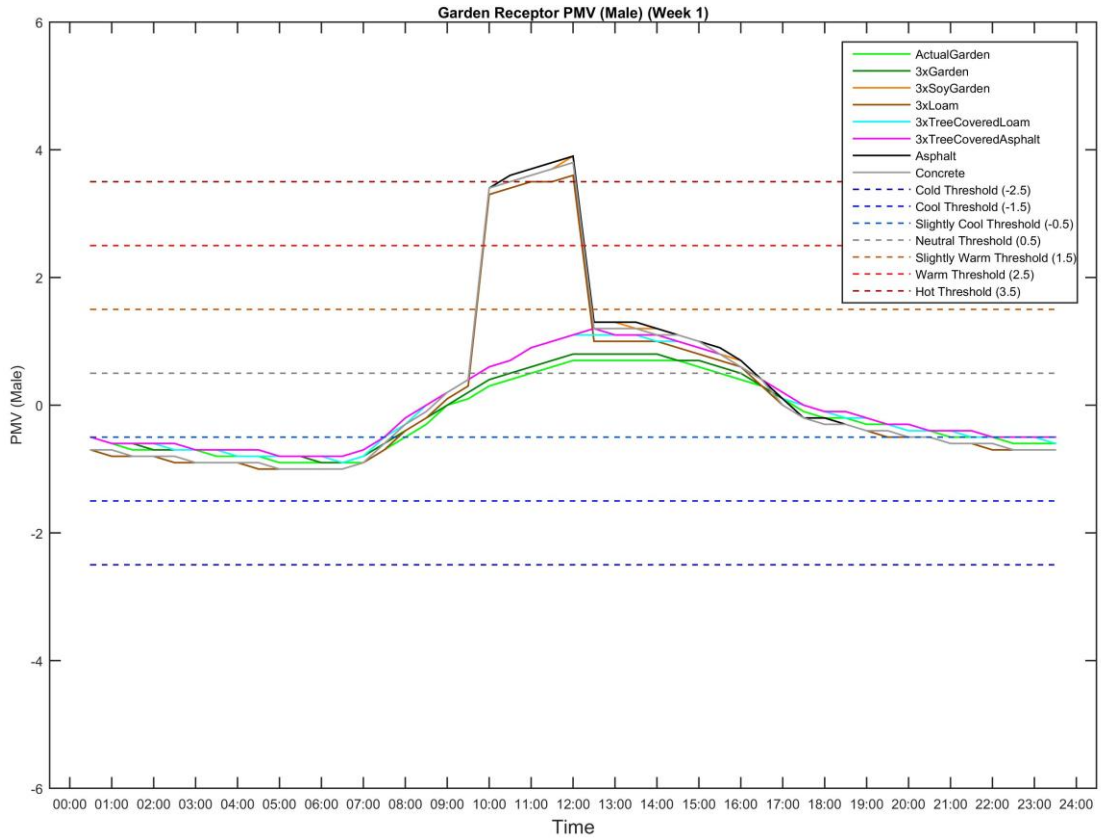


Figure 3.22: The Diurnal Cycle of the Male Predicted Mean Vote (PMV) of the Garden Receptor for Week 1.

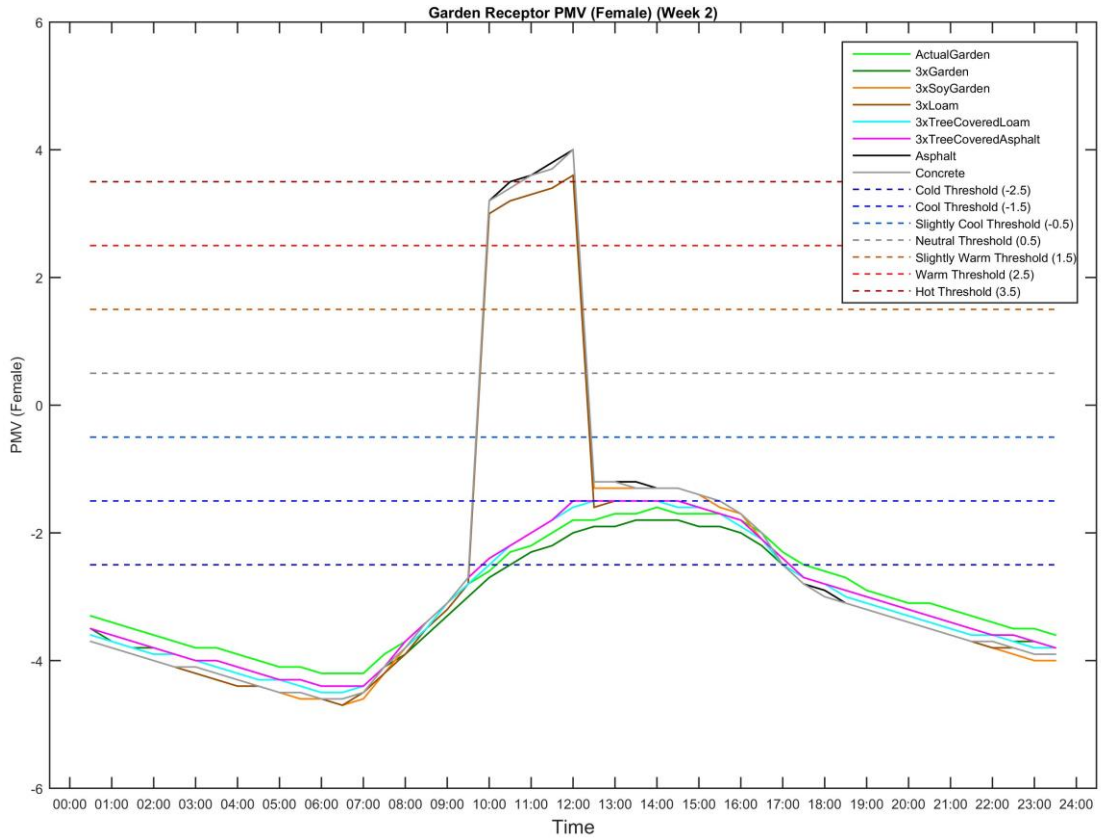


Figure 3.23: The Diurnal Cycle of the Female Predicted Mean Vote (PMV) of the Garden Receptor for Week 2.

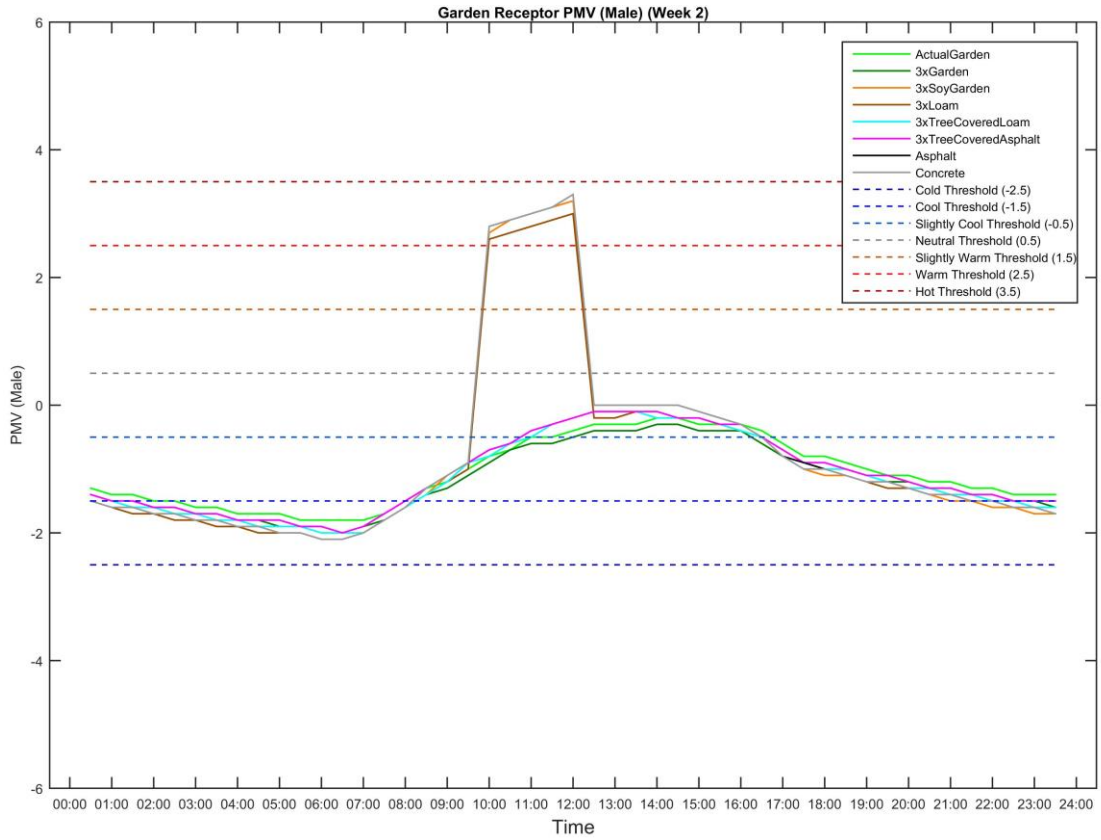


Figure 3.24: The Diurnal Cycle of the Male Predicted Mean Vote (PMV) of the Garden Receptor for Week 2.

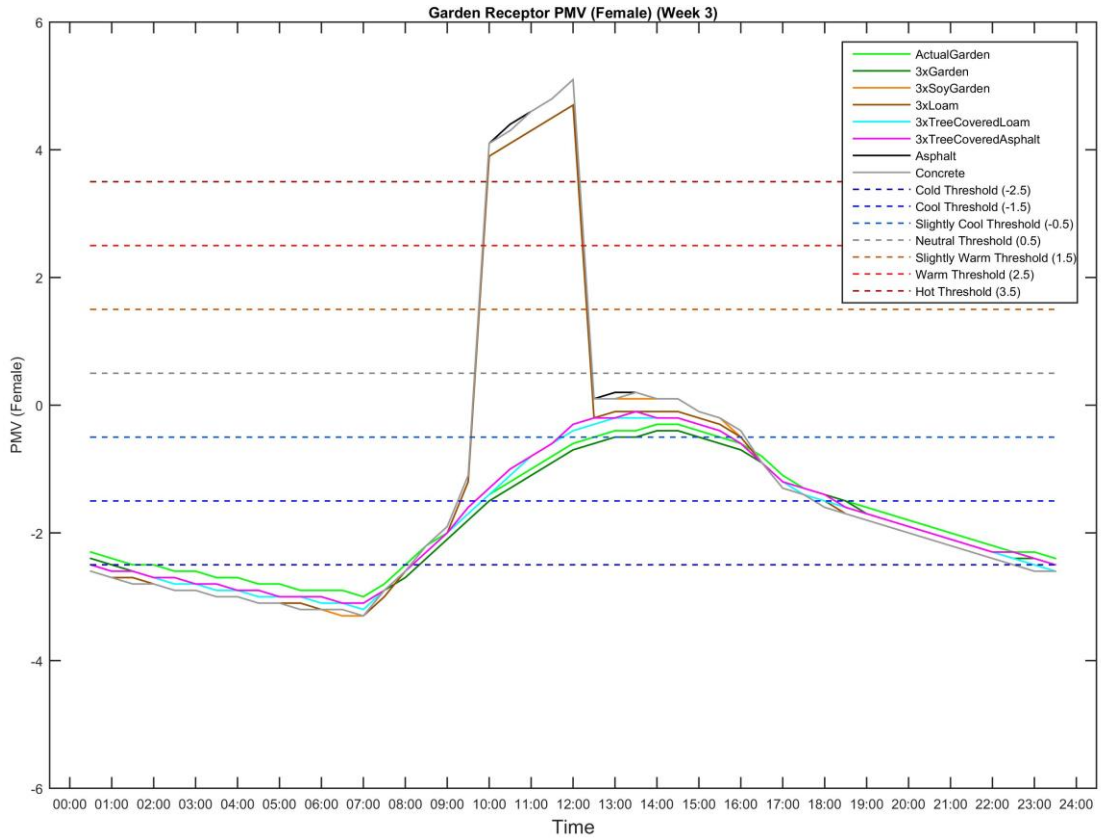


Figure 3.25: The Diurnal Cycle of the Female Predicted Mean Vote (PMV) of the Garden Receptor for Week 3.

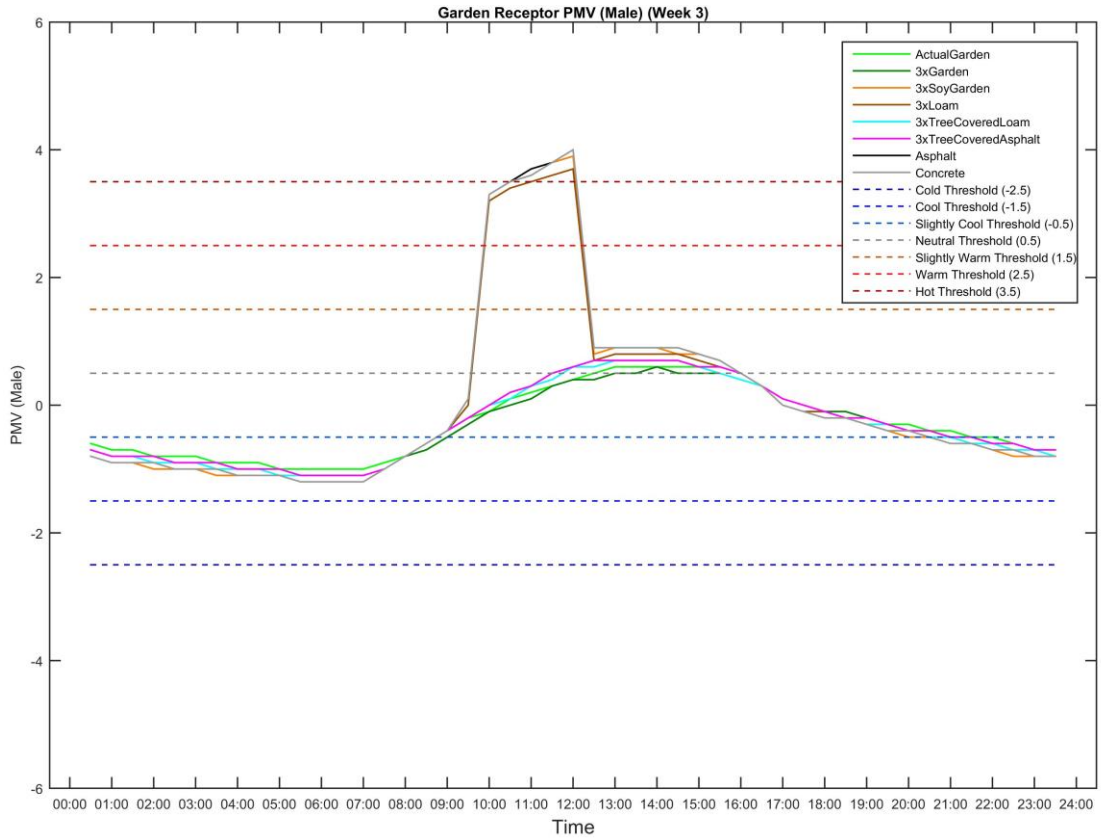


Figure 3.26: The Diurnal Cycle of the Male Predicted Mean Vote (PMV) of the Garden Receptor for Week 3.

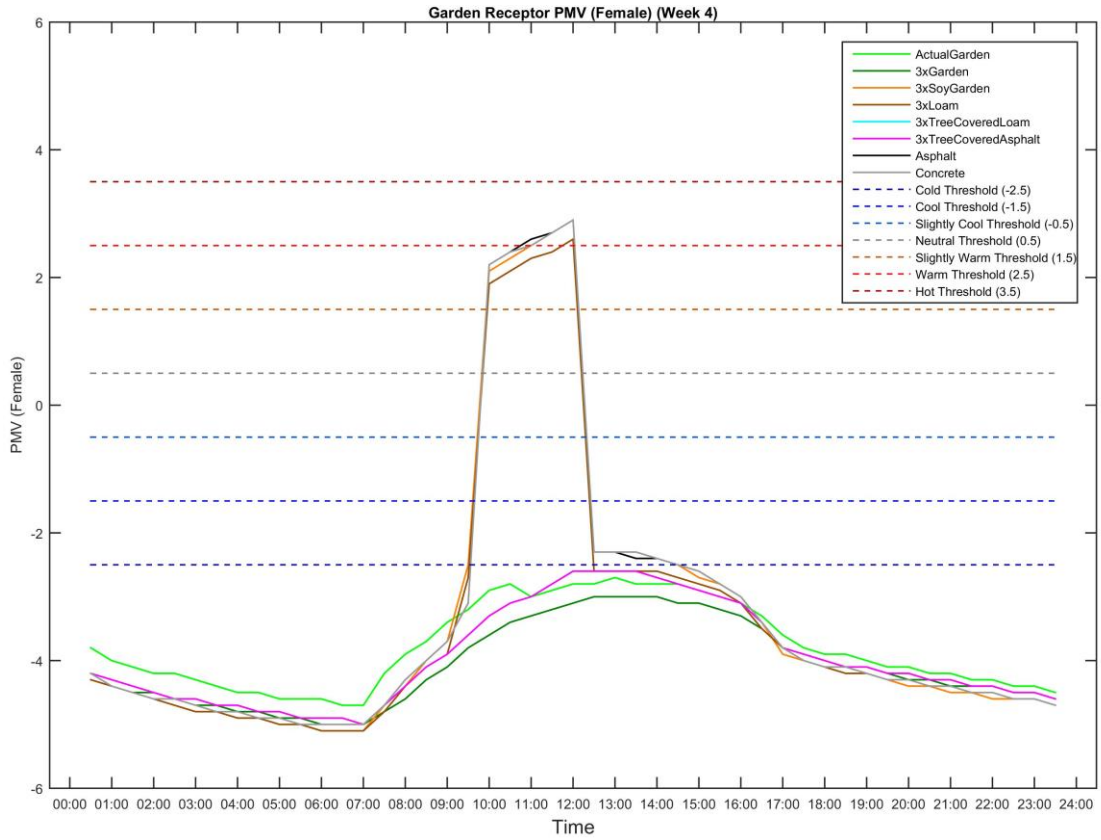


Figure 3.27: The Diurnal Cycle of the Female Predicted Mean Vote (PMV) of the Garden Receptor for Week 4.

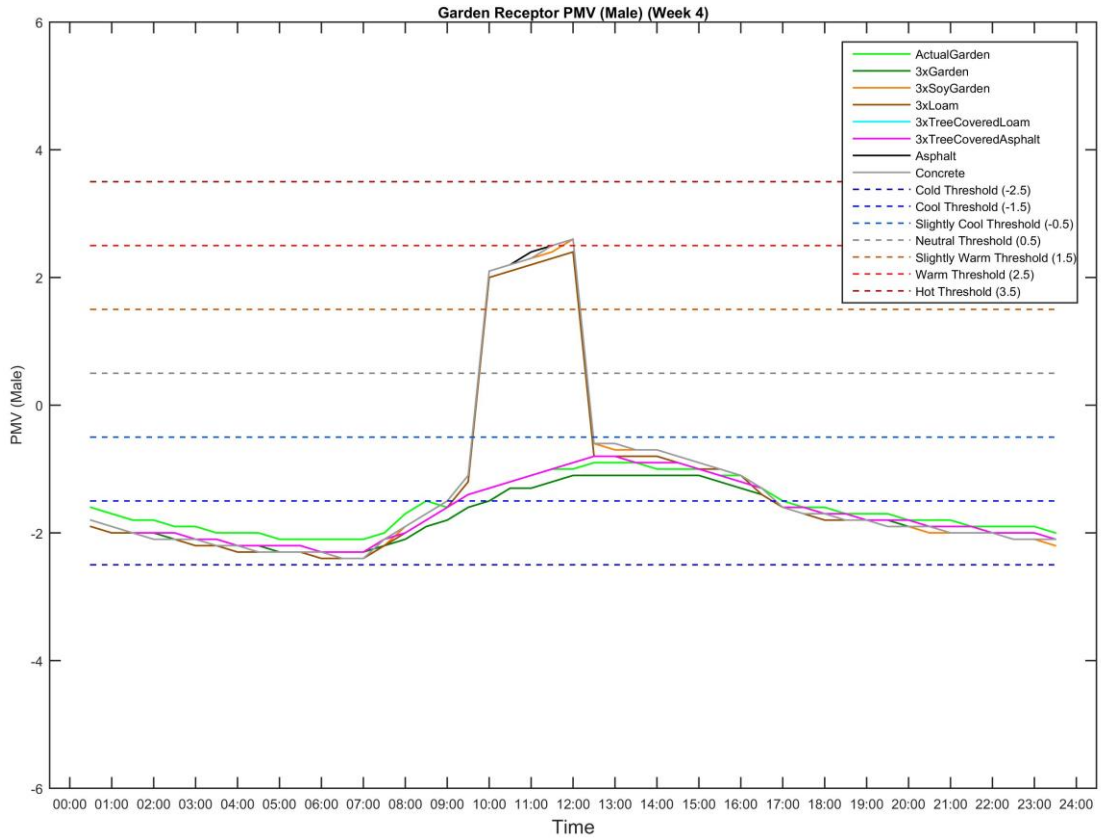


Figure 3.28: The Diurnal Cycle of the Male Predicted Mean Vote (PMV) of the Garden Receptor for Week 4.

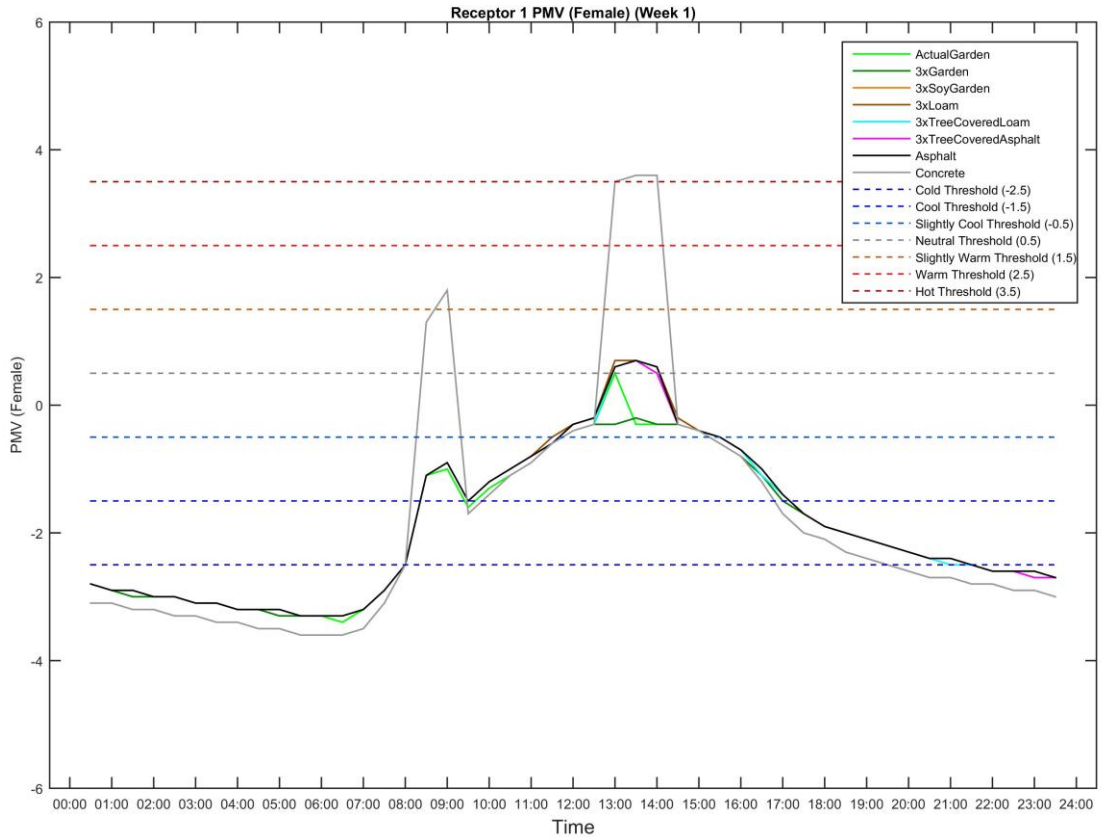


Figure 3.29: The Diurnal Cycle of the Female Predicted Mean Vote (PMV) of Receptor 1 for Week 1.

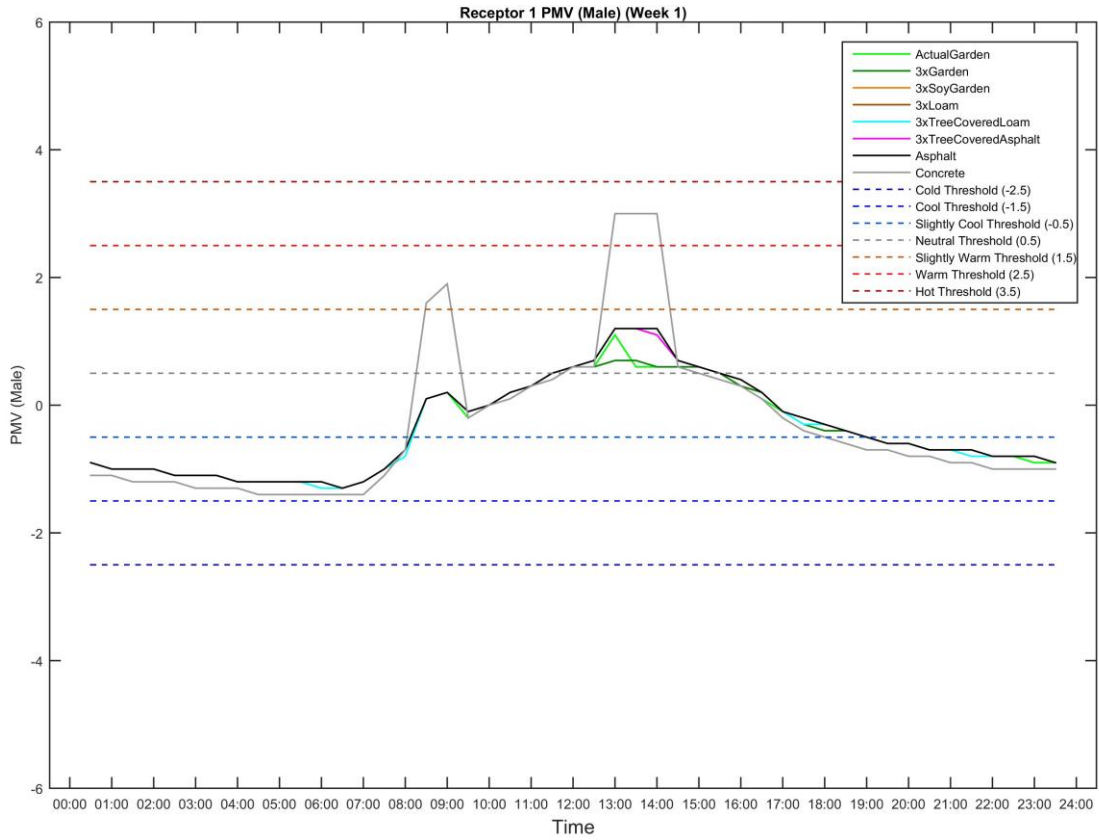


Figure 3.30: The Diurnal Cycle of the Male Predicted Mean Vote (PMV) of Receptor 1 for Week 1.

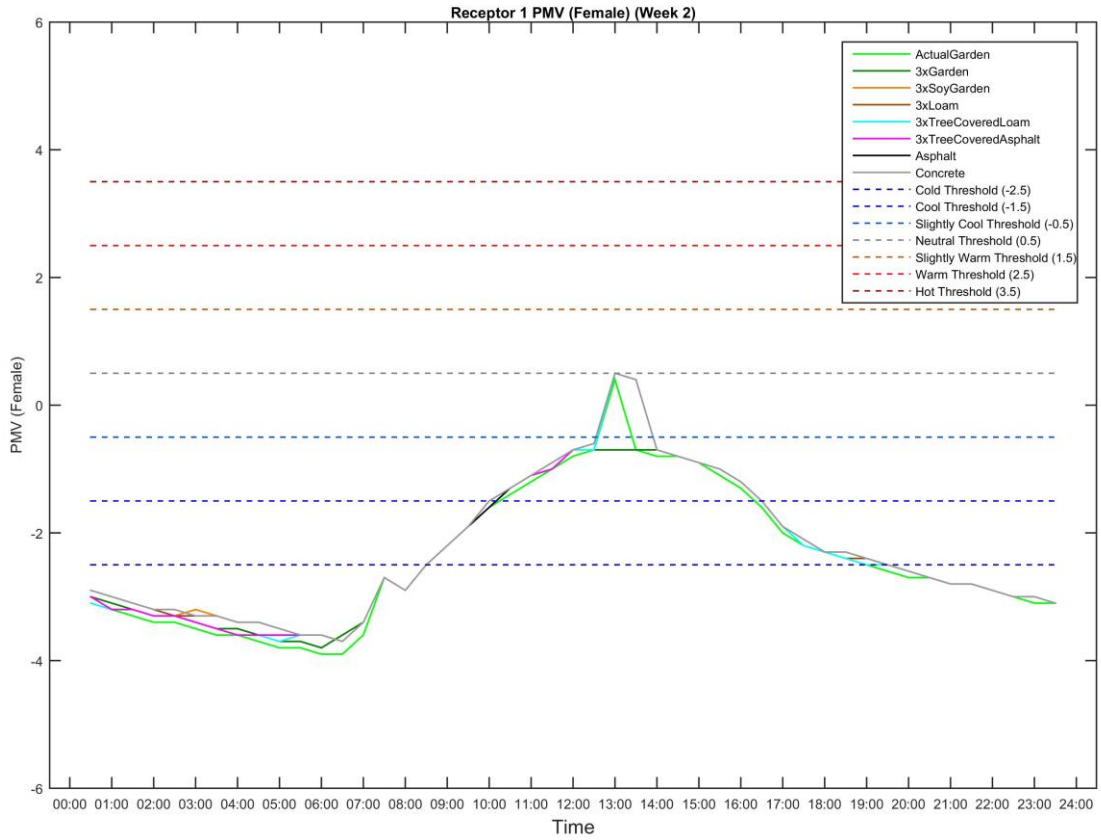


Figure 3.31: The Diurnal Cycle of the Female Predicted Mean Vote (PMV) of Receptor 1 for Week 2.

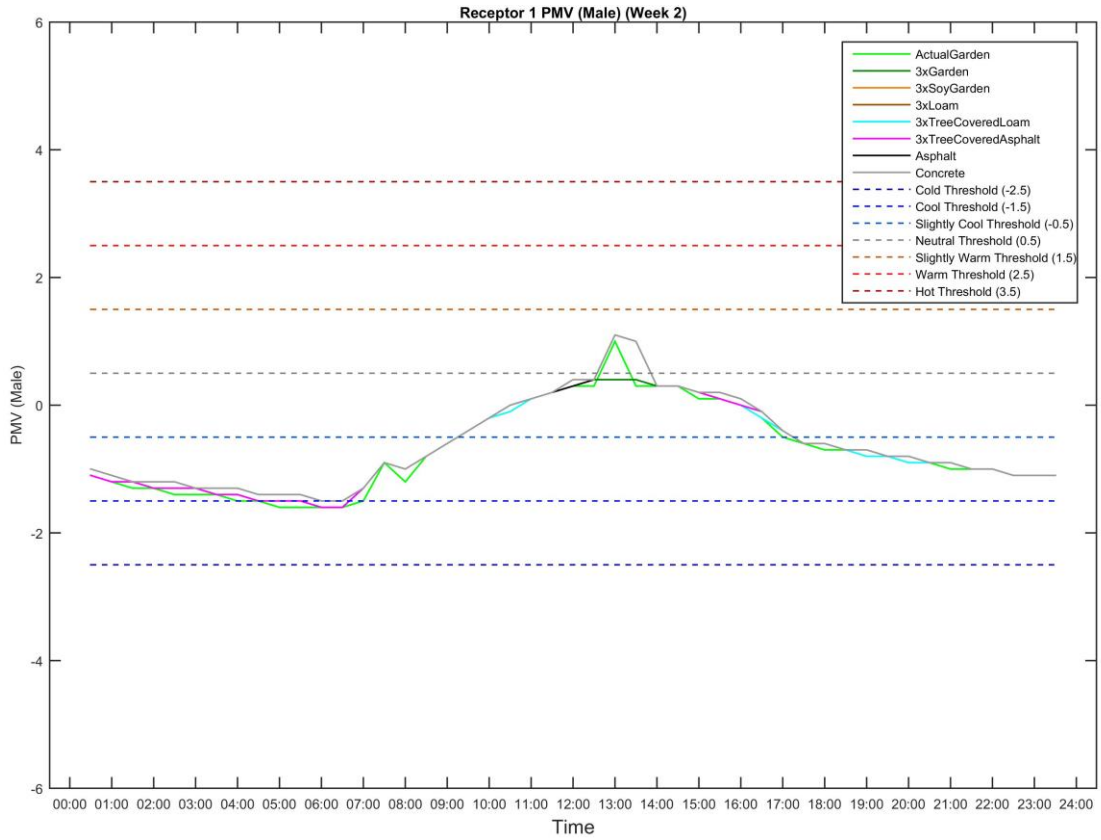


Figure 3.32: The Diurnal Cycle of the Male Predicted Mean Vote (PMV) of Receptor 1 for Week 2.

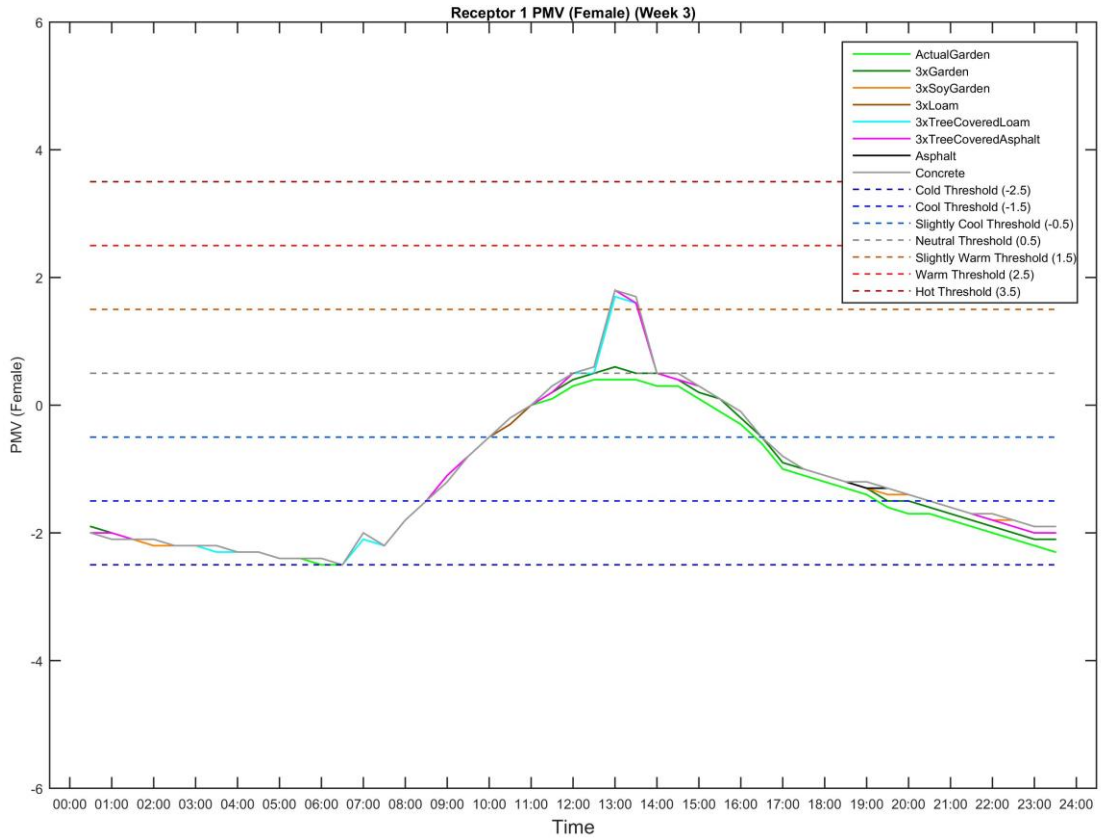


Figure 3.33: The Diurnal Cycle of the Female Predicted Mean Vote (PMV) of Receptor 1 for Week 3.

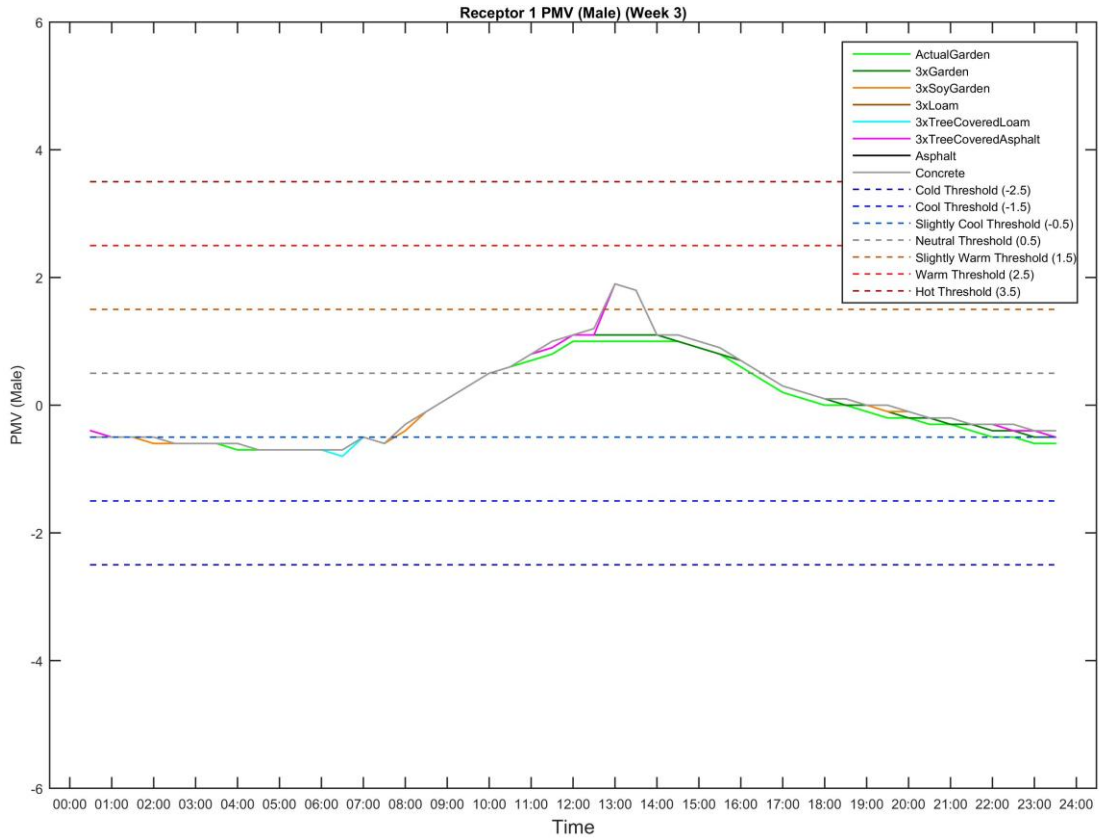


Figure 3.34: The Diurnal Cycle of the Male Predicted Mean Vote (PMV) of Receptor 1 for Week 3.

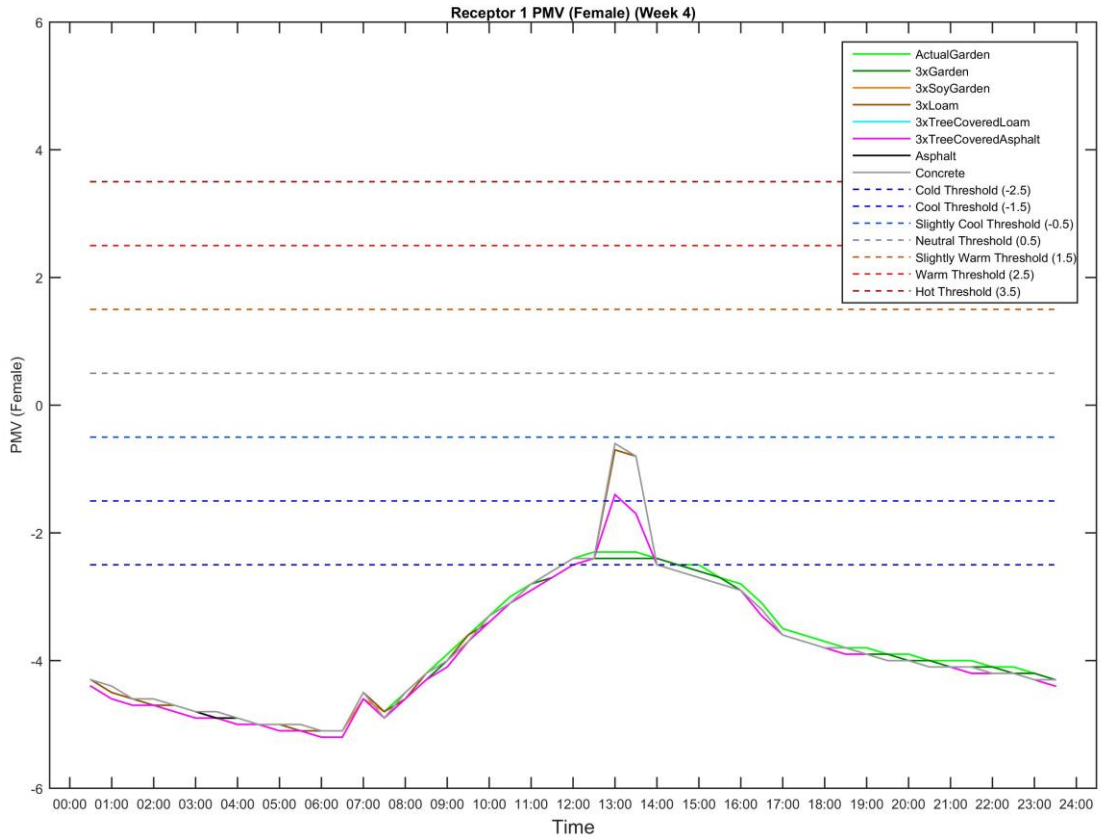


Figure 3.35: The Diurnal Cycle of the Female Predicted Mean Vote (PMV) of Receptor 1 for Week 3.

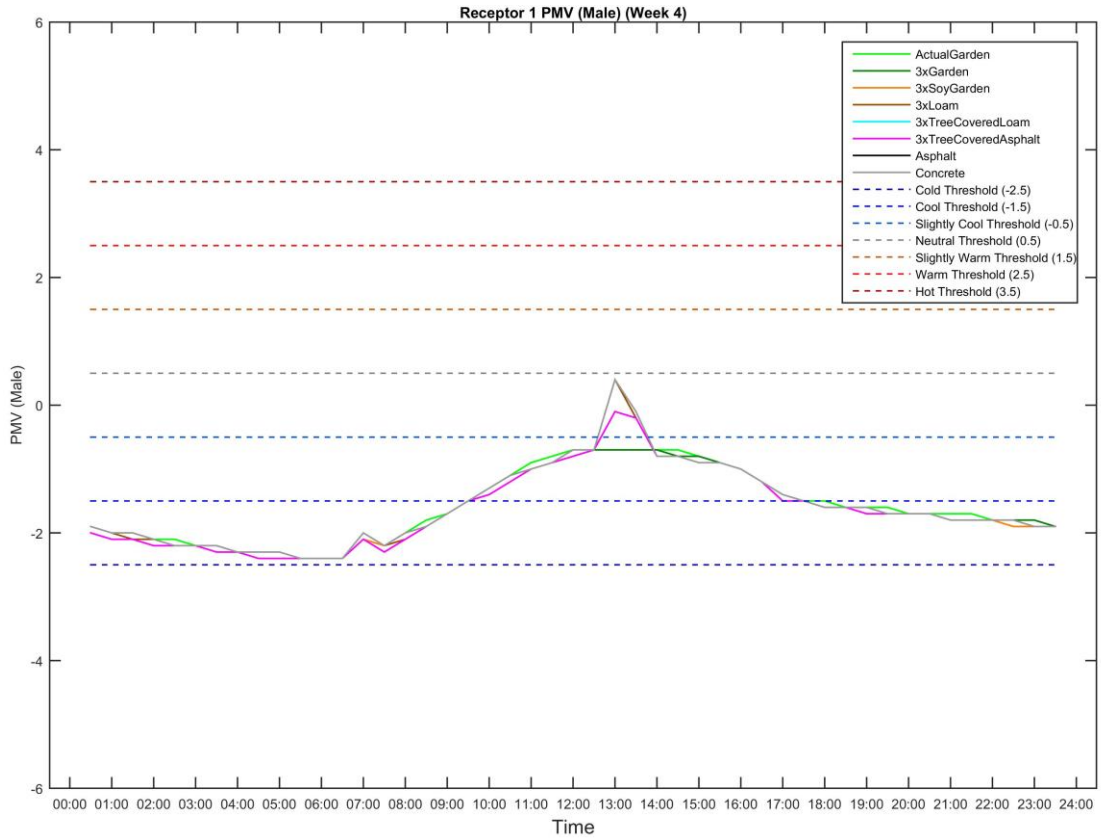


Figure 3.36: The Diurnal Cycle of the Male Predicted Mean Vote (PMV) of Receptor 1 for Week 4.

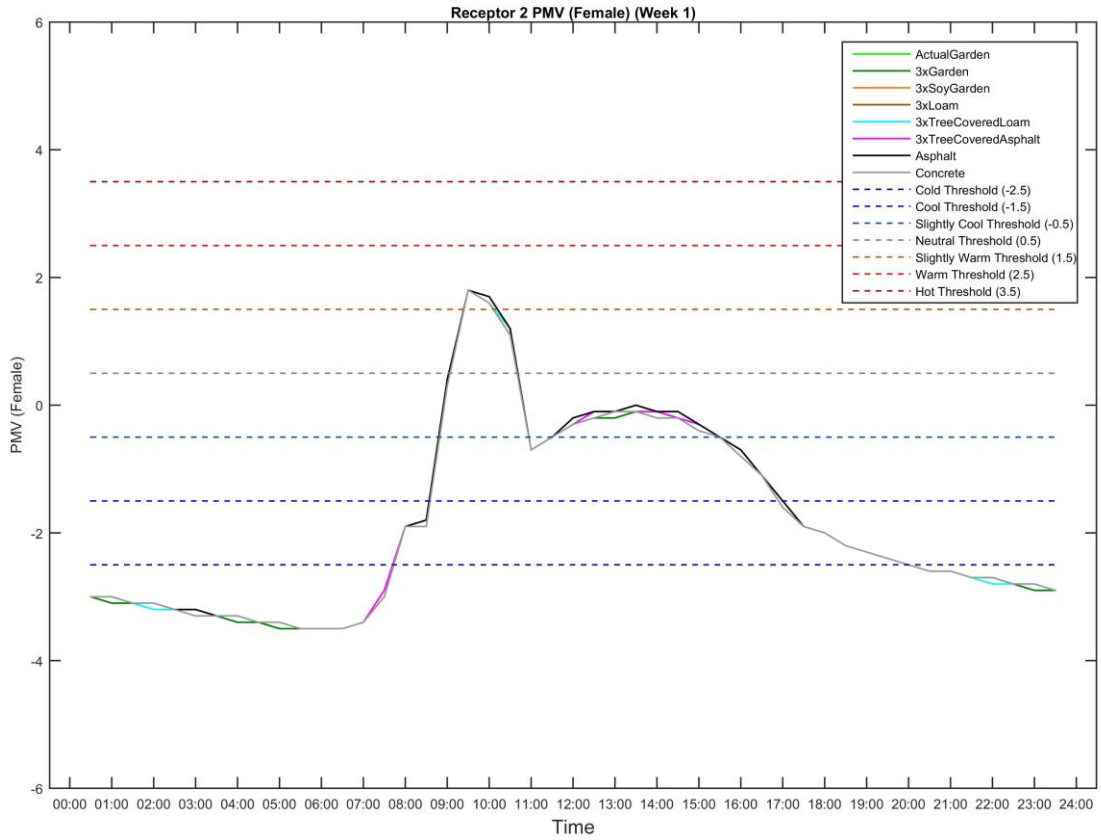


Figure 3.37: The Diurnal Cycle of the Female Predicted Mean Vote (PMV) of Receptor 2 for Week 1.

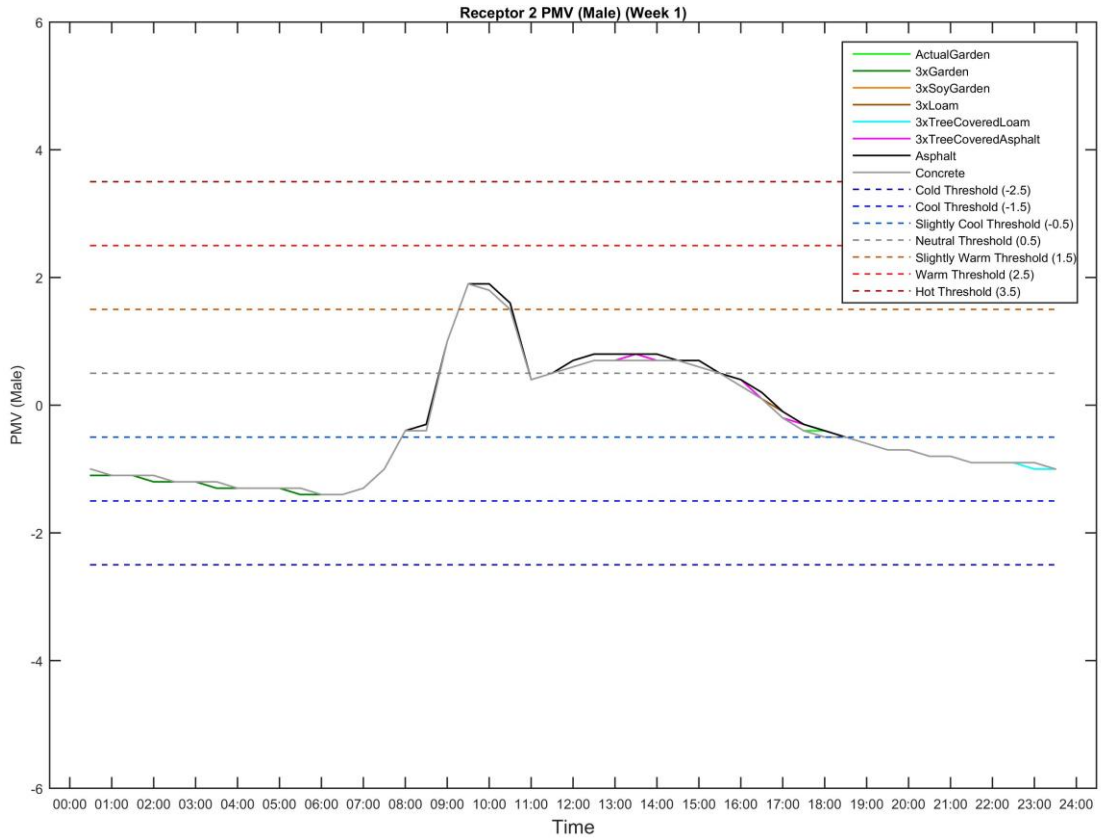


Figure 3.38: The Diurnal Cycle of the Male Predicted Mean Vote (PMV) of Receptor 2 for Week 2.

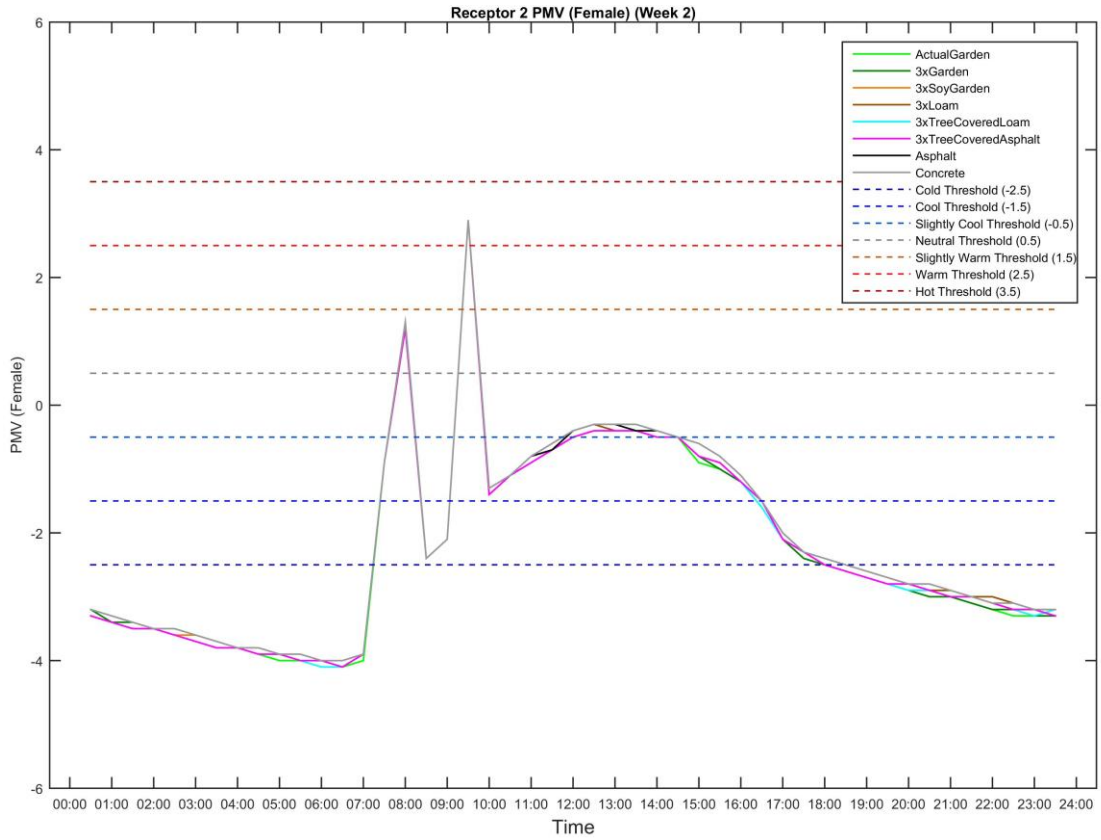


Figure 3.39: The Diurnal Cycle of the Male Predicted Mean Vote (PMV) of Receptor 2 for Week 2.

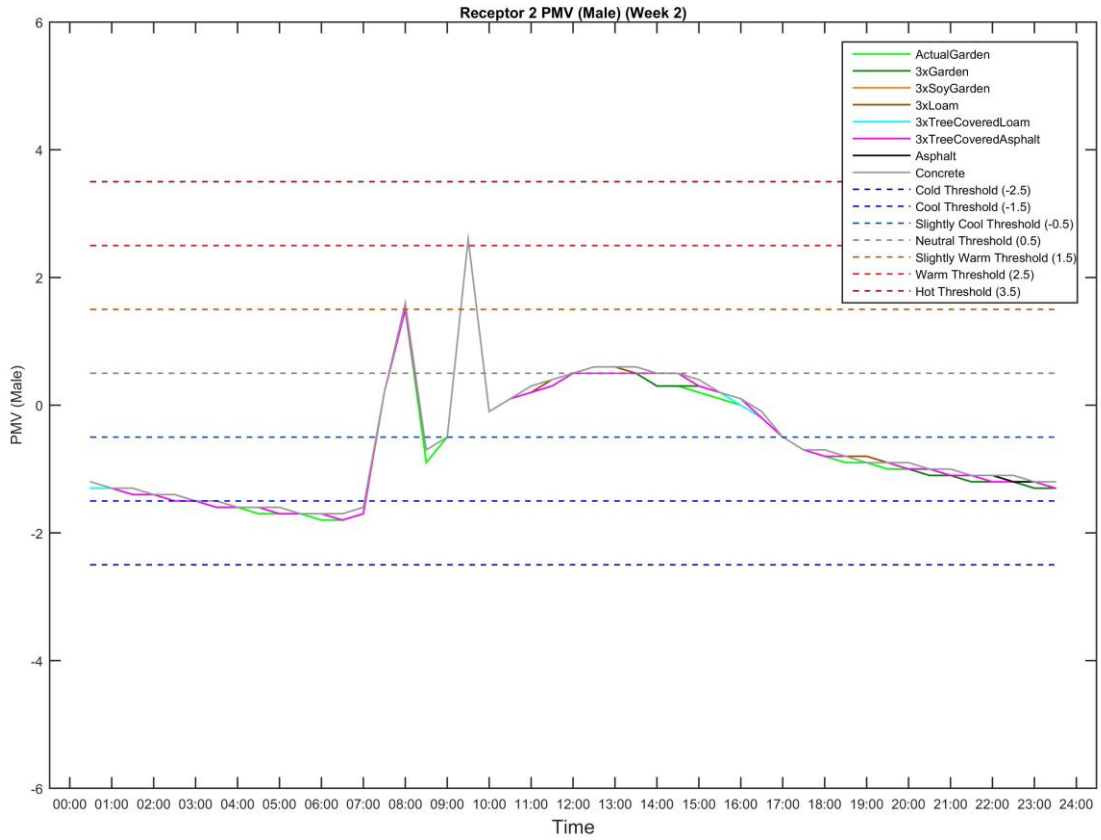


Figure 3.40: The Diurnal Cycle of the Male Predicted Mean Vote (PMV) of Receptor 2 for Week 2.

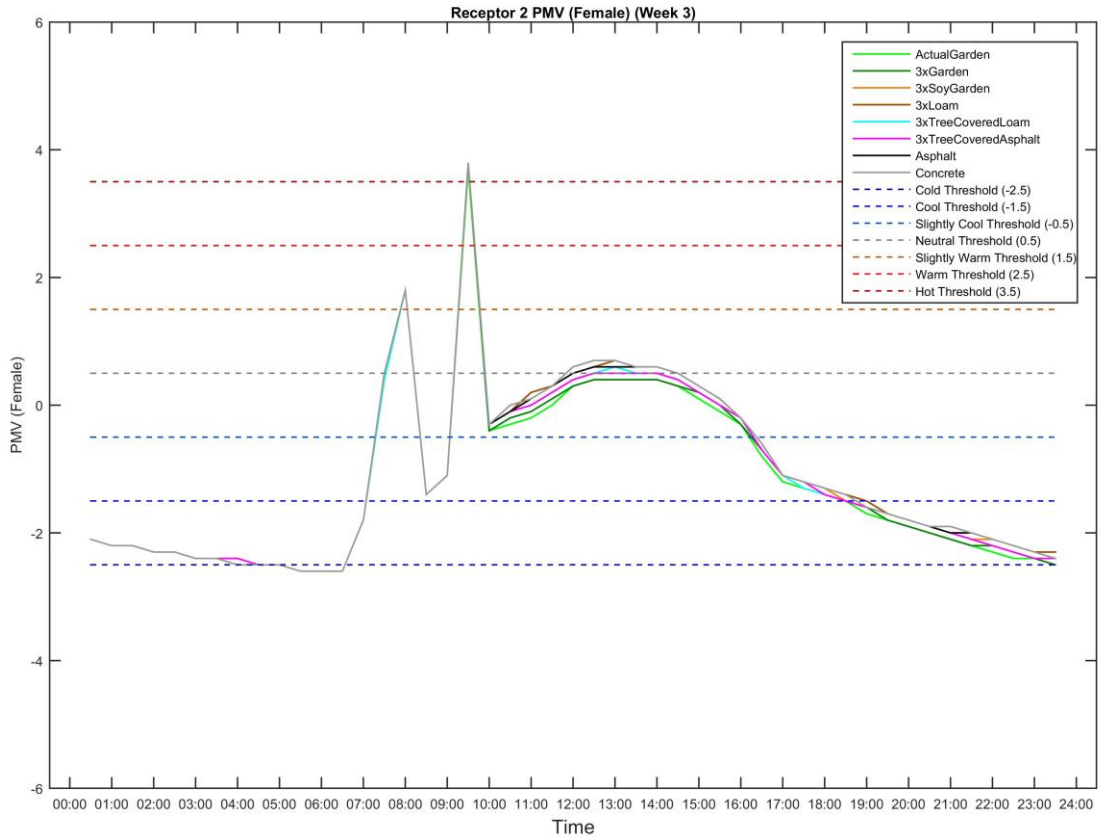


Figure 3.41: The Diurnal Cycle of the Female Predicted Mean Vote (PMV) of Receptor 2 for Week 3.

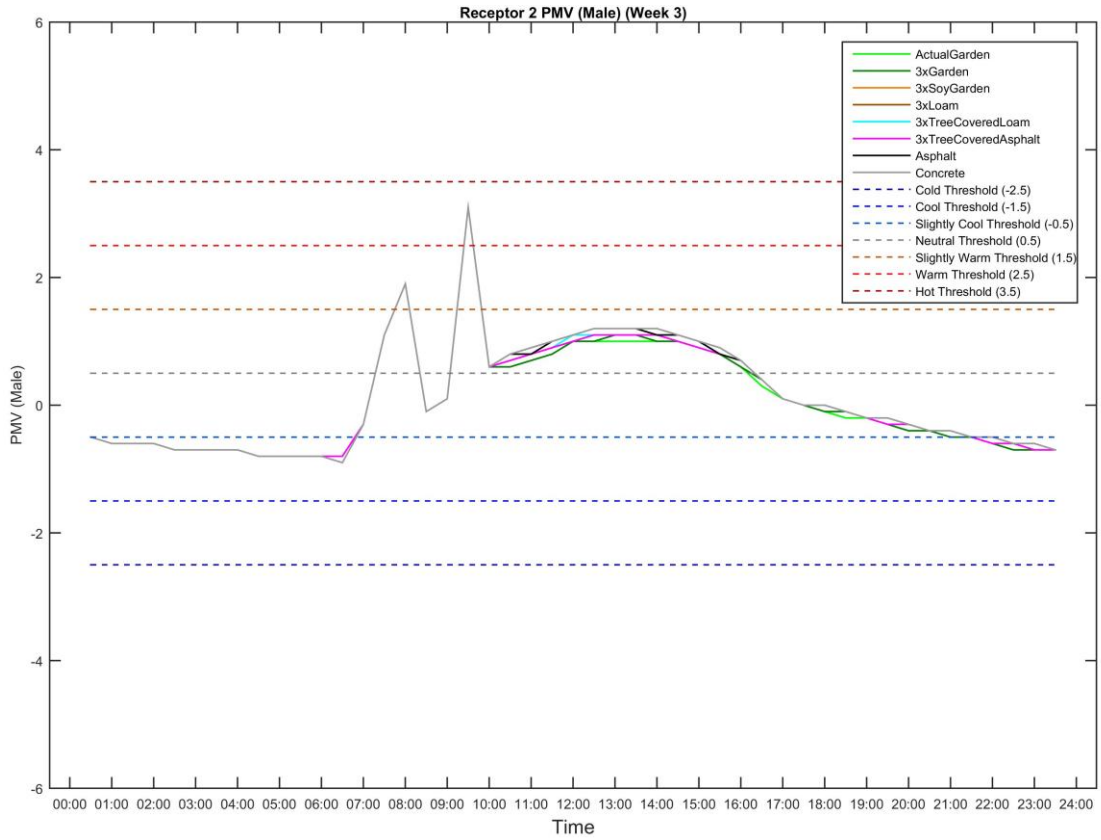


Figure 3.42: The Diurnal Cycle of the Male Predicted Mean Vote (PMV) of Receptor 2 for Week 3.

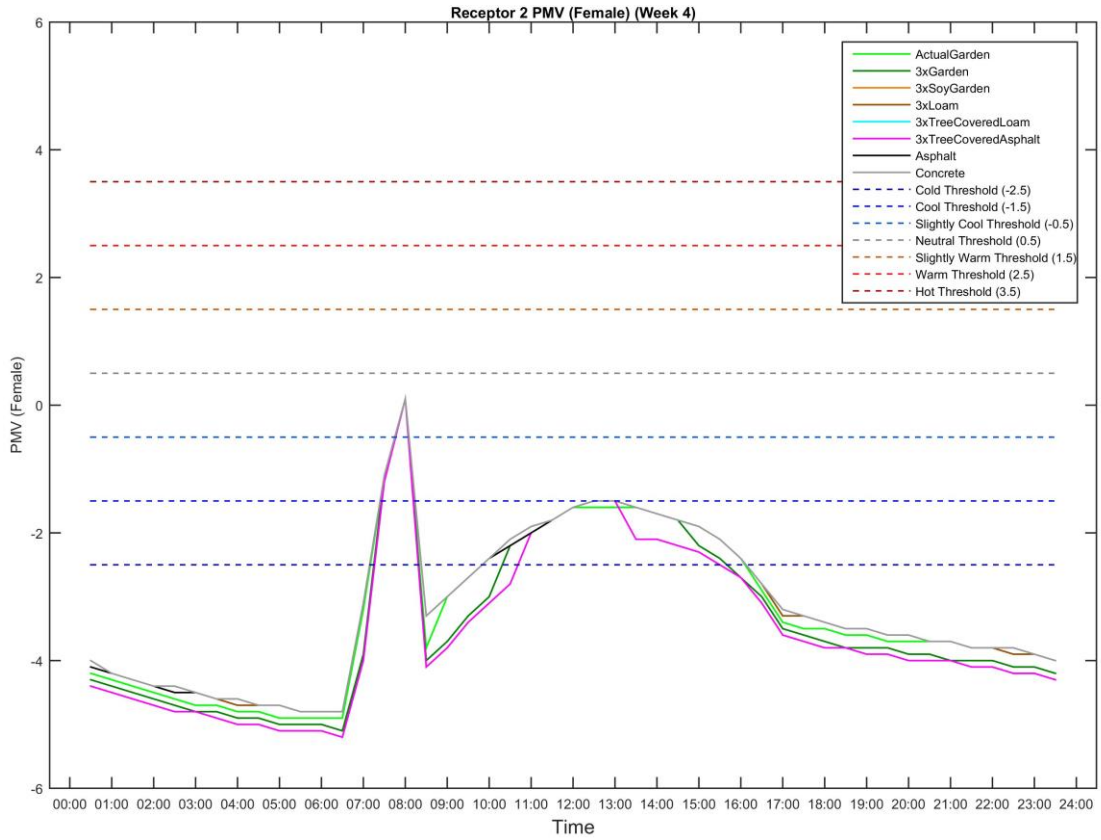


Figure 3.43: The Diurnal Cycle of the Female Predicted Mean Vote (PMV) of Receptor 2 for Week 4.

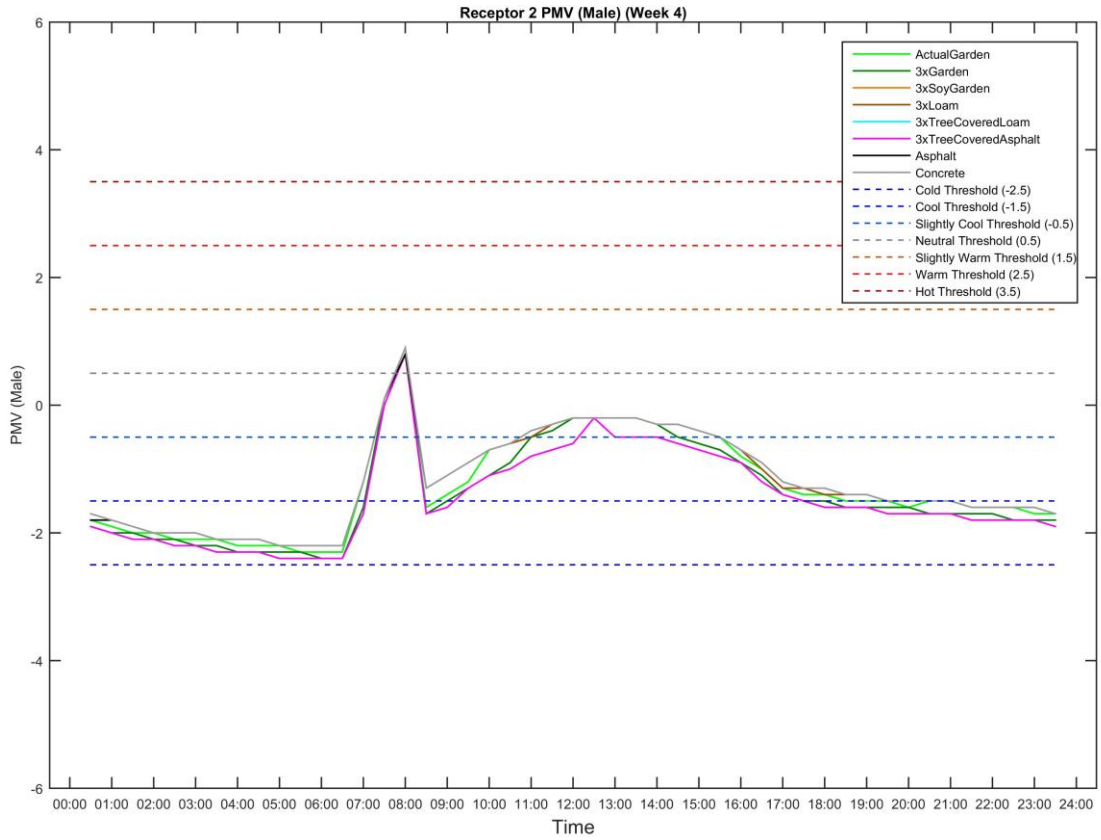


Figure 3.44: The Diurnal Cycle of the Male Predicted Mean Vote (PMV) of Receptor 2 for Week 4.

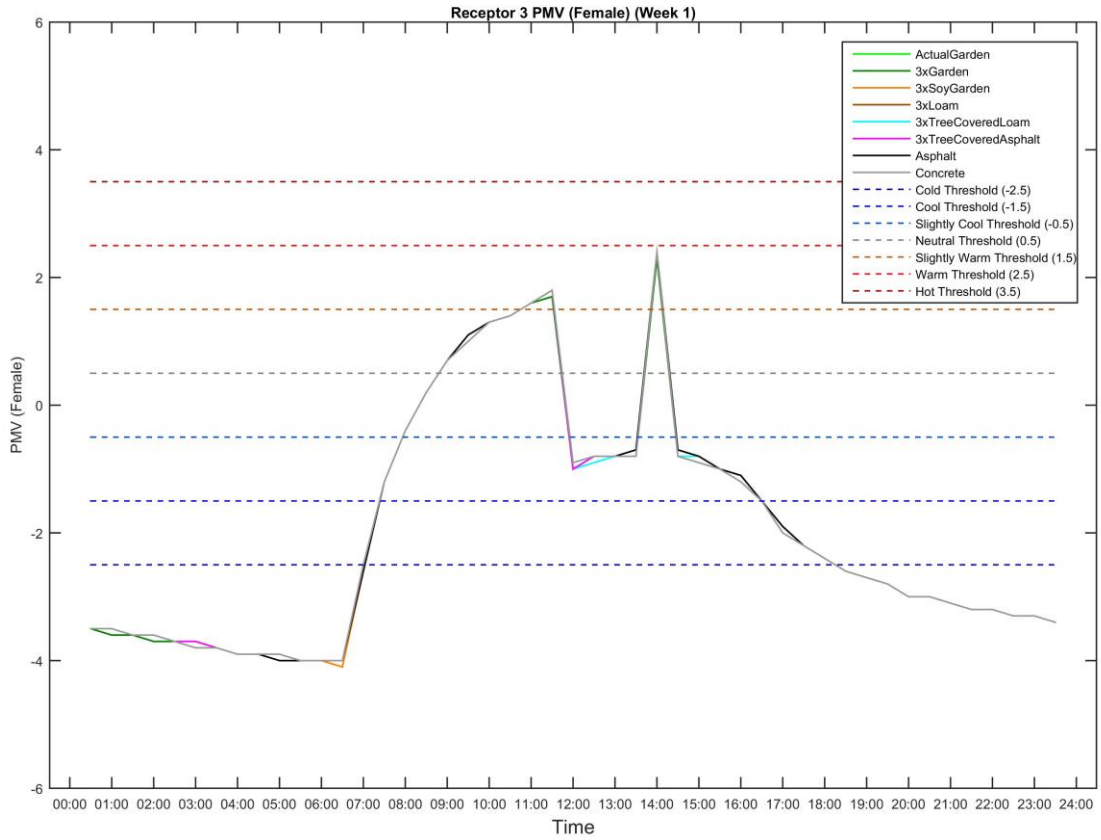


Figure 3.45: The Diurnal Cycle of the Female Predicted Mean Vote (PMV) of Receptor 3 for Week 1.

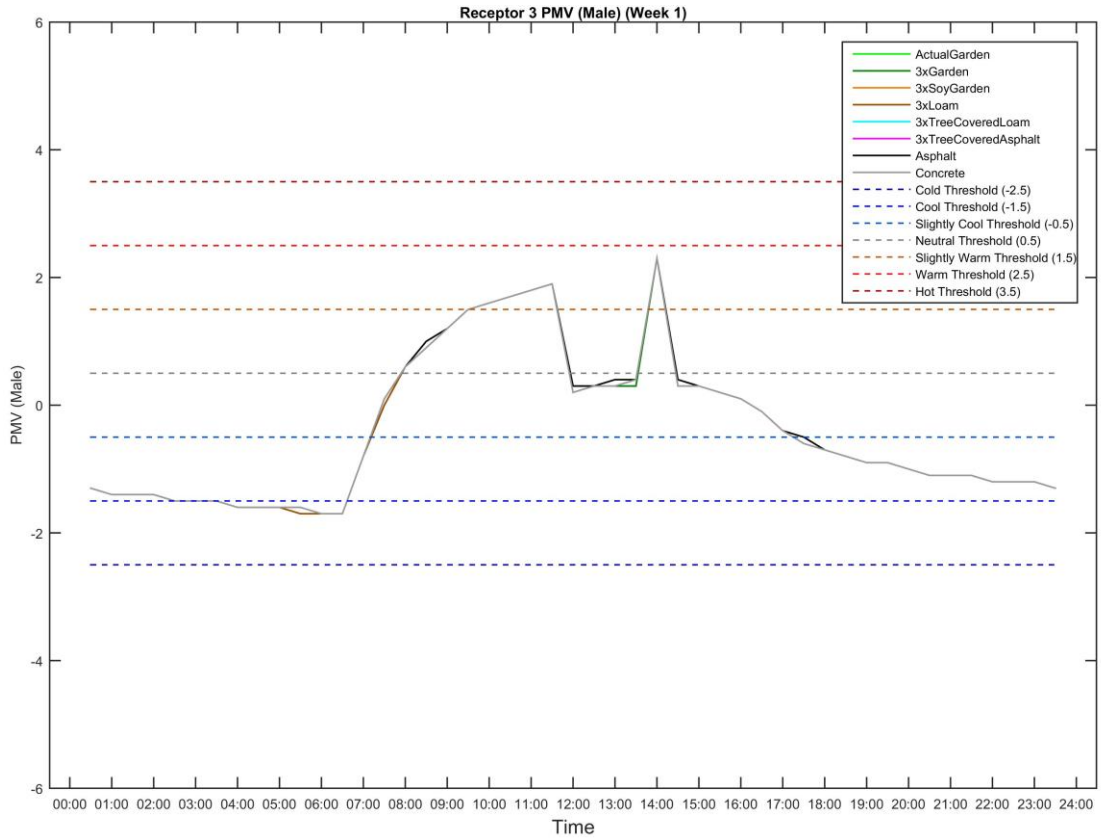


Figure 3.46: The Diurnal Cycle of the Male Predicted Mean Vote (PMV) of Receptor 3 for Week 1.

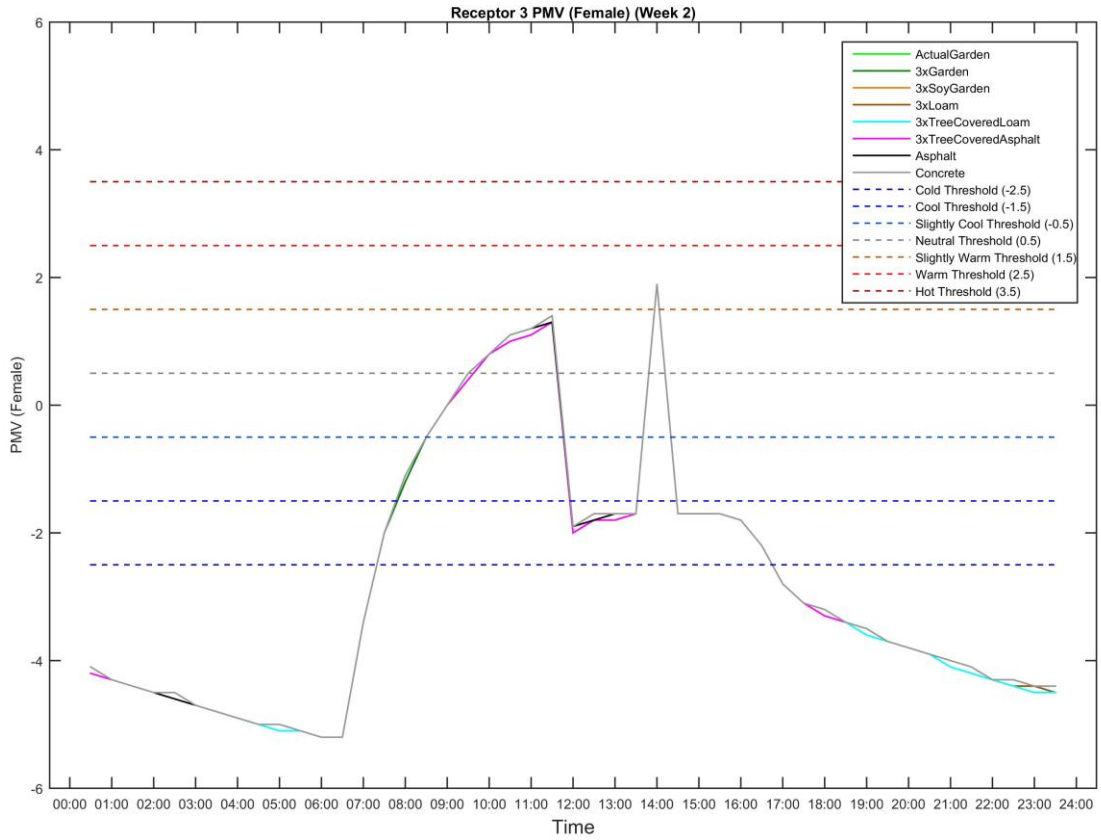


Figure 3.47: The Diurnal Cycle of the Female Predicted Mean Vote (PMV) of Receptor 3 for Week 2.

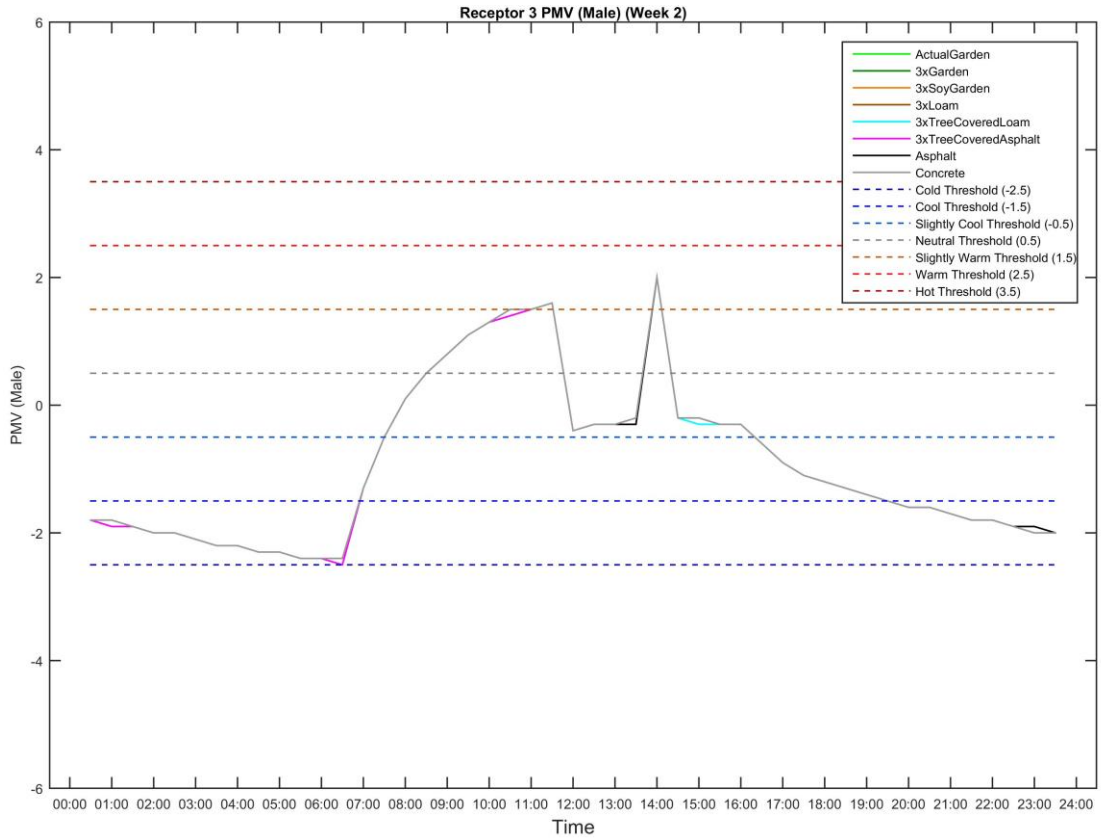


Figure 3.48: The Diurnal Cycle of the Male Predicted Mean Vote (PMV) of Receptor 3 for Week 2.

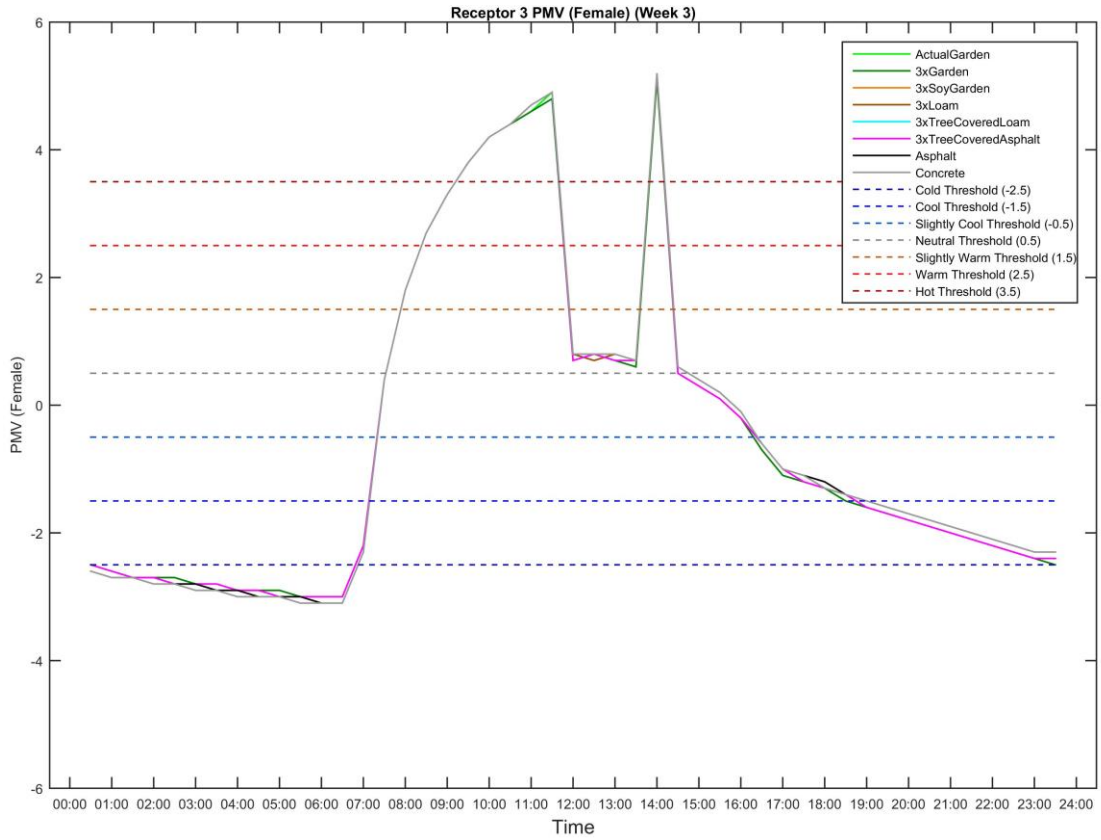


Figure 3.49: The Diurnal Cycle of the Female Predicted Mean Vote (PMV) of Receptor 3 for Week 3.

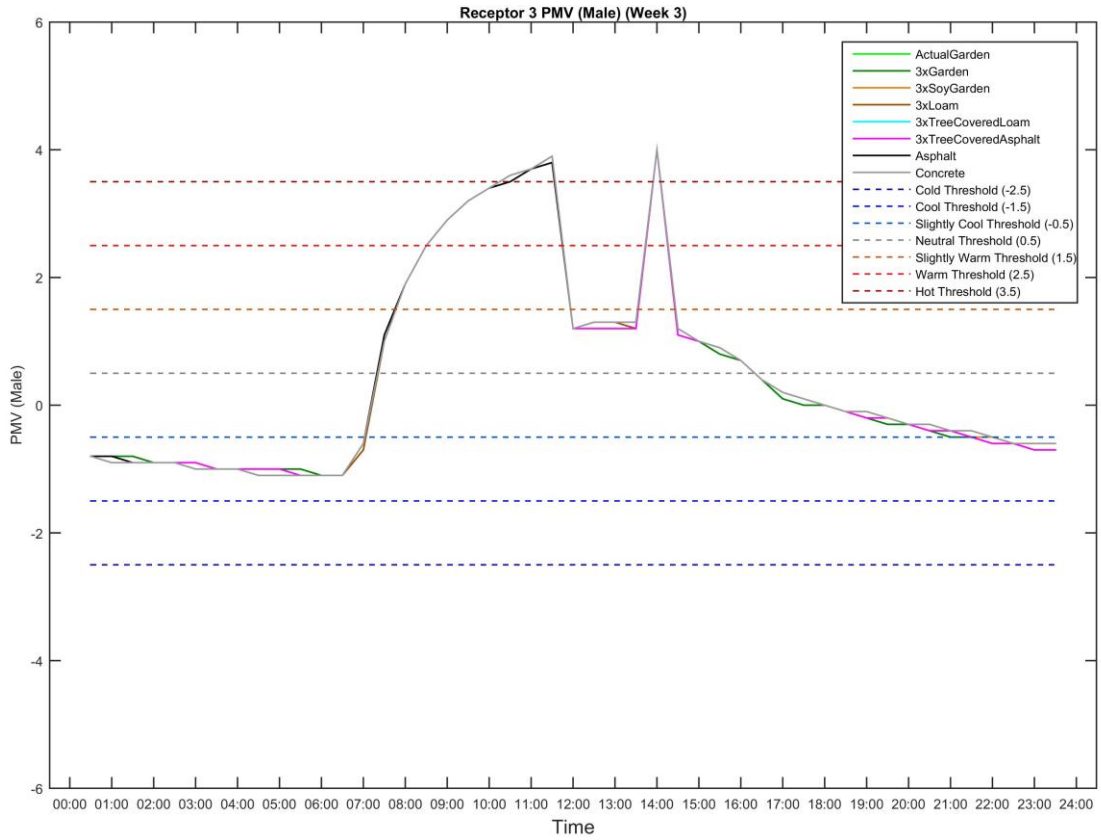


Figure 3.50: The Diurnal Cycle of the Male Predicted Mean Vote (PMV) of Receptor 3 for Week 3.

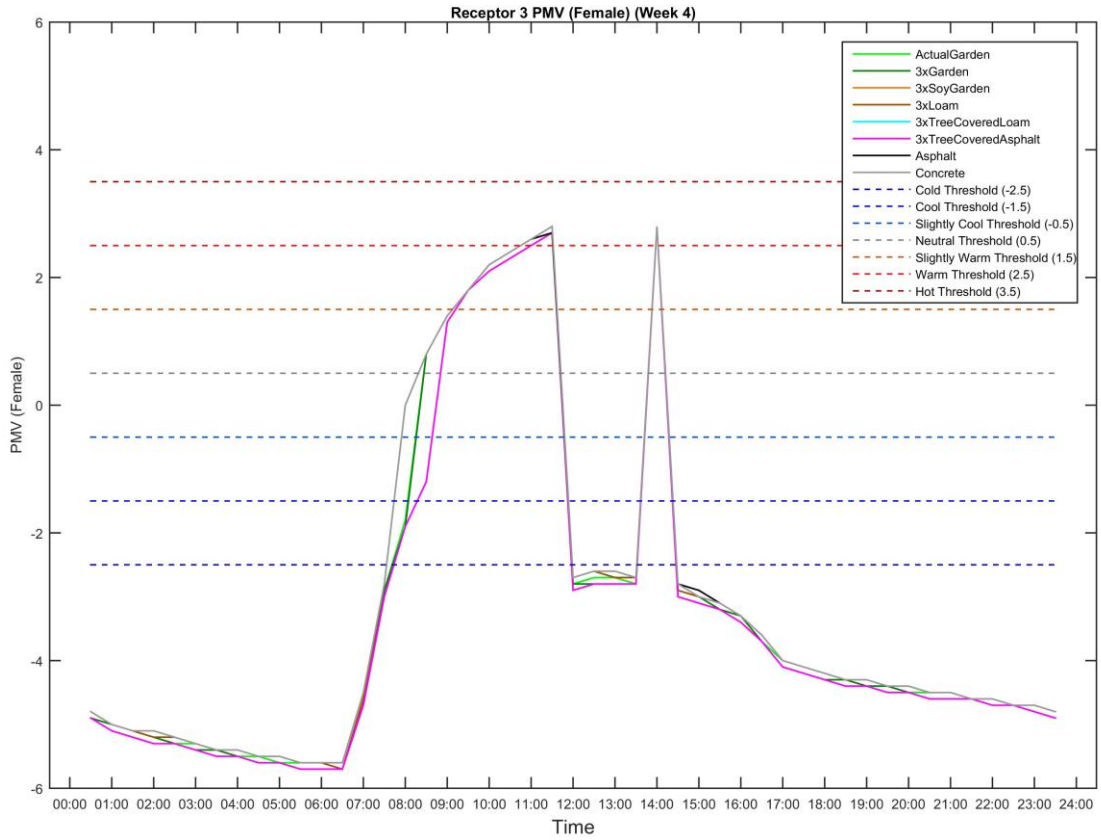


Figure 3.51: The Diurnal Cycle of the Female Predicted Mean Vote (PMV) of Receptor 3 for Week 4.

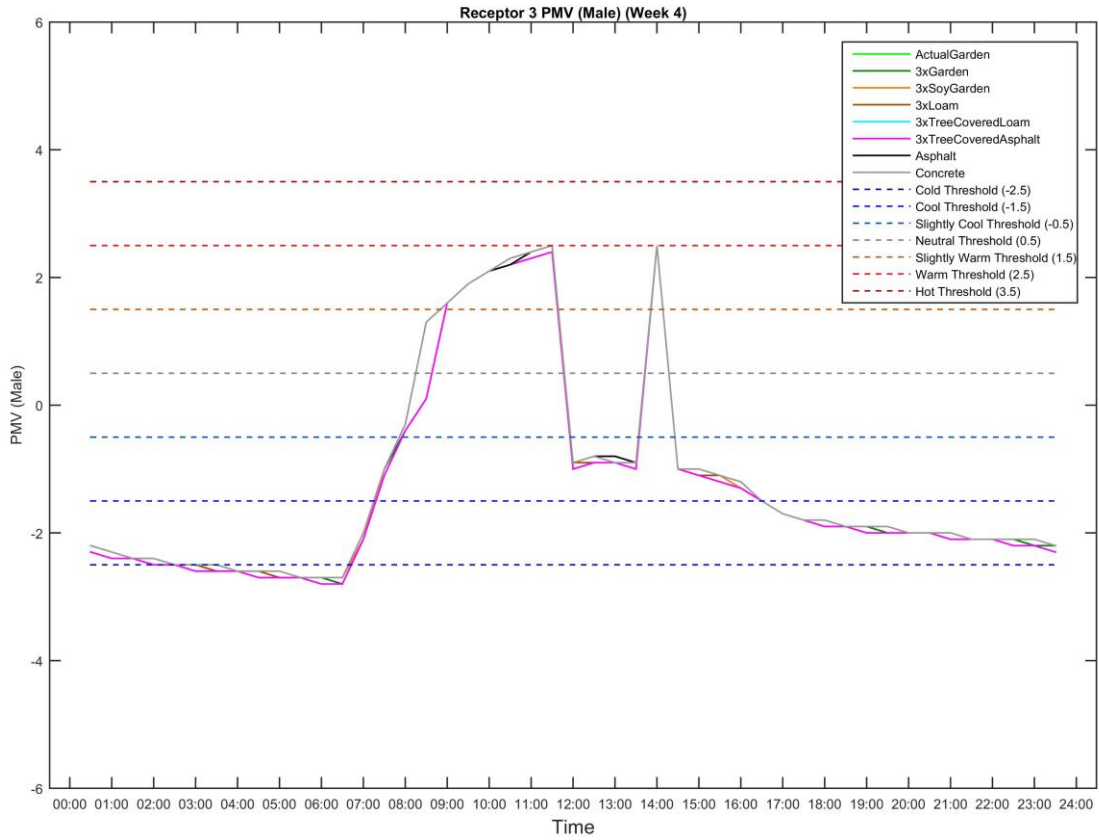


Figure 3.52: The Diurnal Cycle of the Male Predicted Mean Vote (PMV) of Receptor 3 for Week 4.

## **Chapter 4**

### **DISCUSSION**

#### **4.1 Urban Heat Island and Mitigation in Philadelphia**

##### **4.1.1 Philadelphia Urban Heat Island**

Through the comparison of the temperature in the “compact mid-rise” LCZ<sub>2</sub> (Local Climate Zone 2) environment of urban Philadelphia to the nearby “sparsely built” (LCZ<sub>9</sub>) rural sensor E4674, it is apparent that Philadelphia is warmer than the surrounding rural landscape. Among the non-garden urban sites, there was a consistent positive bias in daily maximum temperatures, daily minimum temperatures, and hourly average temperatures compared to E4674. Daily minimum temperatures were an average of 0.91-1.18 °C warmer than the rural sensor E4674, while daily maximum temperatures were an average of 0.62-3.19 °C higher compared to E4674. In addition, hourly average temperatures were also 0.54-1.25 °C warmer at the non-garden urban sites compared to E4674.

These temperature differences are lower than the 7-9 °C increase for the maximum UHI found by Imhoff et al. (2010) in cities replacing temperate forests (which includes Philadelphia). However, this temperature increase was found during the daytime in the summer; the winter and nighttime UHI values were lower, with the summer nighttime UHI around 3 °C, and the winter daytime and nighttime UHI were 3.5 and 1 °C respectively. As this study included both daytime and nighttime temperatures, and was conducted during the early autumn, it is expected the values

would be lower than the extreme UHI values possible during a summer day. It is also possible that, at the “rural” sensor E4674, the sparse buildings (and associated impervious cover) may have also affected the temperature, when compared to an area with no buildings or impervious surface cover (such as a dense forest or state park).

The urban and peri-urban sites also had lower average daily minimum relative humidity (0.46-5.54% lower) and hourly average relative humidity (0.52-2.70% lower) compared to the rural sensor E4674. This is consistent with prior research (Hass et al. 2016), in which urban areas have lower humidity than vegetated and sparsely developed areas.

#### **4.1.2 Urban Garden Heat Mitigation**

The comparison of the Garden Sensor to the other HOBO sensors in the Philadelphia area suggests that the garden has the potential to mitigate warmer temperatures in the surrounding environment. The Garden sensor experienced lower average daily maximum temperatures (between 0.74-2.74 °C lower) and hourly average temperatures (between 0.11-0.55 °C lower) when compared to the other HOBO sensors. However, the Garden Sensor had only a slight decrease in average daily maximum temperature (only 0.02 °C) and warmer hourly average temperatures (0.31 °C higher, on average) when compared to the urban Mesowest sensor E8199. The average daily minimum temperature was also warmer when compared to Sensor 1, Sensor 4, and E8199.

It is possible that, while the garden provides cooling during the day, the cooling effect is minimal during the night. Prior research has shown that, while tree-cover can provide cooling during the day in urban parks, the tree canopy can prevent radiation cooling at night (Bowler et al. 2010, Potchter et al. 2006, Yan and Dong

2015). The garden site has a tree and is bordered by two three-story homes on two sides, limiting its sky-view factor and reducing potential radiation cooling at night. The lack of nighttime radiation cooling may explain the presence of warmer daily minimum temperatures despite the cooler hourly average temperatures and daily maximum temperatures.

The fact that the Garden Sensor's average daily minimum temperature was cooler than Sensor 3 (by 0.60 °C) may be explainable by Sensor 3's corner location. Sensor 3 is located on the corner of Fitzwater Street and S 21<sup>st</sup> Street, which runs perpendicular to Fitzwater Street and receives more direct sunlight than Fitzwater Street. While impervious surfaces such as pavement and concrete are associated with warmer temperatures (Imhoff et al. 2010, Yan and Dong 2015), building can provide cooling shade as well (Bowler et al. 2010, Potchter et al. 2006). It is possible that Sensor 3 temperatures were warmer due to the nearby large, sun-warmed paved area of S 21<sup>st</sup> Street, in contrast to the more shaded Fitzwater Street which is the only other road on which the other HOBO sensors are located.

In regards to relative humidity, the Garden Sensor had a greater average daily minimum relative humidity compared to the other HOBO sensors and rural sensor E4674. The Garden Sensor also recorded greater hourly average relative humidity for Sensors 1-3, but reduced hourly average relative humidity compared to the urban E8199 and E4674. Prior research has shown that the relative humidity of an urban environment is correlated with greater amounts of vegetated surfaces and tree cover (Hass et al. 2016) and it is possible that the increased vegetation in the garden led to greater relative humidity values than the nearby street sensors. The E8199 sensor, however, may be in a location with greater tree cover than the HOBO sensors, and

therefore has a greater hourly average relative humidity. The greater hourly average relative humidity at the rural sensor E4674 is consistent with prior studies which found greater relative humidity values under tree canopies in Pennsylvania and Delaware forests (Matlack 1993). However, the average daily maximum relative humidity was not consistent between sensors. This may be due to local mixing effects, as the Garden Sensor had a higher average daily maximum relative humidity when compared to Sensor 3 (located on a street corner), but a had a lower average daily maximum relative humidity compared to Sensor 1 and 4. Also, The Garden Sensor had smaller average daily minimum relative humidity values and average hourly average relative humidity values when compared to the urban sensor E8199. It is possible that E8199 had a greater level of vegetation (or another source of water vapor) nearby, when compared to the HOBO sensors, giving the sensor a positive bias compared to the Garden Sensor.

## **4.2 Thermal Comfort in Urban Community Gardens**

### **4.2.1 Effects of the Composition of Urban Gardens on Thermal Comfort**

Of all the models tested, the ActualGarden model had lower average PET values than all the hypothetical models except 3xGarden. ActualGarden was 0.28 °C and 0.41 °C cooler at the Garden Receptor for 3xTreeCoveredSoil and 3xTreeCoveredAsphalt (respectively), but the cooling effect was nonexistent past Receptor 2. This suggests that the ground vegetation cover of the ActualGarden and 3xGarden may have provided a small amount of additional cooling compared to the other models, but that this effect is not noticeable beyond a certain extent past the garden boundaries. In contrast, the tree-less models had average PET values that were

1.60-1.98 °C warmer than the ActualGarden model at the Garden Receptor, and average PET values were 0.25-0.29 °C warmer at Receptor 2. This is consistent with prior studies. Tree cover has been previously shown to reduce temperatures in cities (Bowler et al. 2010, Potchter et al. 2006, Shashua-Bar and Hoffman 2000), and in addition, the shade resulting from tree cover causes a reduction in the mean radiant temperature (Matzarakis et al. 1999), which is generally the strongest influence on the PET and PMV indices (Matzarakis et al. 2007).

In comparison to the 3xGarden model, the other hypothetical models had warmer average PET results than compared to the ActualGarden model (and ActualGarden was warmer at the Garden Receptor and Receptor 3), demonstrating that increasing the size of an urban garden increases the cooling impact of the garden in a manner similar to city parks (Jamei et al. 2016). Of the tree-covered hypothetical models, 3xGarden had an average PET that was 0.44 °C cooler at the Garden Receptor (but nonexistent past Receptor 2) for 3xTreeCoveredLoam, and 0.56 °C cooler at the Garden Receptor (but the cooling effect was nonexistent at Receptor 3) for 3xTreeCoveredAsphalt. However, the tree-less models had average PETs that were 1.76-2.14°C warmer than the 3xGarden model, and still had average PETs that were 0.27-0.31 °C warmer at Receptor 2. Because Receptor 3 was near the boundary of the model area, it is possible that the cooling impact of the garden may extend further than Receptor 2 (and potentially even Receptor 3), but the boundary condition forcings caused the PET results to be more similar between models than they may be in reality.

#### **4.2.1.1 The Effect of Tree-Cover and Ground Cover on Thermal Comfort.**

For the eight tested garden models, only the tree-covered gardens had significant cooling effects in the garden when compared to the garden's surroundings.

The Garden Receptor of the tree-covered models had average PET values that were 0.57-0.92 °C cooler than Receptor 1, but 1.84-2.39 °C cooler than Receptor 3. Of the tree-covered models, the bare-ground 3xTreeCoveredAsphalt and 3xTreeCoveredLoam models had the smallest differences between their Garden Receptor and the street receptors, with 3xTreeCoveredAsphalt having the least cooling effect. Similar to the section 4.2.1, this suggests that pervious ground cover and ground vegetation cover has a small cooling effect in addition to the substantial cooling impact of tree shade.

The effect of tree-cover and ground cover are also present in the PET hierarchical analysis as well. ActualGarden and 3xGarden, the two sites with tree-cover and ground vegetation cover, are consistently paired with each other. With the exception of Receptor 1, similar patterns can be found with 3xAsphalt and 3xConcrete (the two tree-less impervious surface models) as well. Cluster analysis also indicated that the main division within the clusters are between the tree-less and tree-covered sites.

The cooling effect of tree shade has been established previously. Shashua-Bar and Hoffman (2000) found that tree canopy shade accounts for 70% of the cooling effect in Tel Aviv. Similarly, Potchter et al. (2006) found that urban parks in Tel Aviv with medium or high tree canopies can reduce temperatures by 2.5 to 3.5 °C respectively. In addition, multiple studies have also shown that air temperatures below tree canopies were lower if the surface is grass instead of concrete (Bowler et al. 2010), as is seen in the differences in cooling between the Garden Sensor and its surroundings in the 3xTreeCoveredSoil and 3xTreeCoveredAsphalt models.

The reason for the large difference between the tree-less and tree-covered models is likely from the influence of direct solar radiation. Petralli et al. (2011) found that the largest differences in temperature between clusters of sites in Florence occurred during summer and fall months, attributing it to a greater influence of solar radiation exposure on the air temperature surrounding their stations. The effect of direct solar radiation is evident in the diurnal cycle of the PET. As solar radiation is a factor in air temperature and the mean radiant temperature of the body, increased solar radiation leads to increases in both in PMV and PET calculations. In the PET and PMV diurnal cycles, the greatest difference between the models occurs at the Garden Receptor. Between the tree-less and tree-covered models, the greatest differences occur during the mid-day, and the tree-less models can reach a PET that is 18 °C greater than the tree-covered models. During the period of direct sunlight, the Garden Receptor had PET values in the range of moderate heat stress (35 °C) for Weeks 2 and 4, and strong heat stress (41 °C) for Weeks 1 and 3 (Wang et al. 2017).

The tree-covered models did have slightly higher PET and PMV values (a difference that is less than 3 °C and 0.3 respectively) during the nighttime, which supports previous findings (Potchter et al. 2006, and Yan and Dong 2015) of tree-less sites having greater nighttime cooling. Despite this, trees moderate daytime thermal comfort to a much greater extent than any of the tree-less models. Of the tree-covered models, the ActualGarden and 3xGarden models were also much cooler during mid-day (between 3 to 5 °C) than 3xTreeCoveredLoam and 3xTreeCoveredAsphalt. In addition, the PET cooling effect of the ActualGarden model is greater than 0.25 °C at Receptor 2 (although only an average of 0.08 °C cooler at Receptor 3), Receptor 2 is 41 meters away from the garden boundary in the model. While this is smaller than the

cooling distance of 100 meters found by Shashua and Hoffman (2000), the garden is smaller than the 60 meter wide green areas in their survey. The ActualGarden model is a maximum of 28 meters wide along its longest axis (north-south), and maximum of 6 meters wide along its shortest axis (east-west). In addition, the ActualGarden model's garden site is less than 100 meters from the edge of the model (Receptor 3, located near the boundary, is only 80 meters away), and the boundary conditions will influence the PET closer to the model boundaries (and reduce differences in the models). Despite this, the cooling distance extends to a greater distance than prior findings that a Park Cool Island extends past the park boundaries by approximately the width of the park (Jamei et al. 2016), extending approximately 1.5 times the longest length of the garden (and approximately 6.8 times the shortest length of the garden), extending from the edge of the garden to Receptor 2 at a minimum possible extent. While this study was limited in number of locations in which PET was calculated, further research can provide greater precision to the cooling range of an urban garden through the use of more receptors at smaller spatial distances, and may be able to demonstrate the influence of wind direction on cooling extent as well.

#### **4.2.1.2 Male and Female Differences in Thermal Comfort**

While the effect of tree-cover on thermal comfort is noticeable for the PET, the intensity of solar radiation's effect on the PMV is different between the sexes. While the Male PMV at the Garden Receptor has high PMV values during the mid-day, the Female PMV has much greater PMV values during the same period of direct sunlight. For example, during Weeks 1 and 3, the Male PMV had a difference of 2.7 and 3.4 between the warmest tree-less and tree-covered models (3xTreeCoveredAsphalt and 3xAsphalt) at 12:00, while the Female PMV had a difference of 4.5 and 5.4. Using

Wang et al.'s (2017) scale of PMV heat stress thresholds, an increase in PMV of 2.5 is equivalent to the difference between no thermal stress and moderate heat stress, and a PMV increase of 3.5 is equivalent to the difference between no thermal stress and strong heat stress. While the Male PMV experiences increases that would cause moderate to strong heat stress, the Female PMV experiences increases that are consistently much greater than the strong heat stress threshold (by a value that is 1 and 1.9 greater than the 3.5 PMV threshold, respectively). The Female PMV of the tree-less models also consistently experienced PMV values greater than 4 while in direct sunlight during Weeks 1 and 3 (which is 0.5 higher than the "strong heat stress" threshold), and the Male PMV only reached a value of 4 during the hotter parts of the day. The maximum Female PMV was warmer by a difference of 1 when compared the maximum Male PMV.

The effect of direct sunlight is noticeable in the average PMV values as well. While the average Female PMV was cooler than the average Male PMV, the direct sunlight increased the average Female PMV. The models 3xTreeCoveredLoam and 3xTreeCoveredAsphalt (at the Garden Receptor) were an average of 1.56 and 1.59 cooler when compared to the Male PMV, but their tree-less counterparts (3xLoam and 3xAsphalt) were both 1.76 cooler. This difference occurs despite the direct sunlight lasting for only two hours of the day.

For Receptors 1-3, the results are similar between individual models at each receptor. However, as the PMV values diverge from neutral values, the Female PMV has a much higher or lower PMV (for hot or cold periods, respectively) when compared to the Male PMV at the same time. While this means that the Female PMV is generally colder than the Male PMV (due to much of the study period being cooler

than neutral at night and dawn/dusk), the Female PMV also has much greater “hot” values than the Male PMV during the mid-day. In addition, when the PMV values are close to neutral, there is less change between the Male and Female PMV. This is most noticeable at Receptor 2, or during Week 3 (for all three receptors), where the daytime PMV values (which are close to neutral) have a difference of approximately 0.5 to 1.0 between the Male and Female PMV, while the nighttime PMV values (which are in the cool or cold values) have a difference of 2.

These results are similar to prior research. Middel et al. (2016) similarly found that women reported slightly cooler average thermal sensations than males. Also, in a review by Karjalainen (2012), multiple studies have shown that while there is no difference in neutral temperatures between male and female subjects, females are more likely to be sensitive to deviations from neutral temperatures and therefore more likely to be dissatisfied with a thermal environment. As female bodies are more sensitive to shifts from optimal temperatures, they are also more likely to be affected by the presence of trees in an urban environment.

The differences between male and female bodies have been considered minor in the past (Fanger 1970, Karjalainen 2012). However, recent studies (Karjalainen 2012) and the results of this experiment show that the differences between the sexes can be significant, especially when deviations from neutral conditions occur. For further research, Karjalainen’s (2012) suggestion to focus on female thermal comfort (as their bodies are more likely to be stressed by thermal differences) would be useful for urban and outdoor thermal environment studies as well.

## **4.2.2 Urban Heat Island Mitigation Strategies for Philadelphia**

### **4.2.2.1 Possibilities**

The cooling ability of urban community gardens is highly dependent on their composition. The greatest amount of cooling occurred in models with tree-cover and ground vegetation cover, but in particular, tree-cover was consistently found to be the greatest influence over thermal comfort between the different models. Unfortunately, urban community gardens in Philadelphia have previously been found to grow a large variety of crops, but all of the most popular species are non-arboreal (Pearsall et al. 2016). If a garden were to have both cooling and food-production uses, it would need to be composed of food trees with shade-tolerant plants beneath the canopy, in a manner similar to “multistrata” gardens.

In many regions of the world, multistrata systems (or “homegardens”) are gardens in which a wide range of annual and perennial plants (that can be edible, medicinal, and utilitarian) are grown in a mixture that can even maintain decades-old trees (Muschler 2014). This system would not necessarily require largely different plants than some of the gardens in Philadelphia. Two of the species popularly grown plants in Philadelphia gardens, collard greens and parsley (Pearsall et al. 2016) are shade tolerant, and other greens (such as lettuce, kale, and spinach) and *Brassicas* (such as broccoli and cabbage) are shade tolerant as well (Dinesh and Pearce 2016). In addition, multistrata systems include species grown as companion species and for pest control (Muschler 2014), which is already done in Philadelphia gardens with marigold, zinnias, cornflowers, and garlic (Pearsall et al. 2016).

In addition, the cooling effect of trees allows for multiple varieties of small-scale greenspaces to promote thermal comfort. In Philadelphia, vacant land within the

city contributes to the UHI effect, and a majority of vacant lots are in areas with higher poverty rates, and lower median income and employment rates. Therefore neighborhoods with greater proportions of residents living in poverty have greater temperatures and higher heat-related mortality rates during extreme heat events. Yet, to reduce the disproportionate amount of vacant lots in poorer neighborhood, the City of Philadelphia is attempting to “green” the vacant lots (through projects such as tree plantings) (Pearsall 2017). As small patches of trees promote thermal comfort, this could reduce heat stress in the surrounding neighborhood, without requiring the use of volunteer labor from a lower-income neighborhoods, where lower-income residents often have little time to garden due to their jobs (Meenar and Hoover 2012).

In addition, Shashua-Bar and Hoffman (2000) suggest placing small parks every 200 meters (double the cooling range of their results) to maximize cooling in urban areas, which would be every two blocks, in a neighborhood like the one surrounding the garden site. As individual trees have been found to reduce air temperatures as well (Bowler et al. 2010), Shashua-Bar and Hoffman’s (2000) suggestion of at least one shade tree per house may also provide better thermal comfort to city residents (and in particular, pedestrians). Furthermore, urban trees have been shown to improve air quality, mitigate flooding and runoff, provide a habitat for urban wildlife, and reduce urban noise levels (Heynen et al. 2006). Street trees provide multiple ecosystem services while using minimal land coverage.

#### **4.2.2.2 Problems**

However, there are multiple obstacles to increasing thermal comfort for city residents. To create an urban garden, or to even grow a small patch of trees for cooling the local environment, requires the use of land that may be used for redevelopment.

While the City of Philadelphia is attempting to green the city's vacant lots by planting trees and maintaining the lots, this requires management and decades of growth to provide cooling benefits to the neighborhood. At the same time, the vacant lot greening program is also being used spur development and increase property values, which will maintain the high temperatures in the neighborhood. This places the long-term use of the vacant lots for cooling the environment in conflict with the short-term use of greening to increase tax revenue from residential, commercial or industrial development (Pearsall 2017). In addition, as this vacant land is greened by the city, property prices rise, especially in poorer neighborhoods (Heckert and Mennis 2012). This can then create a paradox in which the increase in greenspace causes gentrification, which then cause increased costs and drive out the very residents that the greenspace was supposed to protect (Wolch et al. 2014).

This same conflict can be present for the use of a vacant lot as an urban garden. In Philadelphia, urban gardens requires access to vacant land, this is more difficult for neighborhoods with less social and political capital (Meenar and Hoover 2012), and gardens are subject to disparity due to the class and race of the gardeners (Reynolds 2015). Also, even if the gardeners do have access to space, gardeners generally need more space than they have, and often have insecure tenure of their sites (Cohen and Reynolds 2014). As there is pressure to use the land for development, and a lack of social and political capital to support gardens in poorer neighborhoods, it can be difficult for gardens to survive.

Even relying on urban trees to increase the thermal comfort of a neighborhood can potentially reify class differences. Prior research in the city of Milwaukee has demonstrated that urban trees are distributed in relation to household income. Houses

with lower incomes cannot afford to maintain trees on their property, and instead rely on the ecosystem benefits created by the investment in trees on public property (Heynen et al. 2006). In addition, while Philadelphia has a free-tree-planting program (TreePhilly 2016), similar programs in Milwaukee do not provide trees primarily to the poor or to renters (Heynen et al. 2006). This due to a systematic disinvestment in the neighborhoods, where residents and landlords are less likely to invest in properties and upkeep if the neighborhood stability is in question (Heynen et al. 2006).

#### **4.2.3 Limitations and Future Research**

This study was limited in multiple ways. Only one garden was tested for a cooling effect, and it was only possible to get permission to place HOBO sensors to the east of the garden at three locations. In addition, the study period was in autumn, when the greatest urban heat island effect is generally found in the summer. Similarly, as autumn progressed, the trees shed their leaves and the garden plants died as the growing season ended, which would have an impact on the resulting park cool island. To further understand the UHI in Philadelphia (and the potential PCI created by urban gardens), it would be useful to sample multiple gardens simultaneously in the summer, and to include sensors in multiple directions outside of the garden, to find the variability of the PCI (and its extent) between different gardens. Multiple gardens from neighborhoods of varying income levels should be used as well, to determine the differences in the UHI between sections of the city and its connection to the neighborhoods' wealth, and the differences in the gardens' PCI as well.

This study was also limited in terms of the social categories that were analyzed. This experiment discussed only the impact of heat mitigation and thermal comfort with regards to biological sex and a neighborhood's income. However,

minority populations and the elderly are both at risk of increased heat (Harlan et al. 2006). Further research could analyze the impact of urban heat on the elderly through the simulation of PMV at different ages using RayMan. In addition, further research could analyze the connection between thermal comfort and minority status by comparing gardens between neighborhoods with different racial/ethnic compositions.

In addition, the study was limited in the use of a “rural” sensor. The Mesowest sensor E4674 was located in the “sparsely-built” local climate zone (LCZ<sub>9</sub>), which is defined as a “sparse arrangement of small or medium-sized buildings in a natural setting [with an] abundance of pervious land cover (low plants, scattered trees)” (Stewart and Oke 2012). While this is similar to the “scattered trees” (LCZ<sub>A</sub>) or “dense trees” (LCZ<sub>B</sub>) local climate zone types in terms of tree-dominated vegetation and mostly pervious land cover (Stewart and Oke 2012), the presence of buildings (and associated impervious surface cover, such as roads and driveways) in the area surrounding the sensor causes the area to be somewhat “suburban” in land cover, and may affect the temperature and relative humidity at the sensor.

Lastly, the Envi-met model was also limited due to its inability to model rain or short-term cloud cover. While the impact of rain and cloud cover was reduced in the model runs through the calculation of weekly average diurnal cycle, this also reduces the daily (and hourly) variability of the PET. Due to the substantial impact of direct sunlight, it is possible that increased cloud cover may reduce the PET. However, humidity is related to thermal comfort (Fanger 1970, Hass et al. 2016, Höpfe 1999, Matzarakis et al. 2007), and shifts in relative humidity associated with changes in cloud cover and rain were unaccounted for as well. While rain cannot be modelled in Envi-met, further simulations that model both cloudy and sunny days as case studies

may be able to analyze any existing difference in thermal comfort due to the associated differences in the meteorological conditions.

## **Chapter 5**

### **CONCLUSION**

It is well established that urban areas have higher temperatures than their less-developed surroundings (Coseo and Larsen 2014, Imhoff et al. 2010). In addition, exposure to heat can vary across populations in a city due to the presence of vegetation (Declat-Barreto et al. 2013, Jamei et al. 2016, Jenerette et al. 2007); the biological sex of a resident can affect their thermal comfort (Karjalainen 2012, Rupp et al. 2015). Urban community gardens have also been suggested as a form of urban vegetation which may mitigate local temperature increases in a city (Tsilini et al. 2014), which would complement the many social benefits of urban gardens (Poulsen et al. 2014). However, urban greenspace such as parks vary in cooling capability, and the cooling extent of Park Cool Islands has been previously shown to only extend beyond the park boundaries by the width of the park (Imhoff et al. 2010, Jamei et al. 2016). Urban gardens are also subject to social forces that may limit their cooling; the gardens are often limited in size due to their reliance on vacant land, and limited in funding and support from the city due to the social and political capital of the gardeners (Cohen and Reynolds 2014, Meenar and Hoover, and Reynolds 2014).

Through an analysis of observed and modelled data, it has been demonstrated that urban gardens can reduce temperatures within a city as well as promote thermal comfort, primarily due to the presence of tree cover. Tree cover has been previously shown to reduce temperatures in cities (Bowler et al. 2010, Potchter et al. 2006, Shashua-Bar and Hoffman 2000). This effect is likely due to the reduction in direct

solar radiation (Petralli et al. 2011), that results in a reduction of the mean radiant temperature which is a strong influence on thermal comfort (Matzarakis et al. 1999, Matzarakis et al. 2007). With the presence of tree cover, the otherwise-identical gardens can have thermal comfort indices that are reduced from “hot” to “neutral” values, a reduction from “strong heat stress” to “no thermal stress” (Wang et al. 2017). The cooling effect of the tree-covered gardens has also been found to extend past its boundaries, and beyond the width of the garden (and therefore further than urban park cooling). The cooling effect of trees also varies between the sexes; because female bodies are more sensitive to deviations from neutral conditions, direct sunlight causes greater levels of heat stress and discomfort than male bodies in the same conditions. Therefore, tree cover causes a greater reduction in the Female PMV when compared to the Male PMV.

However, while urban gardens (and tree cover) may promote thermal comfort, there are many obstacles to cooling the city in this manner. Many of the most popular Philadelphia urban garden crops are non-arboreal (Pearsall et al. 2016), which may require changing garden composition to promote cooling, and trees take years to mature (Pearsall 2017). Poorer gardeners in Philadelphia also have a harder time accessing vacant land and maintaining their gardens due to a lack of resources (Meenar and Hoover 2012). Relying on public trees may also be problematic for lower-income residents (Heynen et al. 2006), as the addition of trees in poorer neighborhoods increases property costs (Heckert and Mennis 2012), causing gentrification (which drives out the same residents the trees are meant to help) (Wolch et al. 2014). In order to mitigate urban heat islands using urban gardens and tree cover, residents face structural inequality and the risk of gentrification.

## REFERENCES

1. Bowler, D.E., Buying-Ali, L., Knight, T.M., and A.S. Pullin, 2010: Urban greening to cool towns and cities: A systematic review of the empirical evidence. *Landscape and Urban Planning*, **97**, 147-155 doi: 10.1016/j.landurbplan.2010.05.006
2. Cohen, N., and K. Reynolds, 2014: Resource needs for a socially just and sustainable urban agriculture system: Lessons from New York City. *Renewable Agriculture and Food Systems*, **30**, 103-114 doi: 10.1017/S1742170514000210
3. Coseo, P., and L. Larsen, 2014: How factors of land use/land cover, building configuration, and adjacent heat sources and sinks explain Urban Heat Islands in Chicago. *Landscape and Urban Planning*, **125**, 117-129, doi: 10.1016/j.landurbplan.2014.02.019
4. Declet-Barreto, J., Brazel, A.J., Martin, C.A., Chow, W.T.L., and S.L. Harlan, 2013: Creating the park cool island in an inner-city neighborhood: heat mitigation strategy for Phoenix, AZ. *Urban Ecosyst*, **16**, 617-635, doi: 10.1007/s11252-012-0278-8
5. Dimoudi, A. Kantzioura, A., Zoras, S., Pallas, C., and P. Kosmopoulous, 2013: Investigation of urban microclimate parameters in an urban center. *Energy and Buildings*, **64**, 1-9, doi: 10.1016/j.enbuild/2013/04.014
6. Dinesh, H., and J.M. Pearce, 2016: The potential of agrivoltaic systems. *Renewable and Sustainable Energy Reviews*, **54**, 299-308 doi: 10.1016/j.rser.2015.10.024
7. Ellis, K.N., Hathaway, J.N., Mason, L.R., Howe, D.A., Epps, T.H., and V.M. Brown, 2015: Summer temperature variability across four urban neighborhoods in Knoxville, Tennessee, USA. *Theoretical and Applied Climatology*, **127**, 701-710 doi: 10.1007/s00704-015-1659-8
8. Envi-met, 2016: Envi-met 4. Accessed 6/29/16 [Available online at <http://www.model.envi-met.com/hg2e/doku.php>]

9. Fanger, P.O., 1970: Thermal Comfort: Analysis and Applications in Environmental Engineering. McGraw-Hill Book Company, 244 pp.
10. Gaffin, S.R., Rosenzweig, C., Khanbilvardi, R., Parshall, L., Mahani, S., Glickman, H., Goldberg, R., Blake, R., Slosberg, R.B., and D. Hillel, 2008: Variations in New York City's urban heat island strength over time and space. *Theoretical and Applied Climatology*, **94**, 1-11, doi: 10.1007/s00704-007-0368-3
11. Gosling, S.N., Bryce, E.K., Dixon, P.G., Gabriel, K.M.A., Gosling, E.Y., Hanes, J.M. Hondula, D.M., Liang, L., Mac Lean, P.A.B., Muthers, S., Nascimento, S.T., Petralli, M., Vanos, J.K., and E.R. Wanka, 2014: A glossary for biometeorology. *International Journal of Biometeorology*, **58**, 277-308, doi: 10.1007/s00484-013-0729-9
12. Gregory, M.M., Leslie, T.W., and L.E. Drinkwater, 2016: Agroecological and social characteristics of New York City community gardens: contributions to urban food security, ecosystem services, and environmental education. *Urban Ecosyst*, **19**, 763-794, doi: 10.1007/s11252-015-0505-1
13. Harlan, S.L., Brazel, A.J., Prashad, L., Stefanov, W.L., and L. Larsen, 2006: Neighborhood microclimates and vulnerability to heat stress. *Social Science and Medicine*, **63**, 2847-2863, doi: 10.1016/j.socscimed.2006.07.030
14. Hass, A.L., Ellis, K.N., Mason, L.R., Hathaway, J.M., and D.A. Howe, 2016: Heat and Humidity in the City: Neighborhood Heat Index Variability in a Mid-Sized City in the Southeastern United States. *International Journal of Environmental Research and Public Health*, **13**, n. pag. doi: 10.3390/ijerph13010117
15. Heckert, M., and J. Mennis, 2012: The economic impact of greening urban vacant land: a spatial difference-in-differences analysis. *Environment and Planning A*, **44**, 3010-3027 doi: 10.1068/a4595
16. Heynen, N., Perkins, H.A., and P. Roy, 2006: The Political Ecology of Uneven Urban Green Space the Impact of Political Economy on Race and Ethnicity in Producing Environmental Inequality in Milwaukee. *Urban Affairs Review*, **42**, 3-25 doi: 10.1177/1078087406290729
17. Höppe, P., 1999: The physiological equivalent temperature – a universal index for the biometeorological assessment of the thermal environment. *International Journal of Biometeorology*, **43**, 71-75

18. Huang, L., Arens, E., Zhang, H., and Z. Yingxin, 2014: Applicability of whole-body heat balance models for evaluating thermal sensation under non-uniform air movement in warm environments. *Building and Environment*, **75**, 108-113, doi: 10.1016/j.buildenv.2014.01.020
19. Imhoff, M.L., Zhang, O. Wolfe, R.E., and L. Bounoua, 2010: Remote sensing of the urban heat island effect across biomes in the continental USA. *Remote Sensing of Environment*, **114**, 504-513, doi: 10.1016/j.rse.2009.10.008
20. Jamei, E., Rajagopalan, P., Seyedmahmoudian, M., Jamei, Y., 2016 Review on the impact of urban geometry and pedestrian level greening on outdoor thermal comfort. *Renewable Sustainable Energy Rev.* **54**, 1002-1017, doi: 10.1016/j.rser.2015.10.104
21. Jenerette, G.D., Harlan, S.L., Brazel, A., Jones, N. Larsen, L., and W.L. Stefanov, 2007: Regional relationships between surface temperature, vegetation, and human settlement in a rapidly urbanizing ecosystem. *Landscape Ecol*, **22**, 353-365, doi: 0.1007/s10980-006-9032-z
22. Johansson, E., Thorsson, S., Emmanuel, R., and E. Krüger, 2014: Instruments and methods in outdoor thermal comfort studies – The need for standardization. *Urban Climate*, **10**, 346-266, doi: 10.1016/j.uclim/2013.12.002
23. Karjalainen, S., 2012: Thermal comfort and gender: a literature review. *Indoor Air*, **22**, 96-109 doi: 10.1111/j.1600-0668.2011.00747.x
24. Kim, Y.H., and J.J. Baik, 2004: Daily maximum urban heat island intensity in large cities of Korea. *Theoretical and Applied Climatology*. **79**, 151-164, doi: 10.1007/s00704-004-0070-7
25. Matlack, G.R., 1993: Microenvironment Variation within and among the forest edge sites in the Eastern United States. *Biological Conservation*, **66**, 185-194 doi: 10.1016/0006-3207(93)90004-K
26. Matzarakis, A., Mayer, H., and M.G. Iziomon, 1999: Applications of a universal thermal index: physiological equivalent temperature. *International Journal of Biometeorology*, **43**, 76-84 doi: 10.1007/s004840050119
27. Matzarakis, A., Rutz, F., and H. Meyer, 2007: Modelling radiation fluxes in simple and complex environments —application of the RayMan model. *International Journal of Biometeorology*. **51**, 323-334, doi: 10.1007/s00484-006-0061-8

28. Matzarakis, A., Rutz, F., and H. Meyer, 2010: Modelling radiation fluxes in simple and complex environments: basics of the RayMan model. *International Journal of Biometeorology*. **54**, 131-139, doi: 10.1007/s00484-009-0261-0
29. Mayer, H., 1993: Urban bioclimatology. *Experientia*. **49**, 957-963, doi: 10.1007/BF02125642
30. Meenar, M.R., and B.M. Hoover, 2012: Community food security via urban agriculture: Understanding people, place, economy, and accessibility from a food justice perspective. *Journal of Agriculture, Food Systems, and Community Development*. **3**, 143-160, doi: 10.5304/jafscd.2012.031.013
31. Mesowest, 2017a: Mesowest User's Guide. Accessed 25 June 2017 [Available online at <http://mesowest.utah.edu/html/help/userguide.html>]
32. Mesowest, 2017b: Mesowest Main Help. Accessed 25 June 2017 [Available online at [http://mesowest.utah.edu/html/help/main\\_index.html#overview](http://mesowest.utah.edu/html/help/main_index.html#overview)]
33. Mesowest, 2017c: E8199 Station Metadata and Information Page. Accessed 20 April 2017 [Available online at [http://mesowest.utah.edu/cgi-bin/droman/station\\_total.cgi?stn=E8199&unit=0](http://mesowest.utah.edu/cgi-bin/droman/station_total.cgi?stn=E8199&unit=0)]
34. Mesowest, 2017d: Weather Conditions for E8199. Accessed 20 April 2017 [Available online at [http://mesowest.utah.edu/cgi-bin/droman/meso\\_base\\_dyn.cgi?stn=E8199](http://mesowest.utah.edu/cgi-bin/droman/meso_base_dyn.cgi?stn=E8199)]
35. Mesowest, 2017e: KPHL Station Metadata and Information Page. Accessed 20 April 2017 [Available online at [http://mesowest.utah.edu/cgi-bin/droman/station\\_total.cgi?stn=KPHL&unit=0](http://mesowest.utah.edu/cgi-bin/droman/station_total.cgi?stn=KPHL&unit=0)]
36. Mesowest, 2017f: Weather Conditions for KPHL. Accessed 20 April 2017 [Available online at [http://mesowest.utah.edu/cgi-bin/droman/meso\\_base\\_dyn.cgi?stn=KPHL](http://mesowest.utah.edu/cgi-bin/droman/meso_base_dyn.cgi?stn=KPHL)]
37. Mesowest, 2017g: E4674 Station Metadata and Information Page. Accessed 20 April 2017 [Available online at [http://mesowest.utah.edu/cgi-bin/droman/station\\_total.cgi?stn=E4674&unit=0](http://mesowest.utah.edu/cgi-bin/droman/station_total.cgi?stn=E4674&unit=0)]
38. Mesowest, 2017h: Weather Conditions for E4674. Accessed 20 April 2017 [Available online at [http://mesowest.utah.edu/cgi-bin/droman/meso\\_base\\_dyn.cgi?stn=E4674](http://mesowest.utah.edu/cgi-bin/droman/meso_base_dyn.cgi?stn=E4674)]

39. Middel, A., Hüb, K., Brazel, A.J., Martin, C.A., and S. Guhathakurta, 2014: Impact of urban form and design on mid-afternoon microclimate in Phoenix Local Climate Zones. *Landscape and Urban Planning*, **122**, 16-28, doi: 10.1016/j.landurbplan.2013.11.004
40. Middel, A., Selover, N., Hagen, B., and N. Chhetri, 2016: Impact of shade on outdoor thermal comfort a seasonal field study in Tempe, Arizona. *International Journal of Biometeorology*, **60**, 1849-1861 doi: 10.1007/s00484-016-1172-5
41. Muschler, R.G., 2014: Agroforestry: Essential for Sustainable and Climate-Smart Land Use? *Tropical Forestry Handbook*, L. Pancel and M. Kohl, Springer, 2013-2116
42. Pearsall, H., Gachuz, S., Sosa, M.R., Schmook, B., Van der Wal, H., and M.A. Gracia, 2016: Urban Community Garden Agrodiversity and Cultural Identity in Philadelphia, Pennsylvania, U.S. *Geographical Review*, **107**, 476-495 doi: 10.1111/j.1931-0846.2016.12202.x
43. Pearsall, H., 2017: Staying cool in the compact city: Vacant land and urban heating in Philadelphia, Pennsylvania. *Applied Geography*, **79**, 84-92, doi: 10.1016/j.apgeog.2016.12.010
44. Pennsylvania Spatial Data Access (PASDA), 2015: Philadelphia Aerial Photography 2015. Accessed 19 October 2016 [Available online at <http://www.pasda.psu.edu/uci/DataSummary.aspx?dataset=1132>]
45. Pennsylvania Spatial Data Access (PASDA), 2016: Philadelphia Buildings. Accessed 19 October 2016 [Available online at <http://www.pasda.psu.edu/uci/DataSummary.aspx?dataset=146>]
46. Petrali, M., Massetti, L., and S. Orlandini, 2011: Five years of thermal intra-urban monitoring in Florence (Italy) and application of climatological indices. *Theoretical and Applied Climatology*. **104**, 349-356, doi: 10.1007/s00704-010-0349-9
47. Potchter, O., Cohen, P., and A. Bitan, 2006: Climatic Behavior of Various Urban Parks During Hot and Humid Summer in the Mediterranean City of Tel Aviv, Israel. *International Journal of Climatology*, **26**. 1695-1711, doi: 10.1002/joc.1330

48. Poulsen, M.N., Hulland, K.R.S., Gulas, C.A., Pham, H., Dalglish, S.L., Wilkinson, R.K., and P.J. Winch, 2014: Growing an Urban Oasis: A Qualitative Study of the Perceived Benefits of Community Gardening in Baltimore, Maryland. *Culture, Agriculture, Food and Environment*, **36**, 69-82, doi: 10.1111/cuag.12035
49. RayMan, 2006: RayMan 1.2. Accessed 21 June 2016 [Available online at [www.urbanclimate.net/rayman/rayman.htm](http://www.urbanclimate.net/rayman/rayman.htm)]
50. Reynolds, K., 2015, Disparity Despite Diversity: Social Injustice in New York City's Urban Agriculture System. *Antipode*, **47**, 240-259, doi: 10.1111/anti.12098
51. Rupp, R. F., Vásquez, N. G., and R. Lamberts, 2015: A review of human thermal comfort in the built environment. *Energy and Buildings*. **105**, 178-205, doi: 0.1016/j.enbuild.2015.07.047
52. Salata, F., Golasi, I., Petitti, D., de Lieto Vollaro, E., Coppi, M., and A. de Lieto Vollaro, 2017: Relating microclimate, human thermal comfort and health during heat waves: An analysis of heat island mitigation strategies through a case study in an urban outdoor environment. *Sustainable Cities and Society*, **30**, 79-96, doi: 1016/j.scs.2017.01.006
53. SAS, 2017a: Predictive and Specialized Modeling. Accessed 27 March 2017 [Available online at <http://support.sas.com/documentation/onlinedoc/jmp/index.html>]
54. SAS 2017b: Multivariate Methods, Second Edition. Accessed 27 March 2017 [Available online at <http://support.sas.com/documentation/onlinedoc/jmp/index.html>]
55. Shashua-Bar, L., and M.E. Hoffman, 2000: Vegetation as a climatic component in the design of an urban street An empirical model for predicting the cooling effect of urban areas with trees. *Energy and Buildings*, **31**, 221-235 doi: 10.1016/S0378-7788(99)00018-3
56. Stewart, I.D., and T.R. Oke, 2012: Local climate zones for urban temperature studies. *Bulletin of the American Meteorological Society*, **93**, 1879-1900, doi: 10.1175/BAMS-D-11-00019.1
57. Stewart, I.D., Oke, T.R., and E.S. Krayenhoff, 2014: Evaluation of the 'local climate zone' scheme using temperature observations and model simulations. *International Journal of Climatology* **34**, 1062-1080, doi: 10.1002/joc.3746

58. Tree Philly, 2017: Free Trees TreePhilly. Accessed 02 July 2017. [Available online at <http://treephilly.org/free-trees/>]
59. Tsilini, V., Papantoniou, S., Kolokotsa, D., and E. Maria, 2014: Urban gardens as a solution to energy poverty and urban heat island. *Sustainable Cities and Society*, **14**, 323-333, doi: 0.1016/j.scs.2014.08.006
60. Wang, Y., de Groot, R., Bakker, F., Wörtche, H., and R. Leemans, 2017: Thermal comfort in urban green spaces: a survey on a Dutch university campus. *International Journal of Biometeorology*, **61**, 87-101, doi: 10.1007/s00484-016-1193-0
61. Whitlock, M.C., and D. Schluter, 2015: *The Analysis of Biological Data*. Roberts and Company Publishers, Inc., 818 pp.
62. Wolch, J.R., Byrne, J., and J.P. Newell, 2014: Urban greenspace, public health, and environmental justice: the challenge of making cities 'just green enough'. *Landscape and Urban Planning*, **125**, 234-244 doi: 0.1016/j.landurbplan.2014.01.017
63. Yan, H., and L. Dong, 2015: The Impacts of Land Cover Types on Urban Outdoor Thermal Environment: the case of Beijing, China. *Journal of Environmental Health Science and Engineering*, **13**. n. pag. doi: 10.1186/s40201-015-0195-x